2018

CHARACTERIZING THE FUNCTIONAL ROLE AND REGULATED ASSEMBLY OF PROTEIN POLYMERS MIND AND FTSA DURING ESCHERICHIA COLI CELL DIVISION

Joseph Jake Conti
University of Rhode Island, jconti123@gmail.com

CHARACTERIZING THE FUNCTIONAL ROLE AND REGULATED ASSEMBLY OF PROTEIN POLYMERS MIND AND FTSA DURING *ESCHERICHIA COLI* CELL DIVISION

BY

JOSEPH JAKE CONTI

A DISSERTATION SUBMITTED IN PARTIAL FULFILLMENT OF THE

REQUIREMENTS FOR THE DEGREE OF

DOCTOR OF PHILOSOPHY

IN

BIOLOGICAL AND ENVIRONMENTAL SCIENCES

UNIVERSITY OF RHODE ISLAND

2018

DOCTOR OF PHILOSOPHY DISSERTATION

OF

JOSEPH JAKE CONTI

APPROVED:

Dissertation Committee:

Major Professor Jodi L. Camberg

Niall H. Howlett

Abraham Kovoor

Nasser H. Zawia
DEAN OF THE GRADUATE SCHOOL

UNIVERSITY OF RHODE ISLAND

2018

Abstract

It is an immense undertaking for any organism, including a bacterium, to self-replicate. Accurate and rapid division is essential for bacteria to proliferate and produce progeny, especially in environments where there is competition for resources. The nucleoid, the region of the cell that contains the DNA, harbors the genetic information required to achieve robust division, but it is the assembly of the cell division machinery, collectively referred to as the divisome, that produces and coordinates the mechanical force necessary to divide a cell. The hallmark of prokaryotic cell division is the formation of a protein super-structure, called the Z-ring, which spans the circumference of the cell division site on the interior of the cytoplasmic membrane. A nascent Z-ring, or proto-ring, is minimally comprised of polymerized FtsZ tethered to the cell membrane by FtsA, which is anchored directly to the membrane. The proto-ring acts as a scaffold for a sequential pathway of at least 10 essential cell division proteins and more than 15 other accessory proteins, which collectively regulate the spatiotemporal assembly of the mature Z-ring. Once fully assembled, the Z-ring and accessory proteins comprise the divisome that coordinates constriction of the mother cell into two identical daughter cells.

In Manuscript I, I review how proteins physically perturb lipid membranes to achieve a morphological cellular event, with emphasis on how prokaryotes assemble and utilize the Z-ring during division. I discuss current models for how division occurs and describe how dynamic protein conformational changes induce various cellular architectures.

In Manuscript II we discovered a new protein polymer comprised of the prokaryotic cell division proteins MinC and MinD, which copolymerize in the presence of ATP and rapidly depolymerizes in the presence of MinE. We report mechanistic insight into regulation of the protein assembly and propose a model of function for the polymer.

In Manuscript III we report the first natively purified and enzymatically active preparation of FtsA. We show that FtsA intercalates its membrane targeting sequence (MTS) into the lipid bilayer and uses ATP to directly remodel membrane architecture. These observations led us to propose a new model of the cell division pathway whereby FtsA directly exerts constrictive force at the division septum. Using our understanding from the work in Manuscript III we demonstrated in Manuscript IV that FtsA binds to phospholipids in an ATP-dependent manner through a mechanism that is distinct from the MTS. Additionally, we show that FtsA forms polymers in the presence of ATP and that polymerization is concentration dependent. This manuscript advances our model of FtsA-mediated lipid reorganization through mechanistic insight of how FtsA associates with the membrane and forms ATP-dependent polymers.

In conclusion, we report novel protein assemblies of MinC with MinD and, separately, assemblies of FtsA and we propose a model for how each polymer may affect cell division. Altogether, this work elucidates the role of protein polymers during prokaryotic cell division, and more generally, broadens our perspective of how protein polymers affect diverse cellular activities.

ACKNOWLEDGEMENTS

I thank my advisor, Dr. Jodi L. Camberg, for the opportunity to perform this work. Specifically for funding me with a teaching and research assistantship during my time in graduate school, supporting my travels to conferences and spending years of her time and patience training me; her efforts have shaped how I think about, perform and communicate my research. I thank Dr. Jodi L. Camberg, Dr. Niall H. Howlett, Dr. Roberta King, and Dr. Abraham Kovoor, the members of my PhD committee. Their guidance with the comprehensive exam and this dissertation is greatly appreciated. Additionally, I acknowledge the CMB faculty and students, past and present, which have shaped the productive and collegial atmosphere in the department. Finally, I thank my friends, my family, and my parents: I could not imagine this process without your support.

PREFACE

This dissertation has been prepared in the Manuscript Format according to the guidelines of the Graduate School of the University of Rhode Island. Manuscript I, "FtsA and other protein assemblies generate force on phospholipid membranes to coordinate cellular activities" is formatted as a review article for *Current Genetics*. Manuscript II, "The bacterial cell division regulators MinD and MinC form polymers in the presence of nucleotide" was published in *FEBS Letters* in 2015. Manuscript III, "FtsA reshapes membrane architecture and remodels the Z-ring in *Escherichia coli*" was published in *Molecular Microbiology* in 2018. Manuscript IV, "Nucleotide-dependent polymerization and lateral membrane-association by the cell division protein FtsA" was formatted and will be submitted to *Journal of Molecular Biology* for publication.

TABLE OF CONTENTS

CONTENT

ABSTRACT…….. ii

ACKNOWLEDGEMENTS……..……. iv

PREFACE……..…….v

TABLE OF CONTENTS…….…… . vi

LIST OF TABLES……..…….. vii

LIST OF FIGURES……...…….. viii

MANUSCRIPT I…… 1

MANUSCRIPT II ……...…… 26

MANUSCRIPT III…….……...…67

MANUSCRIPT IV…….……150

LIST OF TABLES

TABLES

MANUSCRIPT III

Table 1. Strains and plasmids used in this study…… 112

Table S1. MS/MS Identification of major lipids present in FtsA and FtsA(ΔMTS) …… 149

LIST OF FIGURES

MANUSCRIPT I

Figure 1. Proteins which associate with the membrane can exert force on the membrane promoting bending…… 22

Figure 2. Model of *E. coli* divisome function at the septum……..24

MANUSCRIPT II

Figure 1. Formation of large complexes containing MinD and MinC…… 49

Figure 2. Conditions that promote the formation of large MinCD complexes…… 51

Figure 3. Visualization of MinCD polymers by negative staining and electron microscopy…… 53

Figure 4. MinE disassembles ATP-dependent MinCD polymers…… 55

Figure 5. Cooperative assembly of MinCD polymers and interaction with fluorescent ATP……57

Figure 6. Mutations in MinD impair polymerization with MinC……. 59

Figure S1. ATP-dependent assembly of complexes containing MinC and MinD…… 61

Fig. S2. ATP hydrolysis in the presence and absence of MinE and phospholipids…… . 63

Fig. S3. Size exclusion chromatography of MinD and MinD mutant proteins……. 65

MANUSCRIPT III

Figure 1. FtsA hydrolyzes ATP rapidly in the presence of liposomes…….. 113

Figure 2. Phospholipids are essential for rapid ATP hydrolysis……..115

Figure 3. The C-terminal MTS of FtsA inserts into SUVs and is modified by ATP……117

Figure 4. FtsA(K86A), which contains a mutation in a loop near the active site, is defective for function…….. 120

Figure 5. FtsA recruits FtsZ to phospholipids and destabilizes steady state FtsZ polymers……. 122

Figure 6. Reconstruction of synthetic proto-ring complexes…… 124

Figure 7. Membrane distortion and intracellular vesicle formation in cells overexpressing FtsA…… 126

Figure S1. ATP hydrolysis activity trace of purified FtsA and survey of copurified PLs. …… 128

Figure S2. His-SUMO-FtsA hydrolyzes ATP and reorganizes phospholipid vesicles...130

Figure S3. Nucleotide-induced changes in light scatter by FtsA require an intact MTS and PLs…… . 132

Figure S4. FtsA PL reorganization and particle size distribution under varying nucleotide conditions…… 134

Figure S5. Comparison of FtsA and actin active sites…… 136

Figure S6. Characterization and lipid content of FtsA mutant proteins…… 138

Figure S7. FtsA-dependent recruitment of FtsZ to PLs…… 140

Figure S8. Nucleotide Hydrolysis by FtsA and FtsZ…… 142

Figure S9. TEM of putative FtsA protomers, consistent in size with FtsA cytoplasmic domains, aligned on a phospholipid surface……144

Figure S10. BL21 cells overexpressing FtsA are similar in length and viability to cells with empty vector…… 146

MANUSCRIPT IV

Figure 1. FtsAΔMTS in the presence of ATP induces large protein complexes……172

Figure 2. FtsAΔMTS forms ATP-dependent filaments……174

Figure 3. ATP induces membrane association of FtsAΔMTS to phospholipid vesicles..176

Figure 4. Surface-exposed residues of FtsA are critical for a secondary membrane interaction……178

Fig. S1. Nucleotide Hydrolysis by FtsA and FtsAΔMTS in the presence and absence of SUVs……180

Fig. S2. Subunit-subunit interaction of FtsA325AAAΔMTS…… 182

Manuscript I

Publication status: formatted as a review article for *Current Genetics*

Title: FtsA and other protein assemblies generate force on phospholipid membranes to coordinate cellular activities

Authors: Joseph J. Conti[1], Jodi L. Camberg[1, 2#]

Author Affiliations:

[1]Department of Cell and Molecular Biology

The University of Rhode Island

Kingston, Rhode Island, 02881

[2]Department of Nutrition and Food Sciences

The University of Rhode Island

Kingston, Rhode Island 02881

#**Corresponding author**: Jodi L. Camberg,

120 Flagg Road, Kingston, RI, 02881;

Tel: (401)874-4961;

Email: cambergj@uri.edu

Abstract

Among all organisms it is a common strategy to assemble large protein structures to produce large, diverse morphological changes. In this review, we discuss prevailing models of how various protein assemblies in diverse organisms use similar strategies to physically perturb lipid membranes and achieve a morphological transition or event during the life cycle of a cell. Then, we discuss in further detail how prokaryotes assemble the cell division machinery, referred to as the Z-ring, and highlight three prevailing models of how the Z-ring coordinates prokaryotic cell division. Lastly, we contextualize how recent work from our group corroborates, yet also advances, the underlying theory on the mechanism of prokaryotic cell division.

Introduction

A fundamental task for all organisms is to produce progeny, and this process consists of two major steps in *Escherichia coli*: (1) duplication of the genetic material and segregation into opposite haves of the cell and (2) constriction at the division septum and assembly of new cell wall, which separates the cell into two progeny cells.

Division is an immense and energetically costly undertaking for a cell. Most cells range from one to 20 microns in diameter (Zhao et al. 2008), yet a typical monomeric protein is approximately 50 kilodaltons, or 5 nm in diameter (Kim et al. 2013). Therefore, to achieve global morphological changes at the cellular scale, like membrane scission events or cell division, it requires coordination of many proteins simultaneously and often the assembly of large hierarchical protein complexes and/or

the involvement of cytoskeletal proteins. Prokaryotic cells organize proteins involved in cell division into a dynamic superstructure spanning the circumference of the cell, referred to as the divisome (Szwedziak & Lowe 2012; Haeusser & Margolin 2016; Green et al. 2012). The divisome functions at the cytoplasmic membrane to promote constriction at the septum and direct insertion of new cell wall components (Bisson-Filho et al. 2017; Conti et al. 2017; Liu et al. 2017; Yang et al. 2017; Chen et al. 2017).

In this review we discuss prevailing models of how cells from a variety of organisms generate force to change the shape of a membrane and achieve various morphologies. Finally, we review how recent findings of proteins involved prokaryotic cell division fit into the larger context of the bacterial cell division process.

Membrane shape is influenced by lipid composition and protein content

A phospholipid is comprised of multiple hydrophobic fatty acid chains of variable length bound together by a glycerol head group containing a phosphate. Phospholipids orient so that the polar head groups face outward to interact with aqueous or polar solvents and the acyl chains pack together through hydrophobic interactions, organizing into a double leaflet structure with a nonpolar core (Gruner 1985). The hydrostatic pressure of water promotes the phospholipid bilayer to become spherical due to the surface area to volume ratio being lowest in a sphere (Zhao et al. 2008). Universally, cells use phospholipid bilayers, which are approximately 5-10 nm thick (Bayer 1991, Rawiczet al. 2000), to establish a semi-permeable membrane where the outer leaflet of the bilayer interacts with the

external environment and the inner leaflet of the bilayer interacts with the cytoplasmic interior (Mitra et al. 2004; Nadi 2002). The processes of invaginating the membrane or moving large molecules across the membrane require modifications to the shape and/or composition of the phospholipid bilayer (Phillips et al. 2009). Membrane shape is influenced by the intrinsic properties of the phospholipid components. For example, the phospholipid membrane of *E. coli* consists of several lipids, including cardiolipin (CL), which constitutes ~5% of the PL content (Ganong & Raetz, 1982). CL consists of four acyl chains that pack tightly together due to hydrophobic interactions and a large, bulky diphosphate head group, producing a conical shaped lipid. In the rod shaped bacterium *E. coli*, CL has been shown to cluster together to form microdomains, which localize to highly curved regions of bacterial membranes (Mileykovskaya & Dowhan 2000, Renner & Weibel 2011). The curvature of a membrane is defined by 1/r along a cylindrical region of a cell and 2/r at a cell pole, where r is the radius (Huang & Ramamurthi 2010). Regions of higher curvature, which in *E. coli* are the invaginating region of membrane at the septum and the cell pole, accommodate the geometry of CL and relieves the steric strain generated by a CL microdomain (Renner & Weibel 2011). This supports the hypothesis that the spatial preference of lipids is a consequence of geometric and physical constraints of the cell.

Modifications to the overall shape of a cell can be achieved by the presence of membrane-interacting proteins. Proteins which contain a membrane binding motif can accumulate on the inner leaflet of the membrane nonspecifically due to molecular

crowding, and this can produce an uneven steric strain that is sufficient to alter the physical distribution of phospholipids on one face of the membrane bilayer, generating unorganized deformations in the membrane (Stachowiaket al. 2012). Membrane binding proteins can further self-organize to form a protein scaffold and coordinate localized distortion events to create areas of local curvature, thus producing membrane perturbations which are more uniform (Mcmahon & Boucrot 2015). For example, in *Saccharomyces cerevisiae*, differentially regulated nodes of actin peripherally associate with the membrane marking sites for endocytosis, then clathrin self-organizes by oligomerization into a cage-like structure, with several other coat proteins, leading to vesicle budding. Finally, regulatedactin polymerization at discrete nodes promotes vesicle scission and release (Johansenet al. 2016). In contrast to clathrin and actin, membrane-interacting proteins do not need to form a rigid structure to produce membrane shape changes. For example, specific localization of a membrane binding protein can direct local bilayer changes. Epsin1 localizes specifically to phosphatidylinositol 4,5-bisphosphate (PiP_2) in clathrin coated pits, and inserts its N-terminal amphipathic helix which contributes to generating curvature during the formation of clathrin-coated invaginations (Ford et al. 2002). Altogether, the major mechanisms by which membrane shape is reorganized include: insertion of a region of protein, such as an amphipathic helix, into the membrane, specific recruitment of phospholipids with altered packing densities or forming a rigid, protein scaffold on a surface to deform the underlying membrane (Figure 1).

The Z-ring localizes division proteins and may contribute force necessary for division

A cell can organize a network of proteins to form a cytoskeletal structure with enough scale to generate the force necessary to change the global morphology of the membrane. The canonical cytoskeletal protein, actin, forms the core of the actinomyosin contractile ring in eukaryotes. In *Schizosaccharomyces pombe*, localization of anillin, myosin II and formins at the site of division leads to nucleation of the actin ring and formation of the cleavage furrow (Cheffings et al. 2016). Septin filaments assemble at the membrane on both sides of polymerized actin to stabilize the actinomyosin ring and restrict spreading (Mavrakis et al. 2014). One current model of cell division in *S. pombe* proposes that the actin-ring is cross-linked and attached to the membrane by accessory proteins. Then, disassembly of actin polymers promotes septal closure of the actin ring at the cleavage furrow (Pelham & Chang 2002).

A major challenge to achieve cell division for most cells is to overcome the turgor pressure of the cytoplasm (Harold 2002). The cytoplasm has a high concentration of charged macromolecules and small ions; however, the membrane is permeable to water and some small nonpolar molecules, creating a high osmolality environment with turgor pressure exerted on the membrane (Record et al. 1998; Function et al. 2003). The magnitude of this turgor pressure is still debated and varies from one organism to another (Erickson 2017). To overcome the turgor pressure, the cell must generate force to constrict or remodel the membrane.

During cell division, constrictive force may be generated by the activity and assembly or disassembly of cytoskeletal structures. In addition, generation of new cell membrane at the site of cell division may also contribute to the overall force applied during division as older membrane becomes displaced. In vascular plant cells, insertional force builds from the fusion and accumulation of membrane vesicles in the center of the division plane which are then guided by the constrictive force of laterally translocating microtubules (Smith et al. 2001). In prokaryotes such as *E. coli*, assembly of the Z-ring is spatially restricted to midcell. FtsZ polymerizes into the Z-ring, tethered to the membrane through FtsA, and regions of the Z-ring undergo rapid, dynamic assembly and disassembly. Although FtsZ assembly dynamics has been widely postulated to provide the force for constriction, there is much debate about the precise role of FtsZ polymers. The Z-ring also serves as a landmark to recruit peptidoglycan synthesis proteins, which alters the shape of the periplasmic scaffold at the division site (Tsang & Bernhardt 2015). In archaea which lack a Z-ring, CdvA, CdvB and CdvC form a cell division apparatus (Busiek & Margolin 2011) whereby the membrane connecting two archaeal cells is cleaved during cell division by membrane abscission (Lindås et al. 2008) . The Cdv proteins polymerize between segregating nucleoids and persist throughout cell division forming a successively smaller structure that leads to constriction (Hanson et al. 2008; Härtel & Schwille 2014; Dobro et al. 2013). The Cdv proteins are functionally homologous to the eukaryotic endosomal sorting complexes required for transport (ESCRT) system, which promotes membrane abscission during cytokinesis, in addition to the role of the

ESCRT system in endosomal trafficking (Samsonet al. 2008). Together, these studies suggest that constrictive and insertional force are coordinated to reshape membranes and overcome the turgor pressure.

The Z-ring localizes division proteins and may contribute force necessary for division

Currently, there are several models that describe how the prokaryotic divisome may direct force necessary for division (Figure 2). The Z-ring is composed of polymers of FtsZ which are tethered to the membrane by FtsA, to form a proto-ring (Pichoff & Lutkenhaus 2005). Polymers of FtsZ are further organized laterally by several accessory proteins (Z-associated proteins) (Aarsman et al. 2005). The first model proposes that FtsZ filaments can bend. Both straight and bent filaments have been observed by X-ray crystallography and negative stain TEM and therefore it was suggested that bending force may be coupled to membrane bending constriction (Li et al. 2007). Moreover, FtsZ polymers bound to a non-hydrolyzable analog of GTP, GMPCPP, promotes straight filaments whereas FtsZ incubated with GTP produces polymers which adapt various degrees of curvature (Lu et al. 2000). The bending filament hypothesis proposes GTP-bound FtsZ filaments are straight and, upon GTP hydrolysis, GDP coordination alters the angle of subunits at the protofilament interface. Therefore, the degree of FtsZ polymer bending may correlate with the ratio of GTP:GDP in the FtsZ filament (Lu et al. 2000).

A second model proposes that dynamic FtsZ polymers undergo treadmilling, whereby a polymer grows at one end and disassembles at the opposite end, and the directional motion provides directional force. There is both in vivo and in vitro evidence to support that FtsZ undergoes treadmilling with movement of FtsZ polymers coordinated by cycles of GTP binding and hydrolysis and occurs coordinately with FtsA (Yang et al. 2017; Bission-Filho et al. 2017). These observations of FtsA and FtsZ treadmilling are reminiscent of the eukaryotic polymers actin and tubulin, and notably FtsA and FtsZ are structural homologs of actin and tubulin, respectively (Nogales 1998) (Erickson et al. 1996; Szwedziak et al. 2012). Directional assembly of actin filaments produces polymer locomotion and cell motility in lower eukaryotes (Mitchison & Cramer 1996, Pollard & Borisy 2003). Microtubules also exhibit treadmilling, the minus end of a microtubule is tethered to the centrosome and GTP hydrolysis at the plus end of the microtubule results in directional treadmilling, leading to subsequent chromosome segregation (Mitchison & Kirschener 1984). The FtsZ polymer treadmilling model of prokaryotic cell division postulates that FtsZ and FtsA transit the circumference of the cell directionally positioning the cell wall synthesis enzymes to assemble new peptidoglycan (PG) at the septum (Bission-Filho et al. 2017).

Both models rely on division that is driven by FtsZ-mediated GTP hydrolysis. However, considering the slow rate of GTP hydrolysis by FtsZ and lack of a clear GAP (G activating protein) or GEF (Guanine exchange factor) protein (Mukherjee & Lutkenhaus 1998), and observations which suggest that, in vivo, the Z-ring is

discontinuous (Holden et al. 2014), both models require further investigation (Osawa & Erickson 2018), especially considering that the Z-ring decreases in diameter as constriction proceeds.

A third model for division invokes insertional force generated by periplasmic proteins that synthesize peptidoglycan at the nascent division site. In addition to binding FtsZ, FtsA also recruits FtsN to the division site (Busiek & Margolin 2014). FtsN is a bitopic membrane protein that interacts with additional downstream division proteins and penicillin binding proteins engaging in peptidoglycan synthesis and remodeling, including murein transpeptidases and glycosyltransferases (Gerding et al. 2009) (Pogliano et al. 1997; Leclercq et al. 2017)(Gray et al. 2015). This model proposes that peptidoglycan insertion at the septum produces an insertional force that is transmitted across the cell wall since the inner membrane is attached to the outer membrane via the Tol/Pal system (Cascales et al. 2002). Specifically, this model suggests septal wall synthesis inserts PG at site of cell division to generate insertional force and this provides the force for constriction (Figure 2).

Consolidated model of septal membrane remodeling and cell wall synthesis

In vitro, FtsA promotes organization of FtsZ polymers on a surface into dynamic patterns (Loose & Mitchison 2013), and in another study, FtsA has been observed to form a 12-subunit mini-ring with a diameter of 20 nm, that is thought to oppose FtsZ bundling and stabilize long-range FtsZ protofilaments (Schoenemann et al. 2018; Chen et al. 2017). Recently, FtsA has been reported to robustly hydrolyze

ATP in the presence of phospholipids (Conti et al., 2018). Moreover, the C-terminus of FtsA contains a predicted amphipathic helix that intercalates into the lipid bilayer, and, upon binding ATP, the conformation of FtsA changes and the MTS reorients relative to the interior of lipid bilayer (Conti et al. 2018). Together, polymerization of FtsA on the lipid surface and direct insertion of the MTS promote phospholipid reorganization that deforms the membrane locally. Recent data further suggests that there is a secondary site of membrane association on the surface of FtsA and engagement of the membrane at this site is also regulated by ATP association. Considering that FtsA arrives first and simultaneously with FtsZ at the site of division (Söderström et al. 2016) and FtsA directly interacts with FtsZ (Loose & Mitchison 2013), FtsI (Alexeeva et al. 2010) and FtsN (Pichoff et al. 2018), FtsA is at the core of positioning the cell wall machinery at the site of Z-ring assembly. Therefore, FtsA coordinates the constriction event by regulating FtsZ polymerization, produces localized membrane deformations and directs PG insertion at the nascent division site.

Conclusions

The general theory of prokaryotic cell division has long relied on the description of the Z-ring as a cytoskeletal structure that directly generates constrictive force, while localizing other proteins to generate insertional force. Recent findings implicate the Z-ring, constituted by FtsZ and FtsA, in nucleotide-driven treadmilling and nucleotide-dependent lipid bilayer reorganization that is coupled to new cell wall

generation (Bisson-Filho et al. 2017). Instead of force being generated by the assembly or disassembly of a cytoskeletal structure or the action of a motor protein processively moving along a static filament, recent studies suggest that protein conformation and assembly of complexes on a membrane can reconfigure membrane shape locally, and this may be templated on a dynamic scaffold containing FtsZ and FtsZ-interacting proteins to promote division.

References

Aarsman, M.E., Piette, A., Fraipont, C., Vinkenvleugel, T.M., Nguyen-Disteche, M., & den Blaauwen, T. 2005. Maturation of the Escherichia coli divisome occurs in two steps. *Molecular Microbiology*, 55(6), pp.1631–1645.

Alexeeva, S., Gadella, T.W., Verheul, J., Verhoeven, G.S., & den Blaauwen, T. 2010. Direct interactions of early and late assembling division proteins in Escherichia coli cells resolved by FRET. *Molecular Microbiology*, 77(2), pp.384–398.

Kachar, B. 1995. Direct Visualization of Organelle Movement along Actin Filaments Dissociated from Characean Algae. *Science* , Vol . 227 , No . 4692, pp . 1355-1357

Arias-Cartin, R., Grimaldi, S., Arnoux, P., Guigliarelli, B., & Magalon, A. 2012. Cardiolipin binding in bacterial respiratory complexes: Structural and functional implications. *Biochimica et Biophysica Acta - Bioenergetics*, 1817(10), pp.1937–1949.

Busiek, K.K. & Margolin, W., 2014. A role for FtsA in SPOR-independent localization of the essential Escherichia coli cell division protein FtsN. *Molecular Microbiology*, 92(May), pp.1212–1226.

Busiek, K.K. & Margolin, W., 2011. Split decision: A thaumarchaeon encoding both FtsZ and Cdv cell division proteins chooses Cdv for cytokinesis. *Molecular Microbiology*, 82(3), pp.535–538.

Cascales, E., Bernadac, A., Gavioli, M., Lazzaroni, J.C., & Lloubes, R. 2002. Pal Lipoprotein of Escherichia coli Plays a Major Role in Outer Membrane Integrity.

Journal of Bacteriology, 184(3), pp.754–759.

Cheffings, T.H., Burroughs, N.J. & Balasubramanian, M.K., 2016. Actomyosin Ring Formation and Tension Generation in Eukaryotic Cytokinesis. *Current Biology*, 26(15), pp.R719–R737.

Chen, Y., Huang, H., Osawa, M., & Erickson, H.P. 2017. ZipA and FtsA* stabilize FtsZ-GDP miniring structures. *Scientific Reports*, 7;3650 pp.1–9.

Conti, J., Viola, M.G. & Camberg, J.L., 2017. FtsA reshapes membrane architecture and remodels the Z-ring in Escherichia coli. *Molecular Microbiology*, 00, pp.1–19.

Dobro, M.J., Samson, R.Y., Yu, Z., McCullough, J., Ding, H.J., Chong, P.L., Bell, S.D., & Jensen, G.J. 2013. Electron cryotomography of ESCRT assemblies and dividing Sulfolobus cells suggests that spiraling filaments are involved in membrane scission. *Molecular Biology of the Cell*, 24(15): pp.2319–2327.

Du, S., Pichoff, S. & Lutkenhaus, J., 2016. FtsEX acts on FtsA to regulate divisome assembly and activity. *Proceedings of the National Academy of Sciences*, 23;113(34), pp.5052-61.

Erickson, H.P., Taylor, D.W., Taylor, K.A., Bramhill, D. 1996. Bacterial cell division protein FtsZ assembles into protofilament sheets and minirings, structural homologs of tubulin polymers. *Proceedings of the National Academy of Sciences of the United States of America*, 93(1), pp.519–23.

Erickson, H.P., 2017. How bacterial cell division might cheat turgor pressure- a unified mechanism of spetal division in Gram-positive and Gram-negative bacteria. *BioEssay*s, 1700045, pp.1–10.

Ford, M.G.J., Mills, I.G., Peter, B.J., Vallis, Y., Praefcke, G.J.K., Evans, P.R. & McMahon, H.T. 2002. Curvature of clathrin-coated pits driven by epsin. *Nature*, 419(September) 361-366.

Decad, G.M. & Nikaido, H., 2003. Outer Membrane of Gram-Negative Bacteria. *Journal of Bacteriology*, 128(1), pp.325–336.

Gerding, M.A., Liu, B., Bendezu, F.O., Hale, C.A., Bernhardt, T.G., & de Boer, P.A. 2009. Self-Enhanced Accumulation of FtsN at Division Sites and Roles for Other Proteins with a SPOR Domain (DamX, DedD, and RlpA) in Escherichia coli Cell Constriction. *Journal of Bacteriology*, 191(24), pp.7383–7401.

Gidden, J., Denson, J., Liyanage, R., Ivey, D.M., & Lay, J.O. 2009. Lipid compositions in Escherichia coli and Bacillus subtilis during growth as determined by MALDI-TOF and TOF/TOF mass spectrometry. *International Journal of Mass Spectrometry*, 283(1-3), pp.178–184.

Gray, A.N., Egan, A.J., Van't Veer, I.L., Verheul, J., Colavin, A., Koumoutsi, A., Biboy, Breukink, E., den Blaauwen, T., Typas, A., Gross, C.A., Vollmer, W. et al., 2015. Coordination of peptidoglycan synthesis and outer membrane constriction during Escherichia coli cell division. *eLife*, 4(MAY), pp.1–29.

Green, R.A., Paluch, E. & Oegema, K., 2012. Cytokinesis in Animal Cells. *Annual Review of Cell and Developmental Biology.* 28:29-58

Gruner, S.M., 1985. Intrinsic curvature hypothesis for biomembrane lipid composition: a role for nonbilayer lipids. *Proceedings of the National Academy of Sciences*, 82(11), pp.3665–3669.

Haeusser, D.P. & Margolin, W., 2016. Splitsville: structural and functional insights into the dynamic bacterial Z ring. *Nature reviews. Microbiology*, 14(5), pp.305–319.

Hanson, P.I., Roth, R., Lin, Y., Heuser, J.E. 2008. Plasma membrane deformation by circular arrays of ESCRT-III protein filaments. *Journal of Cellular Biology*, 180(2), pp.389–402.

Harold, F.M., 2002. Force and compliance : rethinking morphogenesis in walled cells. *Fungal Genetics and Biology*, 37, pp.271–282.

Härtel, T. & Schwille, P., 2014. ESCRT-III mediated cell division in Sulfolobus acidocaldarius – a reconstitution perspective. *Frontiers in microbiology*, 5(June), pp.1–7.

Holden, S.J., Pengo, T., Meibom, K.L., Fernandez, C.F., Collier, J., & Manley, S. 2014. High throughput 3D super-resolution microscopy reveals Caulobacter crescentus in vivo. *Proceedings of the National Academy of Sciences*, 111(12) 4566-4571.

Huang, K.C. & Ramamurthi, K.S., 2010. Macromolecules that prefer their membranes curvy. *Molecular Microbiology*, 76(4), pp.822–832.

Johansen, J., Alfaro, G. & Beh, C.T., 2016. Polarized Exocytosis Induces Compensatory Endocytosis by Sec4p-Regulated Cortical Actin Polymerization. *PLoS Biology*, 14(8):e1002534 pp.1–24.

Kim YE, Hipp MS, Bracher A, Hayer-Hartl M, Hartl FU. Molecular chaperone functions in protein folding and proteostasis. Annu Rev Biochem. 201382:323-55.

Krupka, M., Cabre, E.J., Jimenez, M., Rivas, G., Rico, A.R., & Vicente, M. 2014. Role of the FtsA C terminus as a switch for polymerization and membrane association.

mBio, 5(6):02221-14.

Leclercq, S., Derouaux, A., Olatunji, S., Fraipont, C., Egan, A.J.F., Vollmer, W., Breukink, E. & Terrak, M. 2017. Interplay between Penicillin- binding proteins and SEDS proteins promotes bacterial cell wall synthesis. *Scientific Reports*, 7:43306, pp.1–13.

Li, Z., Trimble, M.J., Brun, Y.V., Jensen, G.J. 2007. The structure of FtsZ filaments in vivo suggests a force-generating role in cell division. *EMBO Journal*, 26(22), pp.4694–4708.

Lindås, A., Karlsson, E.A., Lindgren, M.T., Ettema, T.J.G., & Bernander, R. 2008. A unique cell division machinery in the Archaea. *Proceedings of the National Academy of Sciences*, 105(48), pp.18942–18946.

Liu, X., Meiresonne, N.Y., Bouhss, A., & den Blaauwen, T. et al., 2017. The Combined activities of FtsW and MurJ are required for lipid II translocation during cell division in Escherichia coli. *bioRxiv*, pp.1–31.

Loose, M. & Mitchison, T.J., 2013. The bacterial cell division proteins FtsA and FtsZ self-organize into dynamic cytoskeletal patterns. *Nature Cell Biology*, 16(1), pp.38–46.

Lu, C., Reedy, M. & Erickson, H.P., 2000. Straight and Curved Conformations of FtsZ Are Regulated by GTP Hydrolysis. *Journal of Bacteriology*, 182(1), pp.164–170.

Mavrakis, M., Azou-Gros, Y., Tsai, F.C., Alvarado, J., Bertin, A., Iv, F., Kress, A., Brasselet, S., Koenderink, G.H., & Lecuit, T. 2014. Septins promote F-actin ring formation by crosslinking actin filaments into curved bundles. *Nature Cell Biology*,

16(4) 322-334.

Mcmahon, H.T. & Boucrot, E., 2015. Membrane curvature at a glance. , pp.1065–1070.

Mileykovskaya, E. & Dowhan, W., 2000. Visualization of Phospholipid Domains in Escherichia coli by Using the Cardiolipin-Specific Fluorescent Dye 10- N -Nonyl Acridine Orange. *J Bacteriol*, 182(4), pp.1172–1175.

Mitra, K., Ubarretxena, I., Taguchi, T., Warren, G., & Engleman, D.M. 2004. Modulation of the bilayer thickness of exocytic pathway membranes by membrane proteins rather than cholesterol. *Proceedings of the National Academy of Sciences*, 101(12), pp.4083–4088.

Mukherjee, A. & Lutkenhaus, J., 1998. Dynamic assembly of FtsZ regulated by GTP hydrolysis. *EMBO Journal*, 17(2), pp.462–469.

Jaspard, F., & Nadi, M. 2002. Dielectric properties of blood : an investigation of temperature dependence. *Physiol. Meas.*, 23:547.

Osawa, M. & Erickson, H.P., 2013. Liposome division by a simple bacterial division machinery. *Proceedings of the National Academy of Sciences*, 110(27), pp.11000–11004.

Osawa, M. & Erickson, H.P., 2018. Turgor Pressure and Possible Constriction Mechanisms in Bacterial Division. *Frontiers of Microbiology*, 9(January), pp.1–7.

Pelham, R.J. & Chang, F., 2002. Actin dynamics in the contractile ring during cytokinesis in fission yeast. *Nature*, 419(September), pp.82–86.

Pichoff, S., Du, S. & Lutkenhaus, J., 2018. Disruption of divisome assembly rescued by FtsN – FtsA interaction in Escherichia coli. *Proceedings of the National Academy of*

Sciences, pp.32–36.

Pichoff, S. & Lutkenhaus, J., 2005. Tethering the Z ring to the membrane through a conserved membrane targeting sequence in FtsA. *Molecular Microbiology*, 55(6), pp.1722–1734.

Pogliano, J., Pogliano, K., Weiss, D.S., Losick, R., & Beckwith, J. 1997. Inactivation of FtsI inhibits constriction of the FtsZ cytokinetic ring and delays the assembly of FtsZ rings at potential division sites. *Proceedings of the National Academy of Sciences of the United States of America*, 94(2), pp.559–564.

Ramamurthi, K.S. & Losick, R., 2009. Negative membrane curvature as a cue for subcellular localization of a bacterial protein. *Proceedings of the National Academy of Sciences*, 106(32), pp.13541–13545.

Record, M.T., Courtenay, E.S., Cayley, D.S., & Guttman, H.J. 1998. Responses of E . coli to osmotic stress : large changes in amounts of cytoplasmic solutes and water. *Trends in Biochemical Sciences*, Apr;23(4) pp.143–148.

Renner, L.D. & Weibel, D.B., 2011. Cardiolipin microdomains localize to negatively curved regions of Escherichia coli membranes. *Proceedings of the National Academy of Sciences of the United States of America*, 2011.

Schoenemann, K.M., Krupka, M., Rowlett, V.W., Distelhorst, S.L., Hu, B., & Margolin, W. 2018. Gain-of-function variants of FtsA form diverse oligomeric structures on lipids and enhance FtsZ protofilament bundling. *Molecular Microbiology*, 0(0), pp.1–18.

Smith, L.G., Gerttula, S.M., Han, S., Levy, J. 2001. TANGLED1: a microtubule binding

protein required for the spatial control of cytokinesis in Maize. *Journal of Cellular Biology*, 152(1) pp.231-236.

Söderström, B., Mirzadeh, K., Toddo, S, von Heijne, G., Skoglund, U., Daley, D.O. 2016. Coordinated disassembly of the divisome complex in Escherichia coli. *Molecular Microbiology*, 101(3), pp.425–438.

Stachowiak, J.C., Schmid, E.M., Ryan, C.J., Ann, S.H., Sasaki, D.Y., Sherman, M.B., Geissler, P.L., Fletcher, D.A. & Hayden, C.C. 2012. Membrane bending by protein – protein crowding. *Science*, 14(9) 944-949.

Szwedziak, P., Wang, Q., Freund, S.M.V., & Lowe, J. 2012. FtsA forms actin-like protofilaments. *Embo J.*, 31(10), pp.2249–2260.

Szwedziak, P. & Lowe, J., 2013. Do the divisome and elongasome share a common evolutionary past? *Current Opinions in Microbiology*, 16(6) pp.745-751.

Tadros, M., Vicente, M. & Gonza, M., 2005. Visualization of Single Escherichia coli FtsZ Filament Dynamics with Atomic Force Microscopy. *Journal of Biological Chemistry*, 280(21), pp.20909–20914.

Tsang, M. & Bernhardt, T.G., 2015. A role for the FtsQLB complex in cytokinetic ring activation revealed by an ftsL allele that accelerates division. *Molecular Microbiology*, 95(January), pp.925–944.

Vaz, F.M., Houtkooper, R.H., Valianpour, F., Barth, P.G., & Wander, R.J.A. 2003. Only One Splice Variant of the Human TAZ Gene Encodes a Functional Protein with a Role in Cardiolipin Metabolism. *Journal of Biological Chemistry*, 278(44), pp.43089–43094.

Viola, M.G., LaBreck, C.J., Conti, J., Camberg, J.L. 2017. Proteolysis-Dependent Remodeling of the Tubulin Homolog FtsZ at the Division Septum in Escherichia coli. *Plos One*, 12(1):.e0170505.

Bisson-Filho, A., Hsu, Y., Squyres, G.R., Kuru, K., Wu, F., Jukes, C., Sun, Y., Dekker, C., Holden, S., VanNieuwenhze, M.S., Brun, Y.V., & Garner, E.C. 2017. Treadmilling by FtsZ filaments drives peptidoglycan synthesis and bacterial cell division. *Science*, 355:6326 pp 739-743.

Yang, X., Lyu, Z., Miguel, A., McQuillen, R., Huang, K.C., & Xiao, J. 2017. GTPase activity – coupled treadmilling of the bacterial tubulin FtsZ organizes septal cell wall synthesis. *Science*, 747(February)355:6326, pp.744–747.

Zhao L, Kroenke CD, Song J, Piwnica-Worms D, Ackerman JJ, Neil JJ. Intracellular water-specific MR of microbead-adherent cells: the HeLa cell intracellular water exchange lifetime. NMR Biomed. 2008 Feb21(2):159-64

A.

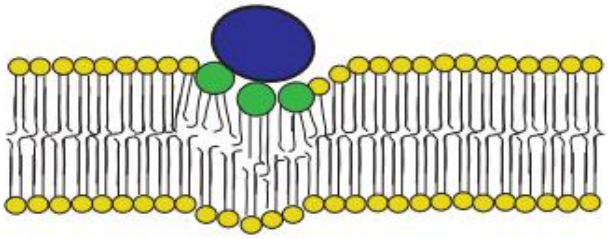

B.

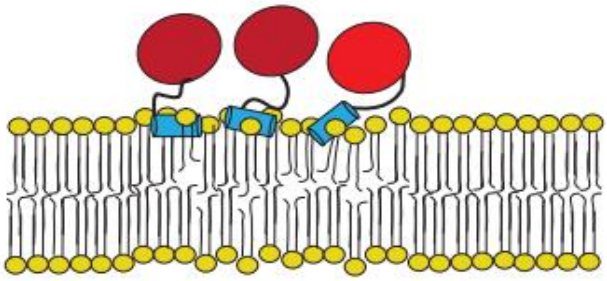

C.

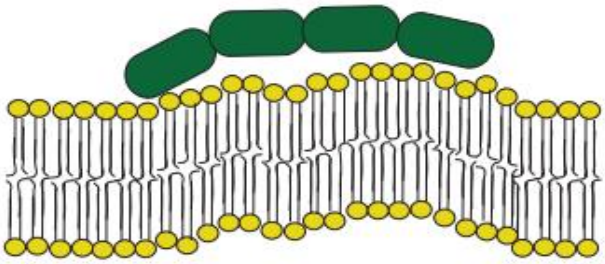

Figure 1. Proteins which associate with the membrane can exert force on the membrane promoting bending

A. Proteins can affect the distribution of lipids in the bilayer by clustering lipids with large head-groups, like cardiolipin, to promote membrane bending B. Clustering of membrane binding proteins, either by insertion of a membrane-embedded anchoring region or nonspecific protein crowding exert an unequal force on one leaflet of the bilayer and promote membrane distortion C. A protein that oligomerizes on the membrane surface can function as a scaffold and promote curvature.

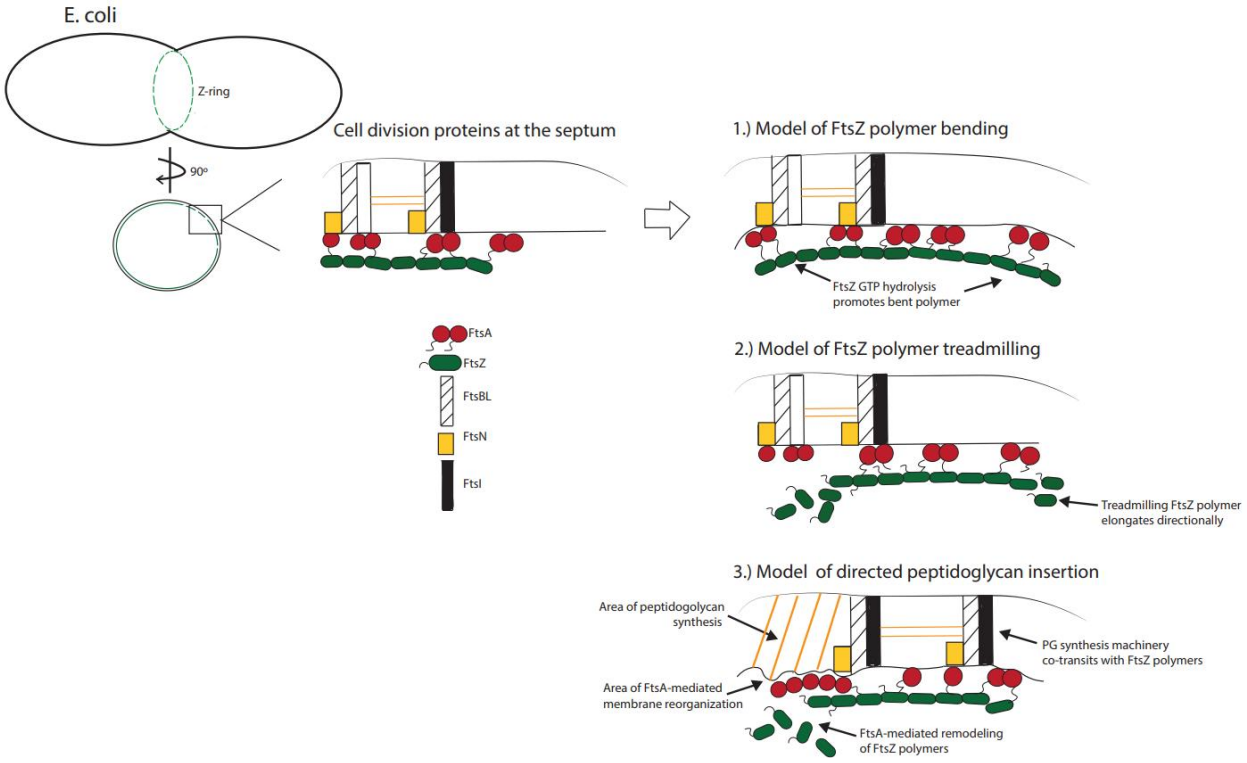
E. coli
Z-ring
90°
Cell division proteins at the septum
FtsA
FtsZ
FtsBL
FtsN
FtsI
1.) Model of FtsZ polymer bending
FtsZ GTP hydrolysis
promotes bent polymer
2.) Model of FtsZ polymer treadmilling
Treadmilling FtsZ polymer
elongates directionally
3.) Model of directed peptidoglycan insertion
Area of peptidogolycan
synthesis
PG synthesis machinery
co-transits with FtsZ polymers
Area of FtsA-mediated
membrane reorganization
FtsA-mediated remodeling
of FtsZ polymers

Figure 2. Model of *E. coli* divisome function at the septum

E. coli divisome depicting 3 models of cell division. 1) FtsZ polymers are recruited to the membrane by FtsA. FtsZ binding GTP promotes a straight polymer, sebsequent hydrolysis of GTP by the FtsZ polymer promotes a change in the conformation of the FtsZ subunits leading to a bent polymer. The force generated by the FtsZ polymer bending may generate some of the force necessary for septation. 2) GTP hydrolysis by FtsZ may promote treadmilling of the FtsZ polymers. Proteins which directly bind FtsZ, including FtsA, may co-transit with a treadmilling FtsZ polymer. 3) FtsA localizes FtsN and FtsI to the site of cell division. These proteins, along with FtsBL, assist in the insertion of new PG in the periplasm: this spatial positioning directs the force generated by new PG insertion. Additionally, polymerization of FtsA on the membrane results in an increased local concentration of FtsA which can remodel FtsZ polymers. Directed PG synthesis, possibly to areas of FtsA-mediated membrane reorganization, may generate some of the force necessary for septation.

Manuscript II

Publication status: Published in *FEBS LETTERS*, 2015

Title: The cell division regulators MinD and MinC form polymers in the presence of nucleotide

Authors: Joseph Conti[1], Marissa G. Viola[1], Jodi L. Camberg[1,2*]

Author Affiliations:

Department of Cell and Molecular Biology,

College of Environment and Life Sciences,

University of Rhode Island,

Kingston, RI, USA

*__Corresponding author__: Jodi L. Camberg, 120 Flagg Road, Kingston, RI, 02881; Tel: (401)874-4961; Email: cambergj@mail.uri.edu

ABSTRACT

The Min system of proteins, consisting of MinC, MinD and MinE, is essential for normal cell division in Escherichia coli. MinC forms a polar gradient to restrict placement of the division septum to midcell. MinC localization occurs through a direct interaction with MinD, a membrane-associating Par-like ATPase. MinE stimulates ATP hydrolysis by MinD, thereby releasing MinD from the membrane. Here, we show that MinD forms polymers with MinC and ATP without the addition of phospholipids. The topological regulator MinE induces disassembly of MinCD polymers. Two MinD mutant proteins, MinD(K11A) and MinD(ΔMTS15), are unable to form polymers with MinC.

INTRODUCTION

The hallmark of cell division in bacteria is the formation of a protein ring at the site of septation, called the Z-ring, which contains FtsZ and FtsZ-interacting proteins. In *E scherichia coli*, Z-ring assembly is inhibited by two systems, SlmA and the Min system [1-4]. The Min system, consisting of MinC, MinD and MinE, prevents assembly of the Z-ring near the cell poles. MinC inhibits FtsZ polymerization in vitro and Z-ring formation in vivo [5-7, 35]. MinD exhibits rapid pole-to-pole oscillation and restricts MinC localization through a direct interaction [8]. MinE functions as a regulator to stimulate the ATPase activity of MinD promoting release from the membrane [4].

MinD is a member of the Walker A Cytoskeletal ATPase (WACA) family, also referred to as the ParA family [9, 10]. Many Par-like proteins are involved in plasmid partitioning or chromosome segregation and are characterized by ATP-dependent dimerization [10, 11]. In the ATP-bound conformation MinD forms a sandwich dimer with two molecules of ATP in the interface, and an amphipathic helix at the C-terminus of each MinD protomer inserts into the lipid bilayer [12, 25]. The regulator MinE, which also forms a membrane-associated dimer, binds to MinD and stimulates ATP hydrolysis in the presence of phospholipids, causing MinD to dissociate from the membrane [14-19, 24]. In the structural model of the MinD dimer in complex with MinE, the MinE binding site is adjacent to the MinD dimerization interface [12, 19].

MinD contains a deviant Walker A ATP-binding motif ($_{10}$GKGGVGKT$_{17}$), which differs from the classical Walker A motif due the presence of an additional lysine at position 11. Lys 11 in MinD is important for dimerization, ATP hydrolysis and interacting with MinC [21, 22]. In the current model, Lys 11 interacts with ATP in the opposing protomer [12, 23]. MinE binds phospholipid-associated MinD and increases the ATP hydrolysis rate 10-fold [15]. ADP-bound MinD then dissociates from the membrane releasing MinE.

Association of MinD with the phospholipid membrane is important for activity in vivo [25, 26]. MinD membrane localization is mediated by a conserved 8–12 residue motif at the C-terminus called the membrane targeting sequence (MTS) [12, 13, 26, 27]. The MTS forms an amphipathic α-helix that inserts into the phospholipid bilayer [12, 13]. Following stimulation of ATP hydrolysis by MinE, the MTS dissociates from the membrane [16, 18]. In the presence of ATP and a regenerating system, cycling of MinD and MinE on and off the membrane produces waves and other patterns on membrane surfaces in vitro [28, 29].

MinC is a dimeric two-domain protein that inhibits FtsZ polymerization at two sites of interaction [6, 7, 20]. In addition to mediating dimerization and FtsZ recognition, the C-domain of MinC also binds to MinD. Amino acid residues in MinC important for binding to MinD include Arg 133, Ser 134 and several surface exposed glycines [22, 30]. MinD residues that interact with MinC are located on the top of the MinD dimer interface, distal to the membrane-associated region. Amino acid mutations that prevent MinD dimerization, and residues in helix 7 (Leu 157, Gly 158

and Ala 161), disrupt the interaction with MinC [12]. Residues on MinD important for the interaction with MinE are more widely distributed along the dimer interface [12].

Some members of the Par family, including ParA, ParF and Soj, undergo ATP-dependent polymerization in vitro, yet polymerization in vivo remains controversial [10, 11, 31, 32]. MinD polymerization is thought to occur on the membrane surface, since several groups observed polymer formation by MinD in the presence of phospholipids and ATP [14, 17].

Here, we describe conditions that support the formation of stable polymers containing MinD, MinC and ATP; however, no phospholipids were added to the reaction. MinE induces disassembly of polymers, which may occur through a direct interaction with MinD that displaces MinC.

EXPERIMENTAL PROCEDURES

Polymerization assays

The *minD, minC* and *minE* genes were amplified from *E. coli* MG1655 and cloned into pET-24b plasmid (Novagen). MinD(DMTS15) was constructed by insertion of a TAA stop codon at position 256 in *minD,* and MinD(K11A) was constructed by site-directed mutagenesis. MinD wild type and mutant proteins were expressed in E. coli BL21(λDE3) cells grown in luria broth containing kanamycin (25 μg ml^{-1}) following addition of isopropyl-β-D-thiogalactoside (IPTG) (0.5 mM). After 3 h, cells were collected and resuspended in 25 mM Tris–HCl, pH 8.0, 50 mM KCl, 10 mM MgCl2, 10% glycerol, 1 mM EDTA and 1 mM tris(2-carboxyethyl)phosphine (TCEP). After French press lysis, soluble extracts were collected by centrifugation at 35 000 x g for 30 min, loaded on a 25

ml Q sepharose fast flow (GE Healthcare) column and eluted with a KCl gradient (50–600 mM). Peak fractions were fractionated on a 50 ml Sephacryl S-100 (GE Healthcare) column equilibrated with 25 mM Tris–HCl, pH 8.0, 150 mM KCl, 10 mM MgCl2, 10% glycerol, 1 mM EDTA and 1 mM TCEP. MinC and MinE were purified as described above except MgCl2 was omitted. Dimer protein concentrations are reported for MinD, MinC and MinE.

Ultracentrifugation assays

Reaction mixtures (25 µl) in assembly buffer (50 mM MES, pH 6.5, 100 mM KCl, 10 mM $MgCl_2$) containing MinD (12 µM), MinC (6 µM) and ATP (4 mM) were incubated for 5 min at 23 C, then centrifuged at 130000g for 30 min. Supernatants and pellets were resuspended in equal volumes and analyzed by SDS–PAGE and Coomassie staining. Where indicated, the following nucleotides or EDTA (15 mM) were included in the reaction: ADP (4 mM), ATP-γ-S (2 mM), AMPPNP (2 mM), GTP (2 mM). Hill coefficients were obtained from reactions titrating MinD in the presence of 2 or 10 µM MinC. Curves were fit to a one-site specific binding model with cooperativity in GraphPad Prism (Version 6.0b) using the following equation B = Bmax [L] n /(Kd n + [L] n); where B is the specific binding, L is the concentration of MinD, and n is the Hill slope. Pre-treatment of MinC and MinD proteins with lipid removal agent (LRA) (Sigma–Aldrich) did not affect assembly in the ultracentrifugation assay.

Light scattering assays

Reactions were carried out in assembly buffer containing MinD (12 µM) and MinC (6 µM) or as indicated with MinE (0–30 µM). Polymerization was followed with time after

the addition of 4 mM ATP by monitoring light scattering using an Agilent Eclipse fluorescence spectrophotometer with excitation and emission wavelengths set to 450 nm with 5 nm slit widths.

Electron microscopy

Reactions containing assembly buffer with 5 µM MinD, 5 µM MinC and 4 mM ATP, where indicated, were incubated for 5 min at 23 C, applied to a 300-mesh carbon/formvar coated grid, fixed with glutaraldehyde (1%), and stained with uranyl acetate (2%). Samples were imaged by transmission electron microscopy using a Morgagni 268100 KV instrument equipped with a 6-megapixel digital camera.

ATPase Assay

ATP hydrolysis was measured by monitoring the amount of phosphate released after 20 min in reactions (25 µl) containing assembly buffer with ATP (4 mM) and MinD (5 µM), MinE 10 (10 µM), MinC (2.5 µM), or E. coli phospholipids (1 mg/ml) (Avanti), where indicated. Total phosphate was detected using Biomol Green (Enzo Life Sciences) and quantified by comparison to a phosphate standard curve. GTP hydrolysis assays were performed as described above except that assembly buffer contained 2 mM GTP.

Analytical Size Exclusion Chromatography

Size exclusion chromatography was performed using a Sephacryl S-100 (5 ml) column equilibrated with assembly buffer containing 1 mM ATP and 0.0005% Triton X-100. MinD, 19 MinD(K11A), and MinD(ΔMTS15) (80 µg) were incubated with ATP (4 mM) for 5 minutes and loaded on the column at a flow rate of 0.2 ml/min. Fractions (100 µl)

were collected using a Gilson fraction collector (203B) fitted for microtiter plate collection. Fractions were analyzed for total protein using a Bradford reagent.

Binding of fluorescent nucleotides.

Fluorescent nucleotide binding was measured with an Agilent Eclipse fluorescence spectrophotometer using an excitation wavelength of 350 nm and an emission wavelength of 400 nm and 5 nm slit widths. Reaction mixtures (75 µL) containing MinD (5 µM) were incubated in assembly buffer with varying concentrations of mant-ATP (0 – 100 µM) or mant-GTP (0 – 30 µM) (Life Technologies), where indicated, and fluorescence intensity was measured. Binding curves were fit to a one site specific binding model in GraphPad Prism using the following equation $F = Fmax \times [L]n / (Kd\ n + [L]n)$; where F is fluorescence intensity, L is ligand concentration and n is unconstrained.

RESULTS

ATP-dependent assembly of polymers containing MinC and MinD in the absence of phospholipids

To further understand the protein interaction that occurs between MinC and MinD, we studied nucleotide-dependent complex formation in vitro. Other Par-like ATPases assemble into polymers, therefore we tested if MinC promotes or stabilizes polymers formed by MinD. MinC and MinD were incubated in the presence and absence of ATP, and then reactions were fractionated by ultracentrifugation. We observed that without ATP, both MinD and MinC, alone or together, were soluble and predominantly localized to the supernatant (Fig. 1 A). However, when MinC and MinD were incubated together

with ATP, the distribution of both proteins shifted to the pellet even though only MinD contains a nucleotide-binding site (46% of MinD fractionated with the pellet). The ratio of MinD to MinC was calculated to be 1.6:1 (Fig. S1A). When MinC or MinD was incubated with ATP alone, each protein was present in the supernatant fraction. These results suggest that with ATP, MinC and MinD form large oligomers.

To confirm these results, we used 90°-angle light scattering to detect the assembly of large MinCD complexes. We measured the light scatter by mixtures of MinC and MinD, then added ATP and monitored the light scattering signal for 15 min (Fig. 1b). We observed that the addition of ATP to reactions containing both MinC and MinD causes a large increase in light scatter, which reaches a plateau after approximately 10 minutes and is stable for longer than 90 min (Fig. 1b, Fig. S1). Addition of ATP to reactions containing either MinC or MinD led to no increase in light scatter (Fig. 1c and 1d). In a control experiment, when buffer instead of ATP was added to reactions containing both MinC and MinD, no increase in signal was detected (Fig. 1e). These results show that the addition of ATP promotes a conformational change in mixtures of MinC and MinD that results in the formation of large complexes that scatter light at 450 nm.

Next, we used 90°-angle light scattering to detect the assembly of large MinCD complexes. We measured the light scatter of mixtures of MinC and MinD, then added ATP and monitored the change in scattered light for 15 min (Fig. 1B). The addition of ATP to reactions containing MinC and MinD caused a large increase in light scatter, which reached a plateau after approximately 15 min and was stable for longer than 90 min (Fig. 1B and Fig. S1B). Addition of ATP to reactions containing either MinC or

MinD led to no increase in light scatter (Fig. 1C and D). No increase in signal was detected when buffer was added to reactions containing both MinC and MinD (Fig. 1E).

Next, to determine if complex formation is dependent on MinC concentration, we titrated the amount of MinC in assembly reactions but kept the amount of MinD constant. We then performed ultracentrifugation and analyzed pellet fractions. Increasing MinC in the reaction also increased the amount of MinD and MinC in the pellet (Fig. 2 A). The ratio of MinD to MinC appeared consistent throughout the titration. Omitting ATP from the reaction did not lead to a significant amount of either MinC or MinD in the pellet.

To further investigate the requirement for ATP in MinCD complex formation, we compared several ATP analogs in ultracentrifugation assays. We performed densitometry on the band corresponding to MinD, since MinD contains the nucleotide-binding site; MinC was present in all fractions that contained MinD. We observed that ATP and the ATP analog ATP-γ-S supported the formation of large complexes containing MinD and MinC, but both the ATP analog AMPPNP and ADP did not (Fig. 2B). MinD-containing complexes were also observed when EDTA was included in the reaction with ATP, indicating that Mg2+-dependent ATP hydrolysis is not important for assembly. Surprisingly, GTP also supported the formation of complexes containing MinD and MinC. MinD binds to mant-GTP; however the interaction is 6-fold weaker than observed with mant-ATP (Fig. S1C). Our results suggest that nucleotide binding by MinD, but not hydrolysis, induces the assembly of large complexes in the presence of MinC.

Next, we identified optimal conditions that promote assembly of large MinCD complexes by comparing different pH and salt concentrations in ultracentrifugation

assays with ATP. We performed densitometry on the band corresponding to MinD to compare relative abundance of MinCD complexes. We varied KCl concentration and observed that as the concentration of salt in the reaction increases, the amount of MinD-containing complexes in the pellet fraction decreases (Fig. 2C). Next, we varied the buffer composition in reactions to identify the optimal pH for assembly. We observed that reactions carried out in MES buffer at pH 6.0 or pH 6.5 support the formation of large MinCD complexes (Fig. 2D). At higher pH using Tris–HCl or HEPES buffer, we observed less MinD (and MinC) in the pellet fractions. Upon testing multiple combinations of ionic strength and pH closer to physiological conditions [38], we continued to observe MinCD complexes at pH 7.3 with 300 mM KCl (Fig. S1D).

To test if the MinD-containing complexes are polymers, as with other Par-like ATPases [11, 32], we performed negative staining and electron microscopy on mixtures of MinD, MinC and ATP. We observed single-stranded polymers of variable length, ~50–800 nm, and approximately 10 nm in width in reactions containing MinC, MinD and ATP (Fig. 3 A). In control experiments, mixtures of MinC and MinD without nucleotide showed background staining with no large structures (Fig. 3B). When either MinC or MinD was incubated with ATP and then visualized, we also observed background staining without discernable structures (Fig. 3C and D). These results show that incubation of MinC and MinD with ATP leads to polymer formation.

MinE promotes disassembly of MinCD polymers

The binding sites for MinC and MinE overlap on MinD, suggesting that the association of MinD with MinC and MinE is mutually exclusive [12, 22]. Therefore, we

tested if MinE dissociates MinCD polymers in a light scattering assay. After assembly of MinCD polymers with ATP, MinE was added and an immediate decrease in light scatter was observed (Fig. 4 A). The decrease continued with time and MinCD polymers dissociated within 10 min. When buffer was added to MinCD polymers instead of MinE, no decrease in the light scatter of MinCD was detected (Fig. 4B).

To confirm that MinCD polymers do not dissociate as a result of ATP hydrolysis stimulated by MinE, we performed ATP hydrolysis assays with MinD in the presence of MinC and MinE. As previously published, we observed that MinE does not stimulate ATP hydrolysis by MinD without the addition of phospholipids [15, 16] (Fig. S2A). Our results suggest that MinE may compete with MinC for binding to MinD. We also detected weak GTP hydrolysis by MinD, however GTP hydrolysis was not stimulated by MinE and phospholipids (Fig. S2B).

To confirm that MinCD polymers observed under our conditions do not dissociate as a result of ATP hydrolysis stimulated by MinE, we performed ATP hydrolysis assays with MinD in the presence of MinC and MinE with and without phospholipids. As previously published, we also observed that MinE does not stimulate ATP hydrolysis in the absence of phospholipids (Fig S2). This result suggests that MinE most likely competes with MinC for binding to MinD and leads to dissociation of polymers.

Assembly of MinCD polymers is cooperative

To determine if polymers assemble cooperatively, we titrated the amount of MinD in polymerization reactions containing a fixed MinC concentration (2 or 10 μM). Then we collected MinCD polymers by ultracentrifugation and analyzed the amount of MinD

in the pellet fractions. The amount of pellet-associated MinD increased as the concentration of MinD in the reaction increased (Fig. 5). The binding curves at both MinC concentrations were used to calculate Hill coefficients of 1.94 ± 0.18 and 1.36 ± 0.17 for curves generated with 10 μM and 2 μM MinC, respectively. Fewer polymers and less cooperativity was observed at the lower MinC concentration likely because MinC is limiting for assembly at high MinD concentration.

Mutations in MinD prevent polymerization with MinC

MinD(K11A) contains a substitution mutation in the deviant Walker A motif of MinD. Lys 11, which is present at the MinD dimerization interface, is important for ATP hydrolysis and essential for dimerization (Fig. 6 A) [21, 22]. However, MinD(K11A) binds nucleotide with similar affinity as wild type MinD [34]. The cooperativity observed with wild type MinD suggests that oligomerization is likely important for polymerization with MinC. Therefore, we tested if MinD(K11A) is defective for polymerization with MinC in ultracentrifugation assays. We did not detect MinD(K11A) in the pellet fractions collected from reactions containing MinC and ATP (Fig. 6B). To confirm that MinD(K11A) is defective for dimerization in the presence of ATP, we performed size exclusion chromatography. MinD(K11A) eluted as a monomer in the presence of ATP, whereas wild type MinD eluted as a dimer, which is in agreement with published results [21, 22] (Fig. S3A). These results suggest that dimerization by MinD is important for polymer formation with MinC.

Phospholipids are not essential for MinCD polymerization: therefore, we hypothesized that the MTS at the C-terminus of MinD would be dispensable for

polymerization with MinC. We constructed a truncated MinD mutant protein deleted for the MTS, MinD(ΔMTS15), and tested it for polymerization with MinC. Interestingly, MinD(ΔMTS15) is unable to form polymers with MinC in ultracentrifugation assays (Fig. 6B). However, MinD(ΔMTS15) is capable of binding nucleotide in experiments with mant-ATP and forms dimers (Figs. S3B and C). These results suggest that the MTS of MinD may be important for mediating the polymer-stabilizing interaction with MinC.

DISCUSSION

Here we describe the nucleotide-dependent polymerization of cell division regulators MinD and MinC in vitro without the addition of phospholipids. Electron microscopy images of MinCD complexes show long single-stranded polymers (Fig. 3A). The MinCD polymers observed in our study are disrupted by MinE, which is consistent with a mechanism where MinC and MinE bind to overlapping regions of MinD near the nucleotide binding site, as suggested in other studies [12, 22, 33].

The mutant protein MinD(K11A) is unable to dimerize or polymerize with MinC, yet is reported to bind ATP (Fig. 6B) [34]. Deletion of the MTS from MinD prevents polymerization with MinC (Fig. 6B). A MinD mutant protein containing a larger C-terminal deletion (MinDΔ19) was shown to maintain thermodynamic properties similar to MinD, suggesting that deletion of the C-terminus does not perturb protein folding [25]. Our results suggest that the MTS of MinD, which is critical for the interaction with phospholipids, may also play a larger role in modulating the interaction with MinC to facilitate polymerization.

Polymerization of MinD with MinC is stimulated by both ATP and GTP (Fig. 2B), however weak GTP hydrolysis activity by MinD is not stimulated by MinE and phospholipids, in contrast to ATP hydrolysis activity (Fig. S2B). MinD was previously reported to bind phospholipid vesicles in the presence of GTP as well as ATP, indicating that MinD associates with either nucleotide [17]. Actin-like ATPases, including ParM, have been shown to polymerize with GTP as well as ATP [39]; however, members of the MinD–ParA family, have not been typically associated with this activity.

The precise molecular arrangement of MinC and MinD in the polymers under our conditions is unknown, however the stoichiometric ratio of MinD to MinC is 1.6:1 (Fig. S1A). Among MinD homologs, filaments have also been described for ParF and Soj, however Soj filaments assemble with DNA [32, 36, 37]. A structural model of the ParF filament has been described recently in a conformation stabilized by AMPPCP, which contains tetrameric units stacked in an antiparallel orientation [32]. An analogous arrangement for MinD would have to accommodate the presence of bound MinC. It is also possible that MinC and MinD may be arranged as alternating MinC and MinD dimers linked together in a 1:1 ratio. If MinCD polymerizes into static filaments in vivo as well as in vitro, then filamentation could sequester cell division regulators or modify the Min oscillation cycle during cell division.

ACKNOWLEDGEMENTS

We thank Linda Kessner and Ryann Murphy for laboratory assistance and Carol Ayala at Rhode Island Hospital for expert technical assistance with the electron microscope. This research was supported by the Rhode Island Foundation.

References

1. Bernhardt, T. G. & de Boer, P. A. (2005). SlmA, a nucleoid-associated, FtsZ binding protein required for blocking septal ring assembly over Chromosomes in E. coli. *Mol Cell* **18**, 555-64.

2. Cho, H., McManus, H. R., Dove, S. L. & Bernhardt, T. G. (2011). Nucleoid occlusion factor SlmA is a DNA-activated FtsZ polymerization antagonist. *Proc Natl Acad Sci U S A* **108**, 3773-8.

3. Tonthat, N. K., Arold, S. T., Pickering, B. F., Van Dyke, M. W., Liang, S., Lu, Y., Beuria, T. K., Margolin, W. & Schumacher, M. A. (2011). Molecular mechanism by which the nucleoid occlusion factor, SlmA, keeps cytokinesis in check. *Embo J* **30**, 154-64.

4. Lutkenhaus, J. (2007). Assembly dynamics of the bacterial MinCDE system and spatial regulation of the Z ring. *Annu Rev Biochem* **76**, 539-62.

5. Dajkovic, A., Lan, G., Sun, S. X., Wirtz, D. & Lutkenhaus, J. (2008). MinC spatially controls bacterial cytokinesis by antagonizing the scaffolding function of FtsZ. *Curr. Biol.* **18**, 235-44.

6. Shen, B. & Lutkenhaus, J. (2009). The conserved C-terminal tail of FtsZ is required for the septal localization and division inhibitory activity of MinC(C)/MinD. *Mol Microbiol* **72**, 410-24.

7. Shen, B. & Lutkenhaus, J. (2010). Examination of the interaction between FtsZ and MinCN in E. coli suggests how MinC disrupts Z rings. *Mol Microbiol* **75**, 1285-98.

8. Raskin, D. M. & de Boer, P. A. (1999). MinDE-dependent pole-to-pole oscillation of division inhibitor MinC in Escherichia coli. *J Bacteriol* **181**, 6419-24.

9. Lutkenhaus, J. (2012). The ParA/MinD family puts things in their place. *Trends Microbiol* **20**, 411-8.

10. Michie, K. A. & Lowe, J. (2006). Dynamic filaments of the bacterial cytoskeleton. *Annu Rev Biochem* **75**, 467-92.

11. Szardenings, F., Guymer, D. & Gerdes, K. (2011). ParA ATPases can move and position DNA and subcellular structures. *Curr Opin Microbiol* **14**, 712-8.

12. Wu, W., Park, K. T., Holyoak, T. & Lutkenhaus, J. (2011). Determination of the structure of the MinD-ATP complex reveals the orientation of MinD on the membrane and the relative location of the binding sites for MinE and MinC. *Mol Microbiol* **79**, 1515-28.

13. Zhou, H. & Lutkenhaus, J. (2003). Membrane binding by MinD involves insertion of hydrophobic residues within the C-terminal amphipathic helix into the bilayer. *J Bacteriol* **185**, 4326-35.

14. Hu, Z., Gogol, E. P. & Lutkenhaus, J. (2002). Dynamic assembly of MinD on phospholipid vesicles regulated by ATP and MinE. *Proc Natl Acad Sci U S A* **99**, 6761-6.

15. Hu, Z. & Lutkenhaus, J. (2001). Topological regulation of cell division in E. coli. spatiotemporal oscillation of MinD requires stimulation of its ATPase by MinE and phospholipid. *Mol Cell* **7**, 1337-43.

16. Lackner, L. L., Raskin, D. M. & de Boer, P. A. (2003). ATP-dependent interactions between Escherichia coli Min proteins and the phospholipid membrane in vitro. *J Bacteriol* **185**, 735-49.

17. Suefuji, K., Valluzzi, R. & RayChaudhuri, D. (2002). Dynamic assembly of MinD into filament bundles modulated by ATP, phospholipids, and MinE. *Proc Natl Acad Sci U S A* **99**, 16776-81.

18. Hu, Z., Saez, C. & Lutkenhaus, J. (2003). Recruitment of MinC, an inhibitor of Z-ring formation, to the membrane in Escherichia coli: role of MinD and MinE. *J Bacteriol* **185**, 196-203.

19. Park, K. T., Wu, W., Battaile, K. P., Lovell, S., Holyoak, T. & Lutkenhaus, J. (2011). The Min oscillator uses MinD-dependent conformational changes in MinE to spatially regulate cytokinesis. *Cell* **146**, 396-407.

20. Cordell, S. C., Anderson, R. E. & Lowe, J. (2001). Crystal structure of the bacterial cell division inhibitor MinC. *EMBO J* **20**, 2454-61.

21. Hayashi, I., Oyama, T. & Morikawa, K. (2001). Structural and functional studies of MinD ATPase: implications for the molecular recognition of the bacterial cell division apparatus. *EMBO J* **20**, 1819-28.

22. Zhou, H., Schulze, R., Cox, S., Saez, C., Hu, Z. & Lutkenhaus, J. (2005). Analysis of MinD mutations reveals residues required for MinE stimulation of the MinD ATPase and residues required for MinC interaction. *J Bacteriol* **187**, 629-38.

23. Park, K. T., Wu, W., Lovell, S. & Lutkenhaus, J. (2012). Mechanism of the asymmetric activation of the MinD ATPase by MinE. *Mol Microbiol* **85**, 271-81.

24. Hsieh, C. W., Lin, T. Y., Lai, H. M., Lin, C. C., Hsieh, T. S. & Shih, Y. L. (2010). Direct MinE-membrane interaction contributes to the proper localization of MinDE in E. coli. *Mol Microbiol* **75**, 499-512.

25. Szeto, T. H., Rowland, S. L., Rothfield, L. I. & King, G. F. (2002). Membrane localization of MinD is mediated by a C-terminal motif that is conserved across eubacteria, archaea, and chloroplasts. *Proc Natl Acad Sci U S A* **99**, 15693-8.

26. Hu, Z. & Lutkenhaus, J. (2003). A conserved sequence at the C-terminus of MinD is required for binding to the membrane and targeting MinC to the septum. *Mol Microbiol* **47**, 345-55.

27. Szeto, T. H., Rowland, S. L., Habrukowich, C. L. & King, G. F. (2003). The MinD membrane targeting sequence is a transplantable lipid-binding helix. *J Biol Chem* **278**, 40050-6.

28. Loose, M., Fischer-Friedrich, E., Ries, J., Kruse, K. & Schwille, P. (2008). Spatial regulators for bacterial cell division self-organize into surface waves in vitro. *Science* **320**, 789-92.

29. Ivanov, V. & Mizuuchi, K. Multiple modes of interconverting dynamic pattern formation by bacterial cell division proteins. *Proc Natl Acad Sci U S A* **107**, 8071-8.

30. Ramirez-Arcos, S., Greco, V., Douglas, H., Tessier, D., Fan, D., Szeto, J., Wang, J. & Dillon, J. R. (2004). Conserved glycines in the C terminus of MinC proteins are implicated in their functionality as cell division inhibitors. *J Bacteriol* **186**, 2841-55.

31. Ebersbach, G., Ringgaard, S., Moller-Jensen, J., Wang, Q., Sherratt, D. J. & Gerdes, K. (2006). Regular cellular distribution of plasmids by oscillating and filament-forming ParA ATPase of plasmid pB171. *Mol Microbiol* **61**, 1428-42.

32. Schumacher, M. A., Ye, Q., Barge, M. T., Zampini, M., Barilla, D. & Hayes, F. (2012). Structural mechanism of ATP-induced polymerization of the

partition factor ParF: implications for DNA segregation. *J Biol Chem* **287**, 26146-54.

33. Ma, L., King, G. F. & Rothfield, L. (2004). Positioning of the MinE binding site on the MinD surface suggests a plausible mechanism for activation of the Escherichia coli MinD ATPase during division site selection. *Mol Microbiol* **54**, 99-108.

34. Okuno, T., Ohgita, T., Sasa, T., Nonaka, A., Funasaki, N. & Kogure, K. (2010). Fluorescence polarization analysis for revealing molecular mechanism of nucleotide-dependent phospholipid membrane binding of MinD adenosine 5'-triphosphate, adenosine triphosphatase. *Biol Pharm Bull* **33**, 1746-50.

35. Hu, Z., Mukherjee, A., Pichoff, S. & Lutkenhaus, J. (1999). The MinC component of the division site selection system in Escherichia coli interacts with FtsZ to prevent polymerization. *Proc. Natl. Acad. Sci. USA* **96**, 14819-24.

36. Leonard, T. A., Butler, P. J. & Lowe, J. (2005). Bacterial chromosome segregation: structure and DNA binding of the Soj dimer--a conserved biological switch. *EMBO J* **24**, 270-82.

37. Barilla, D., Rosenberg, M. F., Nobbmann, U. & Hayes, F. (2005). Bacterial DNA segregation dynamics mediated by the polymerizing protein ParF. *EMBO J* **24**, 1453-64.

38. Camberg, J. L., Hoskins, J. R. & Wickner, S. (2009). ClpXP protease degrades the cytoskeletal protein, FtsZ, and modulates FtsZ polymer dynamics. *Proc Natl Acad Sci U S A* **106**, 10614-9.

39. Camberg, J. L., Viola, M. G., Rea, L., Hoskins, J. R. & Wickner, S. (2014). Location of dual sites in E. coli FtsZ important for degradation by ClpXP; one at the C-terminus and one in the disordered linker. *PLoS One* **9**, e94964.

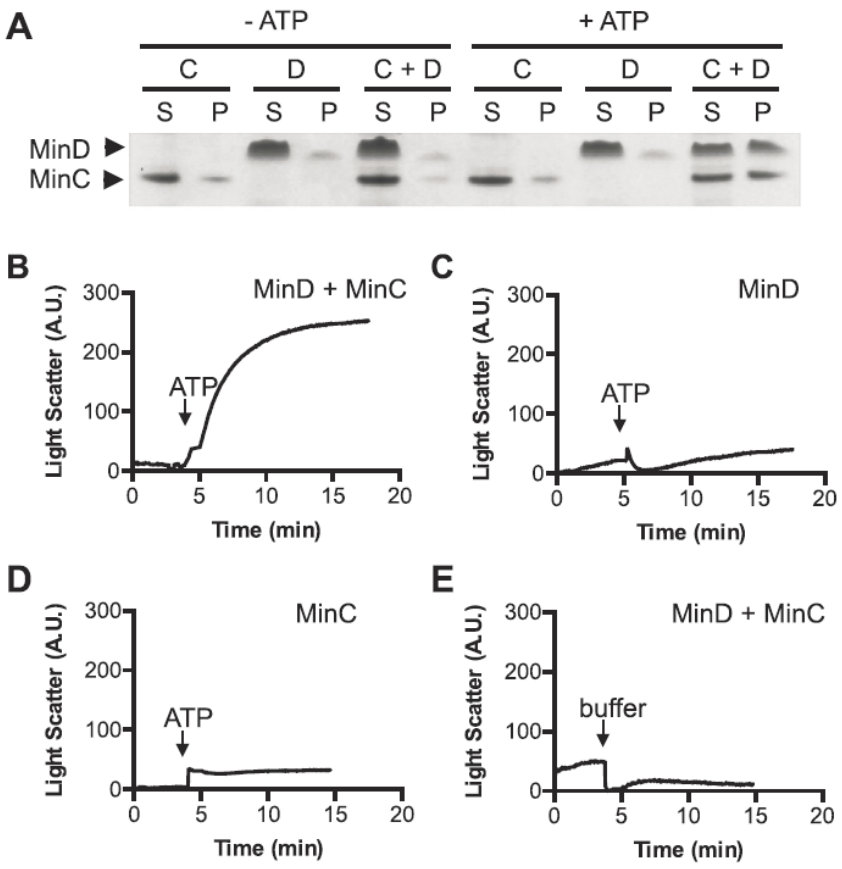
A
- ATP
+ ATP
C
D
C + D
C
D
C + D
S P S P S P S P S P S P
MinD
MinC
B
MinD + MinC
Light Scatter (A.U.)
ATP
Time (min)
C
MinD
Light Scatter (A.U.)
ATP
Time (min)
D
MinC
Light Scatter (A.U.)
ATP
Time (min)
E
MinD + MinC
Light Scatter (A.U.)
buffer
Time (min)

FIGURE 1. Formation of large complexes containing MinD and MinC. (a) Reactions containing combinations of MinC (6 μM), MinD (12 μM), and ATP (4 mM), where indicated, were incubated at room temperature for 5 minutes and then fractionated by ultracentrifugation. Supernatants and pellets were analyzed by SDS-PAGE and staining. The amount of protein in the last lane was quantitated by comparison to a standard curves containing MinC and MinD and calculated to contain 45 pmol of MinD and 22 pmol of MinC. (b) ATP-dependent assembly of complexes containing MinC (6 μM) and MinD (12 μM) was monitored by 90° light scattering as described in Materials and Methods. A baseline was collected for 4.5 min, and then ATP was added when indicated to stimulate assembly. Light scattering was measured for 20 min. (c) Light scattering assay showing MinD (10 μM) alone, with the addition of ATP when indicated, performed as described in (b). (d) Light scattering assay showing MinC (6 μM) alone, with the addition of ATP when indicated, performed as described in (B). (e) Light scattering assay showing reactions containing MinC (6 μM) and MinD (12 μM), with the addition of assembly buffer when indicated, performed as described in (b). Data shown in (b – e) is representative of 3 replicates.

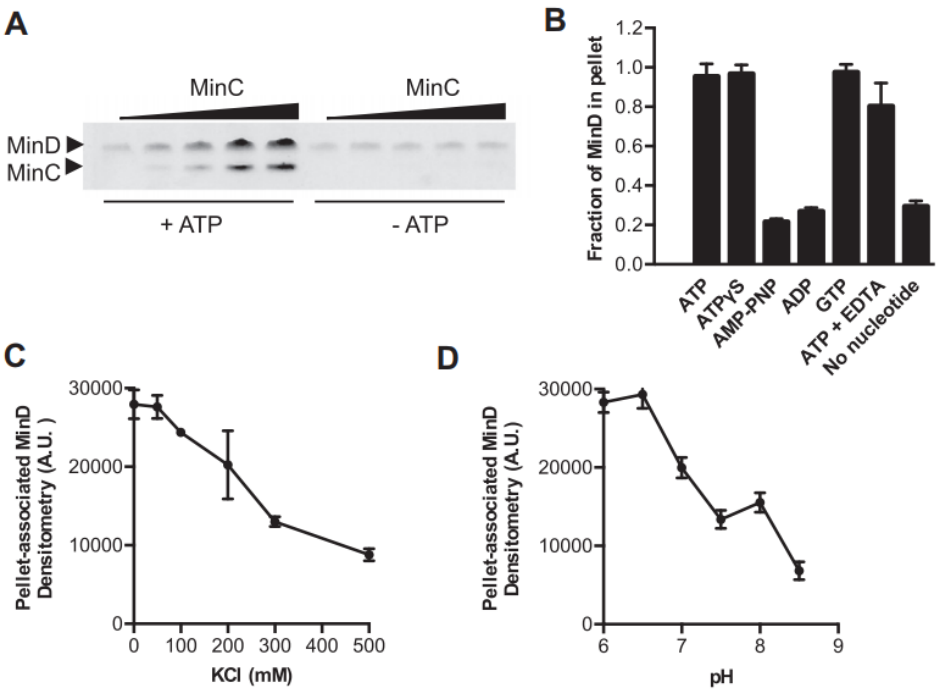
A
MinC
MinC
MinD
MinC
+ ATP
- ATP
B
Fraction of MinD in pellet
1.2
1.0
0.8
0.6
0.4
0.2
0.0
ATP
ATPγS
AMP-PNP
ADP
GTP
ATP + EDTA
No nucleotide
C
Pellet-associated MinD Densitometry (A.U.)
30000
20000
10000
0
0 100 200 300 400 500
KCl (mM)
D
Pellet-associated MinD Densitometry (A.U.)
30000
20000
10000
0
6 7 8 9
pH

FIGURE 2. Conditions that promote the formation of large MinCD complexes. (a) MinD (12 μM) was incubated in assembly buffer with and without ATP, where indicated, and increasing concentrations of MinC (0 – 6 μM). Ultracentrifugation assays to collect MinCD polymers were performed as described in Materials and Methods. Pellet fractions were analyzed by SDS-PAGE and staining. (b) Ultracentrifugation assays were performed on reactions containing MinC (5 μM) and MinD (10 μM) under various nucleotide conditions, where indicated, as described in Materials and Methods. Pellet fractions were analyzed by SDS-PAGE, staining and densitometry of the band on the gel correlating with MinD. (c, d) MinD (10 μM) was assayed for polymer formation with MinC (5 μM) in the presence of ATP and increasing concentrations of KCl (0 – 500 mM) (c) or at various pH (6.0 – 8.5) (d) in ultracentrifugation assays as described in Materials and Methods. Pellet fractions were analyzed by SDS-PAGE, staining and densitometry of the band on the gel correlating with MinD. In (b-d), data from at least three replicates are represented as mean ± SD.

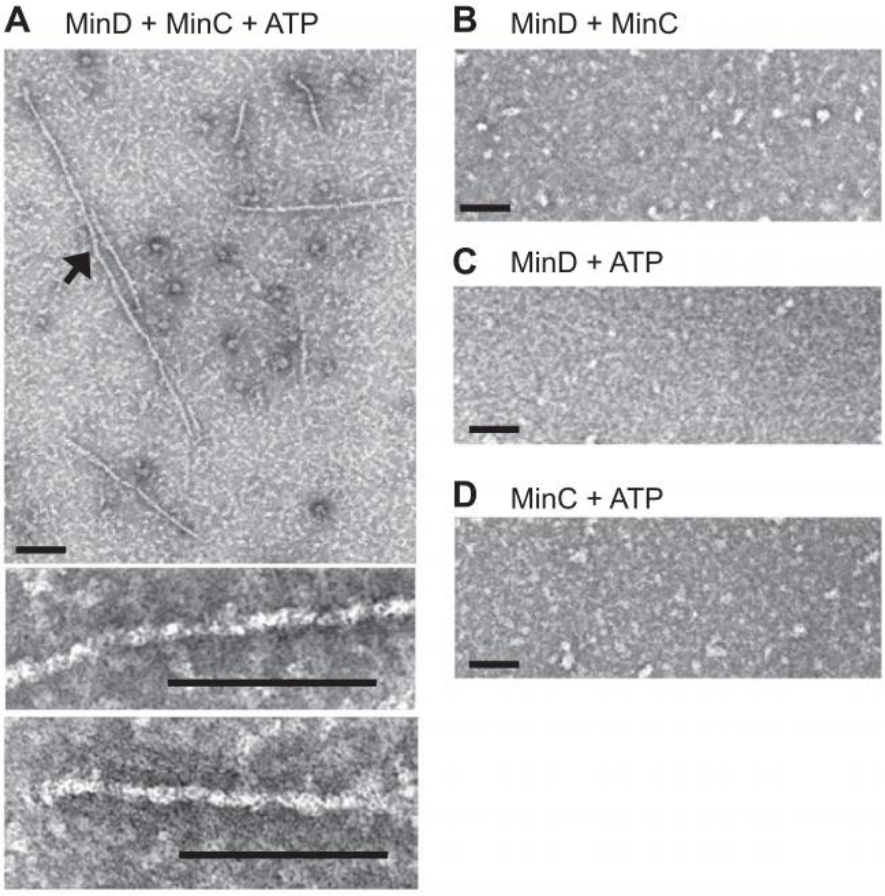
A MinD + MinC + ATP
B MinD + MinC
C MinD + ATP
D MinC + ATP

FIGURE 3. Visualization of MinCD polymers by negative staining and electron microscopy. (A) MinC and MinD were incubated with ATP and visualized by negative staining and electron microscopy as described in Materials and Methods. Single stranded fibers with variable lengths were observed (arrowhead). No fibers were observed in reactions containing MinC and MinD without ATP (b), MinD with ATP (c) or MinC with ATP (d). Size bars in (a-d) are 100 nm.

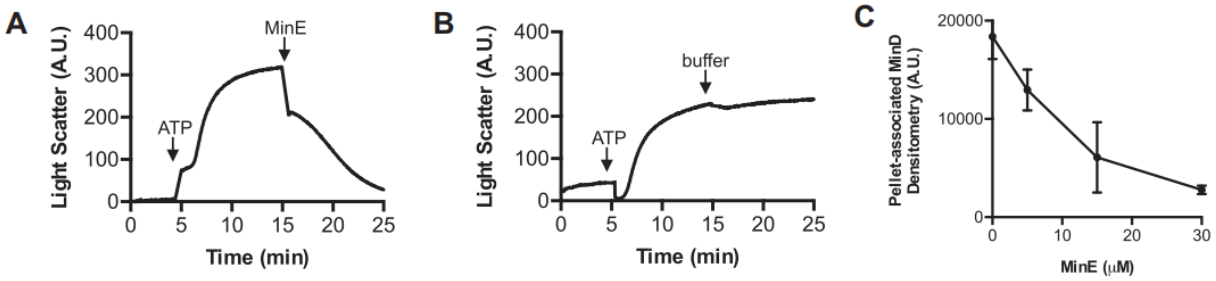
A
Light Scatter (A.U.)
400
300
200
100
0
ATP
MinE
0
5
10
15
20
25
Time (min)
B
Light Scatter (A.U.)
400
300
200
100
0
ATP
buffer
0
5
10
15
20
25
Time (min)
C
Pellet-associated MinD Densitometry (A.U.)
20000
10000
0
0
10
20
30
MinE (μM)

FIGURE 4. MinE disassembles ATP-dependent MinCD polymers. ATP-dependent assembly of complexes containing MinC (5 μM) and MinD (10 μM) was monitored by 90° light scattering as described in *Materials and Methods*. A baseline was collected for 4.5 min, and then ATP was added when indicated to stimulate assembly. Light scattering was measured for 10 min, then MinE (20 μM) (a) or buffer (b) was added to the reaction and light scattering was monitored for an additional 10 min. (c) MinD (10 μM) was assayed for polymer formation with MinC (5 μM) in the presence of ATP and increasing concentrations of MinE (0-30 μM) in ultracentrifugation assays as described in Materials and Methods. Pellet fractions were analyzed by SDS-PAGE, staining and densitometry of the band on the gel correlating with MinD. Data from three replicates are represented as mean ± SD.

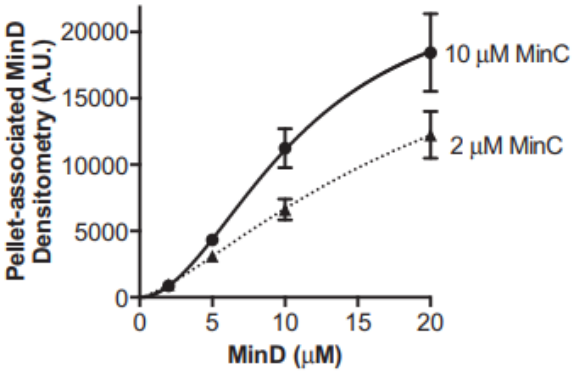
Pellet-associated MinD
Densitometry (A.U.)
20000
15000
10000
5000
0
0
5
10
15
20
MinD (μM)
10 μM MinC
2 μM MinC

FIGURE 5. Cooperative assembly of MinCD polymers and interaction with fluorescent ATP Cooperative assembly of MinCD polymer. MinC (2 or 10 μM) was incubated in assembly buffer with ATP and increasing concentrations of MinD (0-20 μM). Ultracentrifugation assays to collect MinCD polymers were performed as described in Section 2. Pellet fractions were analyzed by SDS-PAGE, staining and densitometry of the band of the gel corresponding to MinD. Data from three Replicates are represented as mean ± S.E.M.

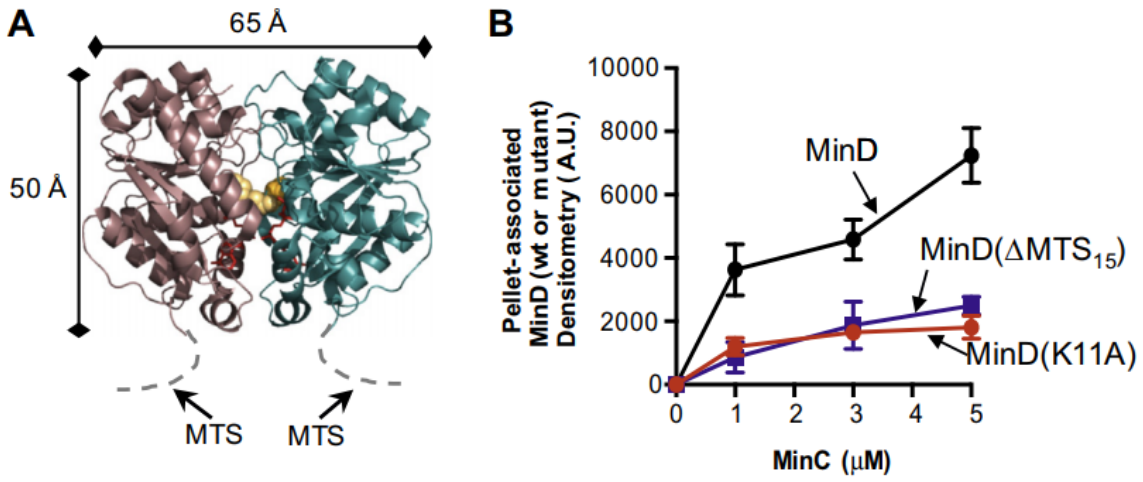
A
65 Å
50 Å
MTS
MTS
B
Pellet-associated MinD (wt or mutant) Densitometry (A.U.)
10000
8000
6000
4000
2000
0
MinD
MinD(ΔMTS15)
MinD(K11A)
0
1
2
3
4
5
MinC (μM)

FIGURE 6. Mutations in MinD impair polymerization with MinC. (a) Structural model of the *E. coli* MinD dimer in association with two molecules of ATP (red) (pdb 3R9I; [12]). One protomer is shown in rose, the adjacent protomer is shown in teal. Lys 11 in each protomer is shown as a Corey-Pauling-Koltun representation at the dimerization interface (yellow). (b) MinD (black), MinD(K11A) (red) and MinD(ΔMTS_{15}) (blue) (10 μM) were assayed for polymer formation with MinC (0 – 6 μM) in the presence of ATP in ultracentrifugation assays as described in Materials and Methods. Pellet fractions were analyzed by SDS-PAGE, staining and densitometry of the band on the gel correlating with MinD wild type or mutant protein. Data from three replicates are represented as mean ± SEM.

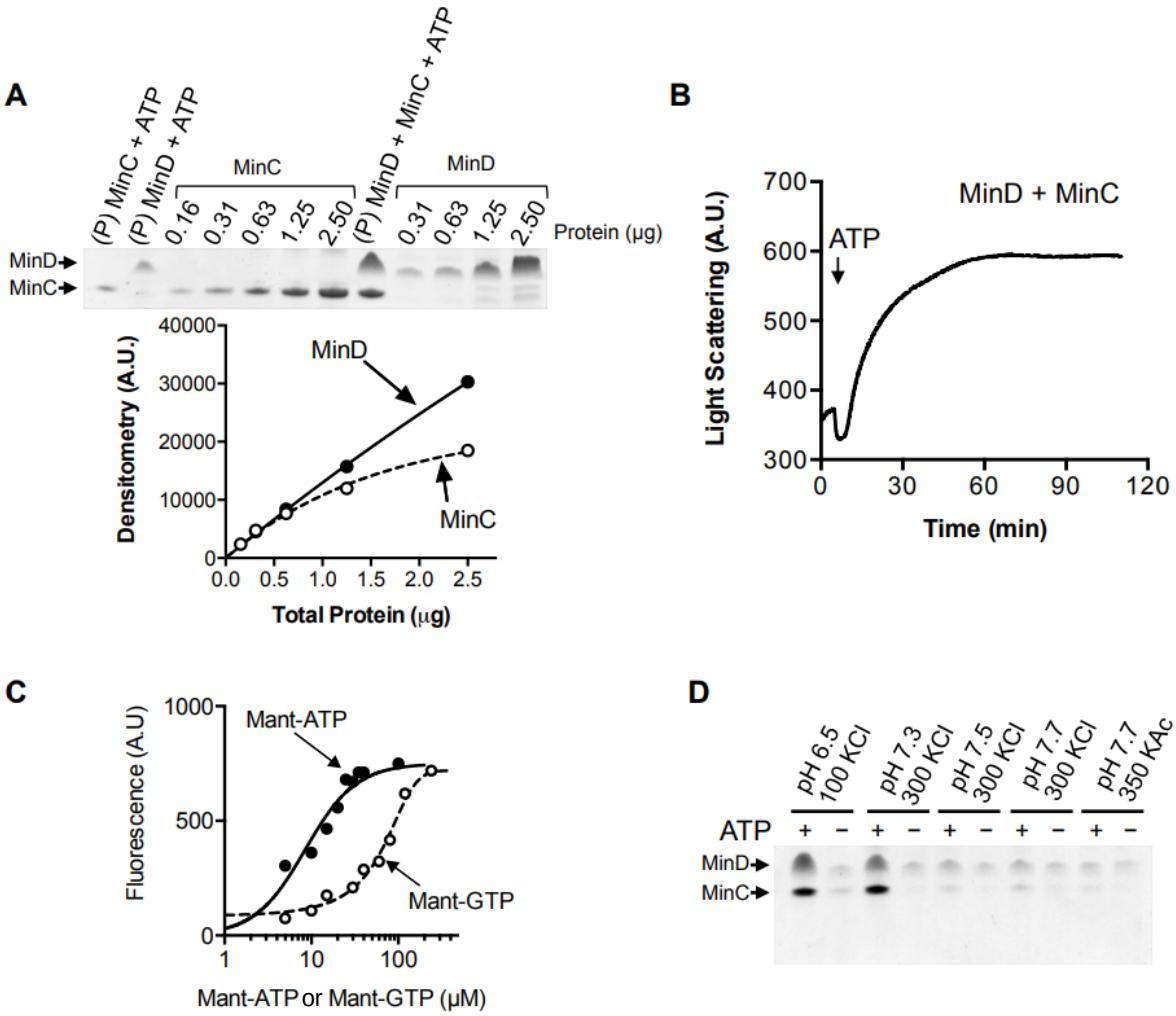
A
(P) MinC + ATP
(P) MinD + ATP
MinC
0.16
0.31
0.63
1.25
2.50
(P) MinD + MinC + ATP
MinD
0.31
0.63
1.25
2.50
Protein (µg)
MinD
MinC
Densitometry (A.U.)
40000
30000
20000
10000
0
MinD
MinC
0.0 0.5 1.0 1.5 2.0 2.5
Total Protein (µg)
B
MinD + MinC
ATP
Light Scattering (A.U.)
700
600
500
400
300
0 30 60 90 120
Time (min)
C
Fluorescence (A.U)
1000
500
0
Mant-ATP
Mant-GTP
1 10 100
Mant-ATP or Mant-GTP (µM)
D
pH 6.5 100 KCl
pH 7.3 300 KCl
pH 7.5 300 KCl
pH 7.7 300 KCl
pH 7.7 350 KAc
ATP + − + − + − + − + −
MinD
MinC

Fig. S1. Large complex assembly of MinD and MinC.

A. Relative stoichiometry of MinC and MinD in pellet fractions was determined by comparing the densitometry of the bands from assembly reactions containing 12 μM MinD, 6 μM MinC and ATP, where indicated, to known standards. To generate protein standard curves, MinD (0.31 – 2.5 μg) and MinC (0.15 – 2.5 μg) were run in adjacent lanes, quantified by densitometry and the results were fit by nonlinear regression. The relative amounts of each protein in the pellet collected from the reactions containing MinC, MinD and ATP were calculated to be 1.3 μg MinD and 0.7 μg MinC, which is equivalent to 22 pmol and 14 pmol, respectively, after background correction by subtracting non-specific pellet-associated bands from control reactions (0.4 μg MinD and 0.3 μg MinC). B. ATP-dependent assembly of complexes containing MinC (5 μM) and MinD (10 μM) was monitored by 90° light scattering as described in Materials and Methods. A baseline was collected for 4.5 min, and then ATP was added when indicated to stimulate assembly. Light scattering was measured for 100 min. C. MinD (5 μM) was incubated with increasing concentrations of mant-ATP (0 – 100 μM) (solid circles) and mant-GTP (0 – 240 μM) (open circles), where indicated. Fluorescence was monitored as described in Supplemental Materials and Methods. Kd values were calculated to be 8.5 ± 1.0 μM (mant-ATP) and 50.6 ± 8.2 μM (mant-GTP) for the interaction with MinD. D. Reactions contained MinC (6 μM) and MinD (12 μM) in the presence or absence of ATP (4 mM). Reactions were incubated at room temperature for 5 minutes and then fractionated by ultracentrifugation. Pellet fractions were analyzed by SDS-PAGE and staining.

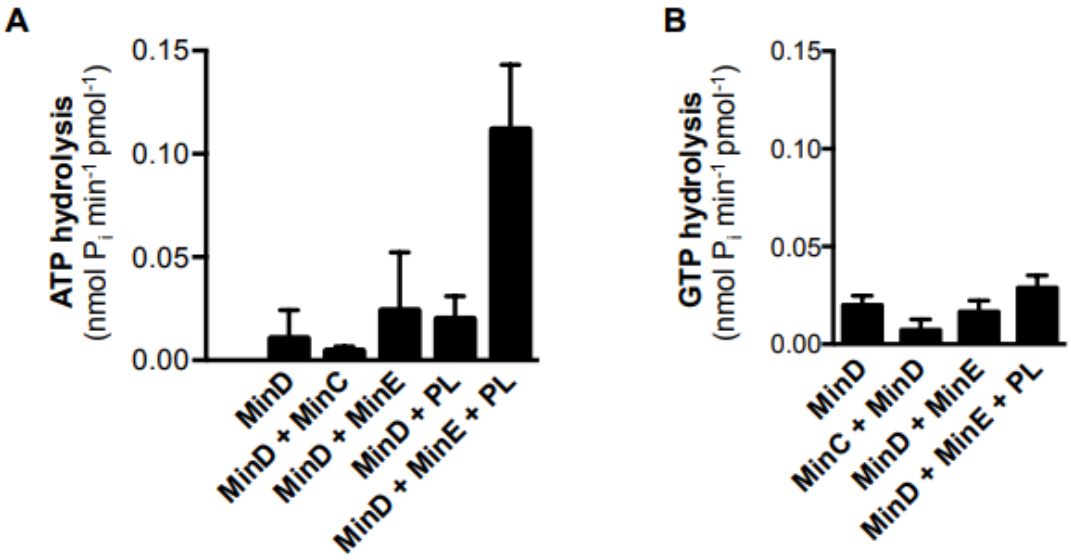
A
ATP hydrolysis
(nmol P_i min^{-1} $pmol^{-1}$)
0.15
0.10
0.05
0.00
MinD
MinD + MinC
MinD + MinE
MinD + PL
MinD + MinE + PL
B
GTP hydrolysis
(nmol P_i min^{-1} $pmol^{-1}$)
0.15
0.10
0.05
0.00
MinD
MinC + MinD
MinD + MinE
MinD + MinE + PL

Fig. S2. Nucleotide hydrolysis.

A. ATP hydrolysis was measured by monitoring the amount of phosphate released after 20 min in reactions (25 µl) containing assembly buffer with ATP (4 mM) and MinD (5 µM), MinE (10 µM), MinC (2.5 µM), or *E. coli* phospholipids (1 mg/ml), where indicated, as described in Supplemental Material and Methods. B. GTP hydrolysis was measured by monitoring the amount of phosphate released after 20 min in reactions (25 µl) containing assembly buffer with GTP (2 mM) and MinD (5 µM), MinE (10 µM), MinC (2.5 µM), or *E. coli* phospholipids (1 mg/ml), where indicated.

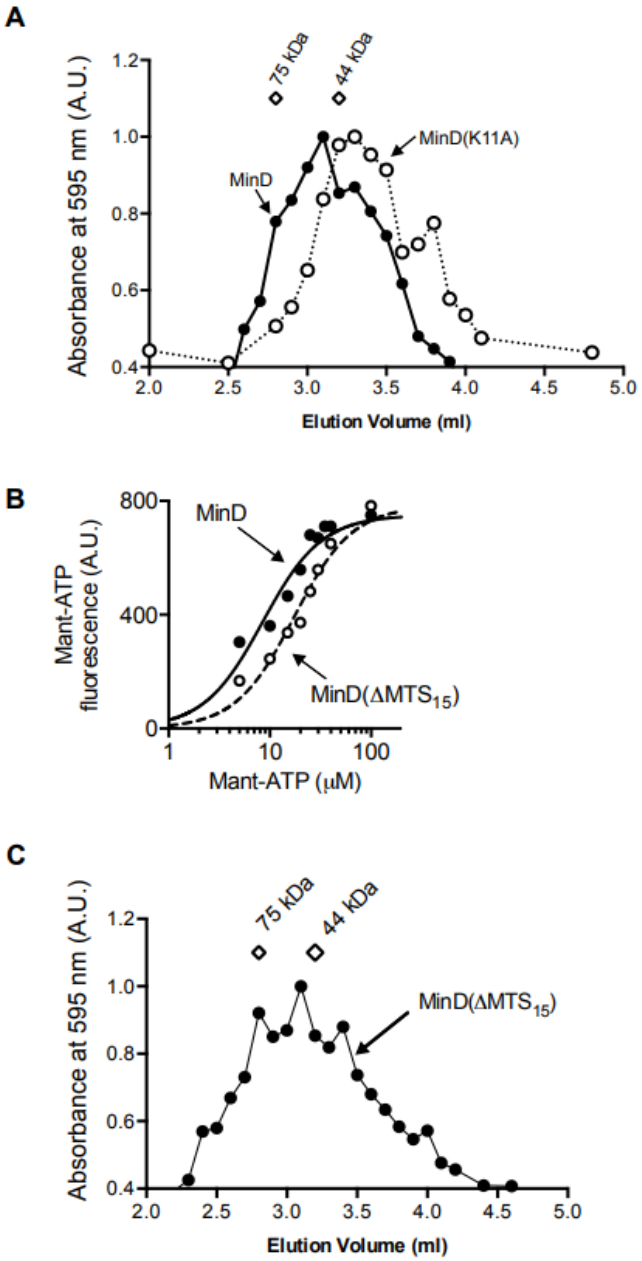
A
75 kDa
44 kDa
MinD(K11A)
MinD
Absorbance at 595 nm (A.U.)
1.2
1.0
0.8
0.6
0.4
2.0
2.5
3.0
3.5
4.0
4.5
5.0
Elution Volume (ml)
B
MinD
800
400
0
Mant-ATP fluorescence (A.U.)
MinD(ΔMTS15)
1
10
100
Mant-ATP (μM)
C
75 kDa
44 kDa
MinD(ΔMTS15)
Absorbance at 595 nm (A.U.)
1.2
1.0
0.8
0.6
0.4
2.0
2.5
3.0
3.5
4.0
4.5
5.0
Elution Volume (ml)

Fig. S3. Size exclusion chromatography of MinD and MinD mutant proteins.

A. Size exclusion chromatography was performed as described in Supplemental Material and Methods. MinD and MinD(K11A) (80 µg) were incubated with ATP (4 mM) for 5 minutes and then fractionated on an S100 column equilibrated with buffer containing ATP (1 mM) . Fractions were analyzed for total protein using a Bradford reagent. B. MinD (5 µM) (solid circles) and MinD(ΔMTS15) (5 µM) (open circles) were incubated with increasing concentrations of mant-ATP (0 – 100 µM) where indicated. Mant-ATP fluorescence was monitored as described in Supplemental Materials and Methods. C. MinD(ΔMTS15) (80 µg) was incubated with ATP (4 mM) for 5 minutes and then fractionated on an S100 column equilibrated with buffer containing ATP (1 mM).

Manuscript III

Publication status: published in *Molecular Microbiology*, 2018

Title: FtsA reshapes membrane architecture and remodels the Z-ring in *Escherichia coli*

Authors: Joseph Conti, Marissa G. Viola, Jodi L. Camberg*

Author Affiliations: Department of Cell and Molecular Biology, College of Environment and Life Sciences, University of Rhode Island, Kingston, RI, USA

***Corresponding author**: Jodi L. Camberg, 120 Flagg Road, Kingston, RI, 02881; Tel: (401)874-4961; Email: cambergj@mail.uri.edu

Abstract

Cell division in prokaryotes initiates with assembly of the Z-ring at midcell, which, in *Escherichia coli*, is tethered to the inner leaflet of the cytoplasmic membrane through a direct interaction with FtsA, a widely conserved actin homolog. The Z-ring is comprised of polymers of tubulin-like FtsZ and has been suggested to provide the force for constriction. Here, we demonstrate that FtsA exerts force on membranes causing redistribution of membrane architecture, robustly hydrolyzes ATP and directly engages FtsZ polymers in a reconstituted system. Phospholipid reorganization by FtsA occurs rapidly and is mediated by insertion of a C-terminal membrane targeting sequence (MTS) into the bilayer and further promoted by a nucleotide-dependent conformational change relayed to the MTS. FtsA also recruits FtsZ to phospholipid vesicles via a direct interaction with the FtsZ C-terminus and regulates FtsZ assembly kinetics. These results implicate the actin homolog FtsA in establishment of a Z-ring scaffold, while directly remodeling the membrane and provide mechanistic insight into localized cell wall remodeling, invagination and constriction at the onset of division

Introduction

Bacterial cell division is a highly regulated process, which, in *E. coli*, proceeds through a septal constriction event executed by a large dynamic protein complex, called the divisome. At the core of the divisome are two highly conserved proteins, FtsZ and FtsA (Haeusser and Margolin, 2016). FtsZ, a homolog of the eukaryotic cytoskeletal protein tubulin, assembles into a ring containing staggered FtsZ polymers,

called the Z-ring (Lutkenhaus et al., 2012). FtsA, which shares structural homology with the actin family of proteins, binds directly to the FtsZ C-terminal region and tethers the Z-ring to the inner face of the cytoplasmic membrane (van den Ent and Lowe, 2000; Szwedziak et al., 2012). Ordered recruitment of proteins to the divisome is essential for rapid division, yet how the divisome promotes septal constriction remains unclear. In *E. coli*, FtsA and FtsZ assemble first at the division site as a proto-ring and then sequentially recruit at least 10 additional cell division proteins (Hale and de Boer, 1997; Pogliano et al., 1997; Wang et al., 1997; Hale and de Boer, 1999; Pichoff and Lutkenhaus, 2002; Goehring and Beckwith, 2005; Aarsman et al., 2005; Alexeeva et al., 2010; Soderstrom et al., 2016). The inner membrane protein ZipA is also recruited early in division and has been reported to function as a static tether for the Z-ring (Pichoff and Lutkenhaus, 2002). In addition to FtsZ, FtsA interacts with FtsEX, an ATP-binding cassette transporter-like complex that may modulate the FtsA multimeric state, recruits FtsI, a murein transpeptidase involved in septal wall synthesis and binds FtsN, a bitopic membrane protein that activates peptidoglycan synthesis (Dai et al., 1996; Corbin et al., 2004, 2007; Bernard et al., 2007; Shiomi and Margolin, 2008; Busiek et al., 2012; Du et al., 2016). After recruitment of FtsN, late septal proteins arrive to insert additional peptidoglycan at the division site and the Z-ring is disassembled following constriction (Rico et al., 2010).

FtsA contains the canonical actin-fold and is a member of the actin/Hsc70/hexokinase superfamily (Bork et al., 1992; van den Ent and Lowe, 2000). The actin fold contains two discrete domains, which are each further divided into two

subdomains. FtsA has structural homology with actin and the bacterial actin homolog MreB in subdomains ‘1A’ and ‘2A’, and despite less homology, subdomain ‘2B’ is positioned in both proteins to coordinate nucleotide. A major structural difference is the presence of the ‘1C switch-domain’ of FtsA. In comparison to the prototypical ‘1B’ subdomain from the actin-like protein MreB, the ‘1C’ subdomain is positioned on the alternate side of domain ‘1A’ (Fig. 1A) (van den Ent and Lowe, 2000; Szwedziak et al., 2012). MreB is important for maintaining cell morphology in rod-shaped bacteria, binds to the membrane and, like FtsA, has been crystallized as an actin-like protofilament (Szwedziak et al., 2012; van den Ent et al., 2014; Errington, 2015). In higher eukaryotes, bundled actin fibers generate constrictive force in collaboration with other proteins (Llinas et al., 2015). In lower eukaryotes, actin forms the core of the cytokinetic contractile ring localizing to the plasma membrane where it may provide the constrictive force for septation (Pelham and Chang, 2002; Pollard and Wu, 2010). Despite FtsA and actin being essential for cell division in many organisms, a major distinction is that FtsA binds directly to phospholipids using a highly conserved C-terminal membrane targeting sequence (MTS) whereas actin requires accessory proteins to associate with the membrane. The MTS is predicted to form an amphipathic helix critical for anchoring the Z-ring to the membrane through an FtsZ-FtsA interaction (Pichoff and Lutkenhaus, 2005). FtsA membrane association is critical for FtsA function during division in vivo (Pichoff and Lutkenhaus, 2005; Szwedziak et al., 2012). Replacement of the FtsA MTS with an analogous motif from MinD or the transmembrane domain from MalF supports essential FtsA functions in vivo,

suggesting that the FtsA MTS is a generic targeting motif. However, overexpression of an FtsA mutant protein truncated at the C-terminus produces a curved cell phenotype (Gayda et al., 1992; Yim et al., 2000; Shiomi and Margolin, 2008). The role of self-association and the influence of phospholipids on oligomerization are even less clear. Several mutations that map to the FtsA protomer interface in the polymer model, including R286W, do not abrogate function in vivo (Geissler et al., 2003; Pichoff et al., 2012). Moreover, cells expressing mutant FtsA deficient for self-interaction require less FtsN and bypass the requirements for ZipA and FtsEX (Geissler et al., 2003, 2007; Reddy, 2007; Pichoff et al., 2012; Du et al., 2016). Protein interaction analyses of yeast and bacterial two-hybrid systems expressing truncated FtsA, without the C-terminal 15 amino acid MTS, generated conflicting reports of self-interaction (Yim et al., 2000; Pichoff and Lutkenhaus, 2005; Pichoff and Lutkenhaus, 2007).

The role of ATP hydrolysis for FtsA function is unknown. ATP hydrolysis activity has been shown to be essential for FtsA function in vivo as several mutations mapping near the ATP-binding pocket cause thermosensitive growth defects (Herricks et al., 2014). FtsA from *E. coli*, *Thermotoga maritima*, *Streptococcus pneumoniae*, *Pseudomonas aeruginosa*, *Deinococcus radiodurans* and *Bacillus subtilis* hydrolyze ATP slowly, with rates ranging from undetectable to a few ATP molecules per minute (Feucht et al., 2001; Paradis-Bleau et al., 2005; Lara et al., 2005; Szwedziak et al., 2012; Herricks et al., 2014; Loose and Mitchison, 2014; Modi et al., 2014). In another

study of *E. coli* FtsA, ATP was important for FtsA to recruit FtsZ on a lipid monolayer and to stimulate FtsZ polymerization dynamics (Loose and Mitchison, 2014).

Here, we provide insight into the molecular events that occur at the interface between the Z-ring and the membrane during early division. We show that ATP binding by phospholipid-associated FtsA is sufficient to remodel membrane architecture, whereby phospholipid binding promotes both affinity of FtsA to ATP and subsequent ATP hydrolysis via communication between the MTS and the ATP-binding site. Finally, we show that FtsA recruits FtsZ to phospholipids to form a large scaffolded network. We propose a model for FtsA function in vivo during cell division that suggests FtsA directly remodels the cell membrane and the Z-ring to promote constriction.

Results

Phospholipid association regulates FtsA ATP hydrolysis

The domain organization of FtsA is similar to actin; however, FtsA contains an additional subdomain ('1C') in lieu of subdomain '1B' of MreB (Fig. 1A) (van den Ent and Lowe, 2000; Szwedziak et al., 2012). Also, FtsA engages the membrane directly through a C-terminal MTS, which is critical for FtsA function in vivo (Pichoff and Lutkenhaus, 2005; Szwedziak et al., 2012). FtsA from *T. maritima* forms linear actin-like polymers, which are thought to assemble adjacent to the membrane surface (Szwedziak et al., 2012; Szwedziak et al., 2014). Currently, it is unknown if binding to the phospholipid membrane regulates FtsA assembly, ATP hydrolysis, or direct protein interactions. To investigate these questions further, we induced expression of

FtsA from a high copy plasmid under the control of an IPTG-inducible promoter in *E. coli* for 20 h at 16°C, lysed the cells and purified native FtsA using ammonium sulfate precipitation, ion exchange chromatography and size exclusion chromatography. Then we assayed fractions containing FtsA for ATP hydrolysis using the malachite green phosphate detection assay and observed that the FtsA protein elution fractions correspond to fractions with robust ATPase activity (Supporting Information Fig. S1A). Next we compared ATP hydrolysis at several concentrations of FtsA; all concentrations of FtsA tested showed robust ATPase activity, with an ATP hydrolysis rate of 20.96 0.5 pmol Pi min^{-1} $pmol^{-1}$ of FtsA for reactions containing 1 μM FtsA (Fig. 1B). The rate of ATP hydrolysis by the native protein is > 10-fold faster than previous reports of *E. coli* FtsA with an N-terminal hexahistidine tag (Herricks et al., 2014). Finally, we also measured ATP hydrolysis using a secondary assay, an NADH enzyme-coupled assay and calculated the rate to be 36.86 ± 0.5 pmol Pi min^{-1} $pmol^{-1}$ (Supporting Information Fig. S1B). This rate is 1.8-fold faster than we detected with malachite green reagent; the difference is due to replenishment of ATP through the activity of pyruvate kinase, preventing ADP accumulation.

Native FtsA rapidly hydrolyzes ATP; therefore, we hypothesized that it may also be competent for assembly into actin-like polymers. To visualize FtsA protein assemblies directly and determine if polymers are present, we analyzed FtsA in the presence and absence of ATP by negative staining with uranyl acetate and transmission electron microscopy (TEM) (Fig. 1C and D). In reactions containing FtsA, we observed large spherical structures of various sizes, ranging from 20 to 500 nm in

diameter. Many of the large structures have smooth, rounded edges with collapsed surface folds and resemble liposomes (Fig. 1C) (Supporting Information Fig. S1C). When FtsA was incubated with ATP and then visualized by TEM, we observed more spherical structures and a heterogeneous population of clustered, spherical vesicles containing long tubulated regions (Fig. 1D) (Supporting Information Fig. S1D). To confirm that the liposome-like structures contain lipids, we stained the reaction mixtures with the lipophilic dye FM 4–64 and then visualized the structures by confocal fluorescence microscopy. FM 4–64 emits fluorescence when bound to lipids and is commonly used to stain membranes of whole cells. As expected, incubation of FtsA with FM4–64 produces fluorescent liposome-like structures consistent with the presence of phospholipids (Fig. 1E).

FtsA localizes to the interior membrane surface in vivo. Therefore, lipids present in the FtsA preparation are most likely derived from the cytoplasmic membrane of *E. coli*. To determine if the copurifying lipids are critical for ATPase activity, we used the nonionic detergent Triton X-100 (TX100) to disrupt the liposomes and then measured the rate of ATP hydrolysis. Increasing TX100 concentration in reactions containing FtsA and lipids results in a concentration-dependent decrease in the rate of ATP hydrolysis (Fig. 2A). At 2% TX100, FtsA hydrolyzes ATP at a rate that is approximately 90% slower than FtsA without detergent (2.3 ± 3.9 min^{-1} and 19.8 ± 3.7 min^{-1} respectively). To confirm that addition of TX100 disrupts liposomes, FtsA was incubated with TX100 (2%) and then fractionated by size exclusion chromatography. In the absence of detergent, FtsA elutes at a position corresponding to the void volume,

indicating that it is present as one or more species larger than 250 kDa, which is consistent with the presence of large structures or liposomes (Fig. 2B). After treatment with detergent, FtsA elutes later, with a calculated size of 94.7 kDa, which could either correspond to an FtsA dimer or an FtsA-detergent micelle (Fig. 2B).

Next, we attempted to restore fast ATP hydrolysis by reconstitution of FtsA into small unilamellar vesicles (SUVs) prepared from *E. coli* phospholipids. As described previously, treatment of FtsA with detergent resulted in slow ATP hydrolysis (Fig. 2A and C) (Supporting Information Fig. S1E). After addition of TX100, residual phospholipids and detergent were then reduced or removed from the FtsA-containing reaction by buffer exchange, where indicated, followed by treatment with detergent- or lipid-removal resin. None of the treatments restores FtsA ATPase activity to the level of untreated FtsA (Fig. 2C); however, after treatment, FtsA was supplemented with SUVs and ATP hydrolysis by FtsA was stimulated (Fig. 2C). These results indicate that rapid ATP hydrolysis by FtsA is promoted by the interaction with phospholipids. As a control, to confirm this, we constructed and purified a truncated FtsA mutant protein, FtsA(ΔMTS), which does not contain the 15 amino acid MTS at the C-terminus. As expected, FtsA(ΔMTS) hydrolyzes ATP at a rate of 0.7 ± 0.3 pmol Pi min^{-1} $pmol^{-1}$, which is < 5% of the activity of wild type FtsA (Fig. 2D). Together, these results indicate that phospholipid engagement by FtsA is essential for rapid ATP hydrolysis. To further identify the lipids that copurify with FtsA, we compared lipid composition profiles of FtsA to FtsA(ΔMTS) and determined that majority of the lipid

signal associated with wild type FtsA is attributable to phosphatidylethanolamine and cardiolipin (Supporting Information Table S1).

Phospholipids stimulate ATP hydrolysis by FtsA suggesting that phospholipid binding shifts the conformation of FtsA to one that has an altered affinity for nucleotide. To test this, we measured binding of FtsA to a fluorescent ATP analog, 30-O-(N-methylanthraniloyl)ATP (mant-ATP), in the presence and absence of phospholipids. Mant-ATP was previously shown to interact with *E. coli* FtsA purified from inclusion bodies (Martos et al., 2012). We observed that phospholipid-free FtsA, prepared by incubation of FtsA with TX100 and subsequent removal of detergent and phospholipids, binds to mant-ATP with a dissociation constant (KD) of 26.2 ± 3.0 μM (Fig. 2E). However, in the presence of phospholipids the interaction between FtsA and mant-ATP is twofold stronger with a KD of 12.8 ± 0.9 μM (Fig. 2E). These results demonstrate that interaction between FtsA and lipids enhances affinity of FtsA for ATP, which could be due to an allosteric change in conformation that is dependent on engagement of the MTS with phospholipids or due to increasing the effective concentration on the vesicle surface.

Finally, we also purified His-SUMO-FtsA, which was previously reported to recruit FtsZ polymers to a lipid surface in vitro yet was defective for ATP hydrolysis (Loose and Mitchison, 2014). Using the expression and purification strategy described here, we observed that His-SUMO-FtsA, purified using the procedure developed for native FtsA, is active for ATP hydrolysis, with a rate that is 58% slower than native FtsA (8.66 ± 0.5 pmol Pi min^{-1} $pmol^{-1}$) (Supporting Information Fig. S2A and B). For

comparison, we also purified His-SUMO-FtsA by metal affinity chromatography as described (Loose and Mitchison, 2014) and determined that, with this method, His-SUMO-FtsA did not copurify with phospholipids and ATP hydrolysis was not restored by supplementation with *E. coli* SUVs (data not shown). Together, these results suggest that the interaction of FtsA with phospholipids preserves ATP hydrolysis activity.

FtsA directly remodels liposome architecture

Since ATP hydrolysis assays showed that prepared *E. coli* phospholipids support rapid ATP hydrolysis and the MTS is predicted to insert into a phospholipid bilayer, we investigated if the addition of FtsA modifies the architecture of SUVs. Therefore, we added phospholipid-free FtsA to purified vesicles and examined protein-lipid architecture by negative stain TEM. We visualized untreated SUVs alone and after incubation with phospholipid-free FtsA (Fig. 3A). There were no observable structures in samples containing phospholipid-free FtsA (Fig. 3Aiii). Also, we observed that prior to incubation with FtsA, the SUVs are small and uniform, with an average diameter of 31.46 8.4 nm (Fig. 3Aiv). After incubation with FtsA, we observed a striking reconfiguration of observable structures. Instead of homogeneous spherical vesicles, we observed many large vesicle clusters and tubulated regions (Fig. 3Ai, ii and inset).

To further investigate the role of ATP in remodeling vesicle architecture, we monitored ATP-dependent reorganization by two independent light scattering

methods. First, we used dynamic light scattering (DLS) to probe heterogeneity and relative particle sizes of purified FtsA, with copurifying lipids, in the presence and absence of ATP (Fig. 3B). We observed that the majority of particles in the preparation of FtsA correspond to approximately 50 nm (Fig. 3B). However, after incubation with ATP, we observed the presence of a large, broad peak centered near 300 nm, which represents approximately half of the volume distribution of all particles present (Fig. 3B). The peak was not observed in reactions of FtsA incubated with ADP or ATPγS. The detection of this additional large peak in the presence of ATP is consistent with the large structures observed by TEM.

Next, we employed a real-time vesicle remodeling assay using 90° angle light scatter to detect physical changes when ATP is added. In this assay, we measured the background light scatter of FtsA and copurifying liposomes, then added nucleotide and monitored the change in light scatter over time. The addition of ATP induces a large light scatter increase, which occurs rapidly and plateaus approximately 15 min after the addition of ATP (Fig. 3C). The increase in light scatter induced by ATP is stable for 15 min, and then the signal falls by approximately 50% over the next 60 min (Supporting Information Fig. S3A). To determine whether ATP binding or hydrolysis is associated with the rapid increase in light scatter, we repeated the 90° angle light scatter assay with ADP and ATP in the presence of EDTA to prevent hydrolysis. In the presence of EDTA, ATP is sufficient to scatter light, although the maximal signal is approximately 20% lower than without EDTA (Fig. 3C). We confirmed that FtsA binds similarly to mant-ATP in both the presence and absence of EDTA (Supporting

Information Fig. S3B). When ADP was added to the reaction, the signal change after 30 min was 74% lower than with ATP (Fig. 3C), suggesting that ADP weakly promotes reorganization. This is further supported by TEM of FtsA in the presence of ADP, which shows isolated, intact vesicles, in contrast to the tubulated vesicles with ATP (Supporting Information Fig. S3C). These results are consistent with ATP promoting lipid reorganization. Furthermore, ATPγS was unable to promote robust light scatter, consistent with DLS results (Fig. 3B) (Supporting Information Fig. S4A), and GTP was also unable to stimulate light scatter (Supporting Information Fig. S4B). In the control experiment, we tested if FtsA(ΔMTS) scatters light when ATP is added, but detected no change, suggesting that the increase in scatter requires engagement of the membrane (Supporting Information Fig. S3D). In addition, TX100 prevents ATP-dependent reorganization by wild type FtsA in 90° light scattering assays and the formation of large 300 nm structures assembled with ATP by DLS (Supporting Information Figs S3E and S4C). As expected, supplementation of FtsA with *E. coli* SUVs after treatment with detergent restores ATP-dependent light scatter (Supporting Information Fig. S3F). Finally, when we tested His-SUMO-FtsA, we also observed that His-SUMO-FtsA scatters light upon addition of ATP and copurifies with phospholipid vesicles (Supporting Information Fig. S2C and D).

Next, we determined if ATP binding changes the orientation of the MTS in the interior of the lipid bilayer, leading to reorientation of the lipid plane relative to FtsA. We used the lipophilic probe diphenylhexatriene (DPH) as an acceptor in fluorescence resonance energy transfer (FRET) assays, with the donor fluorescence emitted by

excitation of two naturally occurring tryptophan residues in the MTS (W408 and W415). In reactions containing FtsA and SUVs pre-incubated with DPH, excitation of the tryptophan residues at 285 nm resulted in a DPH emission signal, which peaked at 430 nm and the intensity was dependent on FtsA concentration (0 to 3 μM) (Fig. 3D). As a control, we measured DPH fluorescence at several phospholipid concentrations and determined that phospholipid concentration does not alter the amplitude at 430 nm under the range of concentrations tested and in the absence of protein (Supporting Information Fig. S3G). To determine if ATP changes FRET efficiency between the FtsA tryptophans and DPH, we compared DPH emission in the presence and absence of ATP. We detected a decrease in the maximum emission amplitude at all FtsA concentrations in the presence of ATP, resulting in a 23% loss of emission at 3 μM FtsA (Fig. 3E). This suggests that when FtsA binds ATP, the MTS repositions within the plane of the lipid bilayer altering the FRET efficiency by limiting access of the DPH acceptor. In the control experiment, we examined the FRET efficiency of FtsA(ΔMTS) and DPH, which does not contain either tryptophan residue near the C-terminus. As expected, we detect no emission of DPH in the presence of FtsA(ΔMTS) (Fig. 3F). These results indicate that the FtsA C-terminal MTS inserts into the lipid bilayer, insertion does not require ATP and the MTS repositions within the membrane when FtsA binds ATP.

A mutation in a loop proximal to the FtsA ATP-binding site impairs function in vitro

To further investigate how nucleotide binding and hydrolysis is coordinated with other regions of the protein, we performed site-directed mutagenesis in a loop near the nucleotide-binding region of FtsA (Fig. 1A, Supporting Information Fig. S5A and B). This loop in the structural model of *E. coli* FtsA (residues 84–89) occupies the space similar to the sensor loop in *Saccharomyces cerevisiae* actin (Sc residues 70–78) (Supporting Information Fig. S5C and D). We identified a lysine residue (K86) in FtsA in this loop near the binding region of the ATP g-phosphate and constructed and purified the FtsA mutant protein FtsA(K86A). FtsA(K86A) is defective for ATP hydrolysis, compared to wild type FtsA, and no stimulation is observed with addition of prepared phospholipids (Fig. 4A). We performed the 90° angle light scatter assay with FtsA(K86A) to detect reorganization; however, the mutant protein failed to scatter light upon addition of ATP (Fig. 4B). To determine if this defect is due to an inability of FtsA(K86A) to bind ATP, we measured binding to mant-ATP and calculated a KD for the interaction of 27.9 ± 0.5 mM (Fig. 4C), which is similar to the KD of wild type FtsA with mant-ATP (Fig. 2E). Next, we tested if the MTS of FtsA(K86A) intercalates into the lipid bilayer using the Trp-DPH FRET assay, but failed to detect a concentration-dependent FRET signal for FtsA(K86A) (Fig. 4D). These results suggest that residue K86 near the ATP-binding site may participate in communication between the nucleotide binding site and the membrane. To determine if FtsA(K86A) localizes to the Z-ring in vivo, we expressed GFP-FtsA(K86A) in cells and monitored localization in live dividing cells. Cells expressing GFP-FtsA exhibited fluorescence at the septa and were determined to be 8.5 ± 0.5 μm (n 5 222) in length.

In contrast, cells expressing GFP-FtsA(K86A) were significantly different in length, 5.6 ± 0.1 μm (n 5 297) ($p < 0.0001$), which is 34% shorter than cells expressing GFP-FtsA (Fig. 4E). These results suggest that expression of GFP-FtsA interferes with cell division, but expression of GFP-FtsA(K86A) is less toxic. We also observed that GFP-FtsA(K86A) localizes to the division ring, although it is impaired for ATP-hydrolysis and membrane insertion in vitro (Fig. 4E).

Lastly, to determine if self-interaction is critical for phospholipid reorganization in vitro, we constructed and purified FtsA(R286W), which was previously reported to be defective for self-interaction and capable of bypassing the requirement for ZipA during division (Geissler et al., 2003; Pichoff et al., 2012). In this study, FtsA(R286W) is defective for rapid ATP hydrolysis compared to wild type FtsA (Fig. 4A). By size exclusion chromatography, FtsA(R286W) elutes as a monomer with a calculated size of 50.6 kDa; however, the peak is very broad with a shoulder overlaying both the dimer position (80 kDa) and the void volume position (Supporting Information Fig. S6A). In contrast, elution of FtsA(ΔMTS) peaks at 108 kDa, which is most consistent with a dimer (Supporting Information Fig. S6B). Confocal fluorescence microscopy of FtsA(R286W) stained with FM 4–64 indicates the presence of a few fluorescent vesicles (Supporting Information Fig. S6C); however, in quantitative assays we determined that there is 89% less copurifying phospholipid associated with FtsA(R286W) than with wild type FtsA (Supporting Information Fig. S6D). Next, we performed the 90° angle light scatter assay and determined that although FtsA(R286W) has an ATP hydrolysis rate that is 81% slower than wild type

FtsA, FtsA(R286W) produces a modest change in light scatter when ATP is added (Fig. 4A and B); however, the amplitude increase develops at a slower rate than for wild type FtsA (Fig. 4B). These results indicate that FtsA(R286W) may be capable of forming large phospholipid complexes, but to a much lesser extent than wild type FtsA. These results further suggest that fast ATP hydrolysis and self-association may be important for promoting robust lipid engagement and reorganization.

FtsA recruits FtsZ to phospholipids and destabilizes steady-state FtsZ polymers through a direct interaction with the FtsZ C-terminus

FtsA functions as a membrane tether for recruitment of FtsZ polymers to the cytoplasmic membrane (Pichoff and Lutkenhaus, 2005). Previous reports also indicate that FtsA recruits FtsZ to a lipid monolayer (Loose and Mitchison, 2014) and TmFtsA recruits TmFtsZ inside liposomes and induces negative curvature (Szwedziak et al., 2014). In low-speed sedimentation assays, approximately 30% of FtsA associates with the pellet fraction due to the presence of copurifying phospholipids, and this amount increases to 84% when the reaction is supplemented with SUVs (Supporting Information Fig. S7A). To identify determinants for the interaction between FtsZ, FtsA and phospholipid vesicles, we performed a low-speed sedimentation assay to collect vesicles and vesicle-associated protein under different nucleotide conditions (Fig. 5A and B). We incubated FtsA with SUVs and ATP and then determined if FtsZ fractionates with the SUV pellet. In the presence of GTP or GMPCPP, conditions that promote FtsZ polymerization, the majority of FtsZ is pellet-associated (62.8% and 76.1% respectively) in reactions containing FtsA, SUVs and ATP (Fig. 5A); however,

with GDP, which does not support FtsZ polymerization, only 18.3% of FtsZ is detected in the pellet in reactions containing FtsA, SUVs and ATP. In the presence of ATPγS, less FtsZ was detected in the pellet under all conditions (GDP, GTP and GMPCPP) in reactions containing FtsA and SUVs, suggesting that ATP promotes the interaction between FtsA and FtsZ better than ATPγS (Fig. 5A). In a control experiment, we observed that when FtsA was omitted, FtsZ polymers fractionated with the supernatant in the presence and absence of SUVs since FtsZ polymers do not bind SUVs directly (Supporting Information Fig. S7B); however, when FtsA was included in the reaction, the majority of FtsZ fractionated with the pellet, indicating that FtsA recruits FtsZ polymers to SUVs (Supporting Information Fig. S7B), and this percentage is higher with ATP (Fig. 5A and B) (Supporting Information Fig. S7B). Finally, we also observed that in the presence of ADP, FtsA can recruit FtsZ polymers to SUVs, but to a lesser extent than without ADP or with ATP (Fig. 5A and B). Together, these results show that FtsA recruits GTP- and GMPCPP-stabilized FtsZ polymers to SUVs, but that non-polymerized FtsZ is not efficiently recruited. Moreover, the presence of ATP likely stabilizes this interaction.

To directly visualize recruitment of FtsZ to FtsA-associated phospholipid vesicles, we used confocal fluorescence microscopy. Active fluorescent FtsZ, labeled with Alexa fluor 488 (FL-FtsZ), was incubated with GTP, added to a channel slide with an 80 μm thick flow chamber and visualized. We observed large, fluorescent FtsZ sheets and bundles, likely composed of long, networked FtsZ polymers (Fig. 5Ci), which have been described previously (Camberg et al., 2009). FtsA-decorated

liposomes were stained with FM 4–64 (Fig. 5Cii) and then incubated with FL-FtsZ in the presence of GTP and ATP, and both fluorophores were visualized (Fig. 5Ciii). We observed overlapping fluorescence between FLFtsZ and FtsA-decorated liposomes, consistent with our observations of direct recruitment of FtsZ to phospholipids by FtsA.

After incubation of GTP-induced FtsZ polymers with FtsA and phospholipids, the FL-FtsZ structures observed by fluorescence microscopy resembled vesicles rather than the networked, polymer bundles (Fig. 5Ciii), suggesting the interaction with FtsZ may destabilize FtsZ polymers. To test this directly and determine if FtsA affects the abundance of FtsZ polymers under steady state conditions, we assembled FtsZ with GTP and a bifunctional GTP/ATP-regenerating system in the presence of increasing FtsA, and collected FtsZ polymers by ultracentrifugation. We observed that with the addition of GTP, FtsZ fractionates predominantly with the high-speed centrifugation pellet indicating that FtsZ polymerizes (Fig. 5D). However, when FtsA is added to the reaction, there is a concentration-dependent decrease in the amount of FtsZ present in the pellet (Fig. 5D). This suggests that as FtsA approaches equimolar stoichiometry with FtsZ, FtsA is effective at destabilizing FtsZ polymers**.**

If an FtsZ-interacting protein prevents GTP-dependent assembly, then this protein should also reduce the rate of FtsZ GTP hydrolysis. This has been reported for the cell division inhibitor SulA, which binds to the FtsZ protofilament interface and reduces the rate of GTP hydrolysis by FtsZ (Mukherjee et al., 1998; Cordell et al., 2003). Regarding FtsA, previous studies have produced conflicting results; purified

FtsA from Staphylococcus aureus and *D. radiodurans* stimulates the GTPase activity of cognate FtsZ, which could lead to destabilization of FtsZ filaments (Fujita et al., 2014; Modi et al., 2014). By contrast, FtsA from *D. radiodurans* decreases GTPase activity of *E. coli* FtsZ (Modi et al., 2014). We performed GTP hydrolysis assays with EcFtsZ and observed a rate of 4.8 ± 0.1 pmol Pi min^{-1} $pmol^{-1}$, which agrees with previous reports (Camberg et al., 2014). In control experiments, we detected no GTP hydrolysis activity by FtsA (Supporting Information Fig. S8A). When FtsA was added to reactions containing FtsZ, the rate of GTP hydrolysis decreased by 55%, suggesting that the FtsA-FtsZ interaction decreases FtsZ GTP hydrolysis (Fig. 5E). Reciprocally, we tested if FtsZ inhibits FtsA ATP hydrolysis but observed no effect (Supporting Information Fig. S8B).

In the crystal structure model of TmFtsZ by Szwedziak et al., Arg 301 forms a salt bridge with Asp 338 of TmFtsA (Szwedziak et al., 2012). Therefore, we constructed a mutation at the analogous residue in EcFtsA, Arg 379, to disrupt the interaction between FtsZ and FtsA. This mutant was previously reported to have a GTP hydrolysis rate similar to wild type FtsZ and is competent for GTP-dependent polymerization (Camberg et al., 2014; Viola et al., 2017). FtsA does not inhibit polymerization of FtsZ(R379E), which is in agreement with residues in the FtsZ C-terminus mediating the interaction with FtsA (Fig. 5D). To confirm impaired interaction, we performed fluorescence microscopy to observe if FtsA can recruit FL-FtsZ(R379E) to phospholipid vesicles. Although FL-FtsZ(R379E) polymers were visible and appear similar to wildtype, they do not overlay with fluorescent FtsA-

associated liposomes (Fig. 5Civ), indicating that Arg 379 of FtsZ is a critical residue for interacting with FtsA. We also tested if FtsA recruits GTP- or GMPCPP-stabilized FtsZ(R379E) polymers to SUVs in a low-speed sedimentation assay, but detected only 35.6% of total FtsZ(R379E) in the pellet fraction with GTP and ATP suggesting that FtsZ(R379E) is impaired for the interaction with FtsA (Supporting Information Fig. S7C).

Reconstruction of synthetic proto-ring complexes containing phospholipids, FtsA and polymerized FtsZ

To investigate the detailed architecture of FtsA-decorated liposomes in association with FtsZ polymers, we visualized complexes of FtsA, FtsZ and SUVs in the presence of ATP and GMPCPP by TEM. FtsA, ATP and SUVs, without FtsZ, form distorted and tubulated liposomes. Tubulated liposomes were frequently observed with a smooth surface and an opposing surface lined with projections approximately 50 A˚ from the lipid surface (Fig. 6A). These projections, observed in images of reactions containing FtsA, ATP and either copurifying lipids or supplemental SUVs, are consistent in size with FtsA cytoplasmic domains aligned on the phospholipid surface (Fig. 6Aii, box) (Supporting Information Fig. S9). The majority of aligned projections are present at regions of neutral or negative curvature (Supporting Information Fig. S9). Next, FtsZ was added to a mixture of FtsA, ATP and SUVs, but did not noticeably change the architecture of the proteo-lipid structures (Fig. 6B). Finally, we constructed synthetic proto-ring complexes by incubating stable FtsZ polymers, assembled with the GTP analog GMPCPP, FtsA, ATP and SUVs. In the presence of FtsZ polymers,

long bundled fibers reaching 3.5 mm in length and 50 to 80 nm in width were observed (Fig. 6Ci–v). The bundles appear to contain FtsZ polymers coated in phospholipids, recruited by the direct interaction with FtsA. Bundles assembled into a twisted helical network, periodically containing branches or bifurcations (Fig. 6Cii and v), with several bundles appearing frayed at the ends (Fig. 6Civ). In contrast, FtsZ polymers alone, without FtsA and SUVs, appeared as single stranded and laterally associated fibers reaching 450 nm in length, with single protofilaments 5 nm thick (Fig. 6D). Addition of SUVs to FtsZ polymers had no effect on the dimensions of the FtsZ polymers (Fig. 6E). These results shows that lipid-associated FtsA forms a large structural scaffold with FtsZ polymers in vitro.

Accumulation of membrane in cells overexpressing FtsA

E. coli BL21 cells expressing *ftsA* (Fig. 7A) or containing the control vector (Fig. 7B) were fixed, embedded, prepared as thin sections and visualized by negative stain TEM. Cells expressing FtsA at 16°C for 20 h remained viable and were on average 15% longer than cells containing the control vector (2.69 ± 0.07 μm and 2.33 ± 0.04 μm respectively) (Supporting Information Fig. S10A–C). In cells expressing FtsA, we observed an extensive network of membranes at the septum (Fig. 7Aii). We also observed clusters of membrane-lined regions and a large number of intracellular vesicles that appeared empty and had accumulated at the cell poles (Fig. 7Aiii and inset), similar to intracellular membranes and vesicles observed in cells overexpressing the Lipid A disaccharide synthase (LpxB) or other membrane glycosyltransferases (Eriksson et al., 2009; Metzger and Raetz, 2009). In contrast, in cells containing the

control vector, membrane was observed along the edge of the cell at the site of cell wall invagination and polar vesicles were only occasionally observed (Fig. 7Bi and ii). These results suggest that overexpression of FtsA in vivo leads to the formation of intracellular vesicles and increased membrane surface area throughout the cell and at the division site.

Discussion

Here, we report that FtsA, the membrane-associated actin homolog from *E. coli*, hydrolyzes ATP robustly, directly reorganizes phospholipid membranes and recruits FtsZ to the membrane. The native FtsA preparation used in this study copurifies with lipid vesicles and efficiently inserts into prepared lipid vesicles composed of purified *E. coli* membrane phospholipids. Extraction of FtsA from phospholipids abolishes rapid ATP hydrolysis, but this activity is restored by which is consistent with our finding that FtsA(ΔMTS) hydrolyzes ATP at <5% of the wild type FtsA hydrolysis rate (Fig. 2D).

Although ATP is not required for the direct interaction of FtsA with phospholipids, ATP binding promotes remodeling of lipid vesicle architecture of reconstituted complexes (Fig. 3A–C). Direct membrane remodeling was also previously described for *S. pneumoniae* FtsA in a report suggesting that SpFtsA could bind to phospholipids in the presence of ATP and induce local changes in membrane architecture (Krupka et al., 2014), and ATP dependent lipid tubulation and/or remodeling has also been described for several other membrane-associated proteins including MinD, amphiphysin and epsin (Peter et al., 2004; Hu et al., 2002; Ford et al.,

2002). Notably, we observed that when phospholipid-free FtsA was added to purified vesicles, the vesicles adopted large, curving tubulated clusters (Fig. 3A). The C-terminal helix of FtsA inserts directly into the phospholipid bilayer in the absence and presence of ATP, as determined by FRET; however, the FRET efficiency is modified in the presence of ATP indicating that the position of the MTS and/or the accessibility of the MTS within the membrane changes between nucleotide occupancy states (Fig. 3D and E).

How then does FtsA modify membrane architecture? Membrane bending likely occurs as a result of insertion of the C-terminal helix into the bilayer and the additional collaboration among adjacent domains on the surface of the membrane, which may be regulated by nucleotide cycling and, in vivo, by other cell division proteins. Our results support that there is communication between the active site where ATP binds and the C-terminal helix of FtsA. First, the ATP analog mant-ATP binds FtsA with higher affinity when phospholipids are present, indicating that phospholipid engagement either directly modifies the conformation of FtsA to promote tighter nucleotide binding (Fig. 2E) or, alternatively, may concentrate FtsA on the vesicle surface, increasing the effective concentration. Second, activation of DPH fluorescence by tryptophan residues in the C-terminal helix is reduced in the presence of ATP (23% lower FRET signal when ATP is present, Fig. 3E), which suggests that although the MTS remains inserted, its relative position in the membrane changes to limit access of the acceptor probe. Consistent with this, a previous report indicated that FtsA(R286W) and a fluorescent FtsZ chimera, FtsZ-YFP, incorporate into liposomes and produce concave

membrane perturbations, which occasionally produced liposome scission events, suggesting FtsA may be critical for membrane scission (Osawa and Erickson, 2013). The oligomeric state of FtsA likely plays an additional role, but key details remain unclear. It was reported that FtsA is capable of polymerization with ATP and further suggested that FtsA may assemble more robustly when the MTS has been removed (Szwedziak et al., 2012; Krupka et al., 2014). In this study, we observed FtsA as tightly arranged subunits of FtsA aligned on the surface of the membrane consistent with the presence of FtsA polymers; however these were observed in both the presence and absence of ATP (Fig. 6A). In light scatter experiments, ATP-dependent reorganization is supported by FtsA(R286W) (Fig. 4B); however, FtsA(R286W) is defective for rapid ATP hydrolysis and self-interaction indicating that oligomerization is not the primary driver of membrane remodeling. FtsA self-interaction could, however, modulate cycles of ATP binding, hydrolysis and/or nucleotide release. Consistent with this hypothesis, although FtsA(R286W) is capable of ATP-dependent membrane reorganization, the amplitude change is lower and occurs more slowly than wild type FtsA (Fig. 4B), which may be attributable to slow nucleotide hydrolysis and/or exchange as well as fewer phospholipids. Several reports obtained from in vivo genetic studies have suggested that interactions between FtsA and other division proteins, including ZipA, FtsN and FtsEX, may prevent FtsA self-association and promote monomerization (Pichoff et al., 2012; Du et al., 2016). Therefore, FtsA-interacting proteins may function to inhibit polymerization, thereby regulating cycles of ATP binding and release and cycles of membrane reorganization. Further study will be

required to determine the precise roles of FtsA-interacting proteins with respect to membrane remodeling by FtsA and if there is equilibrium between FtsA monomers and polymers associated with the membrane.

The structural model of actin from S. cerevisiae shows several key functional regions at the nucleotide binding site, including P loop 1 and P loop 2, as well as the sensor loop (amino acids 70–78), which has been suggested to play a critical role in phosphate release after ATP hydrolysis (Supporting Information Fig. S5C and D) (Rould et al., 2006; Murakami et al., 2010; Kudryashov and Reisler, 2013). However, in the *E. coli* FtsA structural model showing a repositioned '1C' subdomain, FtsA appears to be missing an analogous sensor loop. However, two loops are situated in a similar location as the actin sensor loop, one of which contains K86 (Supporting Information Fig. S5A and B). FtsA(K86A) is capable of nucleotide binding, yet is defective for ATP hydrolysis and membrane insertion (Fig. 4A–D). Lys 86 and the surrounding loop regions may serve as a sensor to regulate g-phosphate occupancy and/or relay to nearby regions and the C-terminal helix. However, further study will be required to determine the conformational steps involved in regulating FtsA function.

Although FtsA conformations during division remain insufficiently clear, recent work has suggested that FtsZ polymers treadmill around the circumference of the cell in association with FtsA during division (Bisson-Filho et al., 2017). We investigated the function of FtsA to directly recruit FtsZ to the membrane and observed that FtsA at substoichometric ratios recruits FtsZ to phospholipid vesicles in vitro

through a direct interaction with Arg 379 in the FtsZ C-terminal conserved region (Fig. 5C and D). Under conditions when FtsA is in excess over FtsZ, FtsA destabilizes steady state FtsZ-GTP polymers in sedimentation assays and reduces the overall rate of GTP hydrolysis by FtsZ, suggesting that protofilament assembly is also disrupted (Fig. 5E). FtsA was recently reported to form minirings on a lipid surface and destabilize FtsZ polymers through preventing FtsZ polymer lateral interactions (Krupka et al., 2017). When FtsA and phospholipids are incubated with GMPCPP-stabilized FtsZ polymers in vitro, large twisted bundles are observed. These bundles are likely composed on the interior of FtsZ polymers, and phospholipids wrap around the exterior. We propose that FtsA-mediated membrane reorganization occurs in vivo at the septum where FtsZ polymers undergo active remodeling. In our current model of FtsA during early division (Fig. 8): (i) FtsA directly interacts with the cytoplasmic leaflet of the inner membrane and inserts the

C-terminus into the phospholipid bilayer, (ii) in the phospholipid bound conformation, ATP binding induces a conformational reorientation of FtsA, promoting membrane distortion and (iii) FtsZ polymers provide a scaffold to direct the FtsA-mediated remodeling of the membrane. FtsA then recruits cell wall synthesis and remodeling enzymes, including FtsI and FtsN, adjacent to the distorted region of the membrane on the periplasmic side to add new peptidoglycan. In this model local membrane deformations by FtsA at multiple locations around the circumference of the cell serve as sites of peptidoglycan synthesis, which is consistent with recent work suggesting that interactions of FtsZ polymers with FtsA at the division site guides peptidoglycan

insertion (Bisson-Filho et al., 2017; Yang et al., 2017). Creation of a membrane adjacent protein scaffold may ultimately be a key driver of division, as protein crowding has recently been reported as sufficient to promote membrane fission events in vitro (Snead et al., 2017). Altogether, this study provides direct evidence that FtsA self-organizes, forms a scaffold with FtsZ and restructures membranes to direct cell wall remodeling at the Z-ring during early constriction.

Experimental procedures

Bacterial strains and plasmid construction

E. coli strains and plasmids used in this study are listed in Table 1. The ftsA gene was amplified from *E. coli* MG1655 and cloned into pET-24b using NdeI and EcoRI restriction sites. Site-specific mutants in ftsA were constructed by site-directed mutagenesis of ftsA expression plasmids using the QuikChange mutagenesis system (Agilent) and confirmed by sequencing. Plasmid pSEB293, containing GFP-FtsA, was mutagenized to create GFP-FtsA(K86A); pET-ftsA was mutagenized to create FtsA(K86A), FtsA(R286W) and truncated FtsA, FtsAΔMTS, by inserting a TAA stop codon at amino acid position 405 in ftsA. Where indicated, cell viability was measured by serial dilution of liquid cultures and spread plating onto solid media. Plates were incubated at 37°C for 20 h to count single colonies.

Protein purification

FtsZ and FtsZ(R379E) were purified as previously reported for wild type FtsZ (Camberg et al., 2009, 2014). FtsA, FtsA mutant proteins and, where indicated, His-SUMO-FtsA (Loose and Mitchison, 2014) were expressed in BL21 (de3) carrying pET

vectors encoding wild type or mutant FtsA. The cells were grown in in LB Lennox broth supplemented with 50 μg ml^{-1} kanamycin at 37°C to an OD600 of 1.2. Expression was induced with 0.5 mM isopropyl-b-D-thiogalactoside (IPTG) for 20 hours at 16°C. Cells were harvested by centrifugation for 30 min at 6,000 *x* g at 4°C and resuspended in 25 ml of cold lysis buffer [25 mM Tris-HCl pH 8.5, 50 mM KCl, 10 mM $MgCl_2$, 10% glycerol, 1 mM EDTA, 1 mM tris(2-carboxyethyl)phosphine (TCEP)]. Cells were lysed by French press and soluble cell extracts were obtained by centrifugation at 30,000 x g for 30 min. Extracts were fractionated with 25% ammonium sulfate, and precipitant was resuspended in cold lysis buffer, applied to Q sepharose fast flow (GE Healthcare, Piscataway, NJ) column equilibrated with lysis buffer and eluted using a linear KCl gradient (50–1000 mM). The peak fractions were pooled, precipitated with 50% ammonium sulfate, resuspended in buffer containing [25 mM Tris-HCl pH 7.5, 200 mM KCl, 10 mM $MgCl_2$, 10% glycerol, 1 mM EDTA, 1 mM tris(2-carboxyethyl)phosphine (TCEP)] and fractionated on a Sephacryl S-200 column (50 ml) (GE Healthcare, Piscataway, NJ) at 0.5 ml min^{-1}. Unless otherwise indicated all FtsA used in assays contained copurified phospholipid. For experiments with FtsA that was extracted from PLs, as indicated, FtsA was removed from copurifying phospholipid vesicles by adding TX100 (2%), incubating for 15 min on ice and then exchanging the buffer on G25 Sephadex resin and removing residual detergent with a detergent removal spin column (ThermoFisher). Where indicated, residual PLs were removed by treatment of sample with calcium silicate lipid removal agent (250 mg added per 50 μg of protein) (Sigma-Aldrich). After treatment protein

was used immediately. Protein concentrations were determined by bradford assay with comparison to a bovine serum albumin standard curve using Bio-Rad Protein Determination Reagent and are reported as FtsZ monomers and FtsA monomers.

Analytical size exclusion chromatography of FtsA, FtsA(K86A), FtsA(ΔMTS) and FtsA(R286W) was performed in the presence or absence of TX100 using a Sephacryl S200 (45 ml) column equilibrated with buffer containing 25 mM Tris-HCl (pH 7.5), 200 mM KCl, 10 mM $MgCl_2$, 1 mM EDTA and 1 mM TCEP. Where indicated, FtsA was incubated with 2% TX100 for 10 min and applied to a column equilibrated with buffer containing 0.5% TX100. Eluting fractions were analyzed for FtsA content by SDS-PAGE and coomassie staining and intensity was measured by densitometry using NIH Image J.

Nucleotide binding and hydrolysis assays

To detect ATP binding, reaction mixtures (75 µl) of FtsA (2 µM) with and without SUV (0.5 mg ml^{-1}) were incubated for 5 min (23°C) in reaction buffer containing 25 mM Tris-HCl (pH 7.5), 200 mM KCl and 10 mM $MgCl_2$, with increasing concentrations of mant-ATP (1–250 µM) (Life Technologies). Fluorescence intensity was measured with an Agilent Eclipse fluorescence spectrophotometer using an excitation wavelength of 350 nm and an emission wavelength of 400 nm and 5 nm slit widths. Binding curves were fit to a one site specific binding model in GraphPad Prism (version 4.0b) to calculate KD values using the following equation F 5 Fmax 3 [L]n/(KDn1 [L]n); where F is fluorescence intensity, L is ligand concentration and n is unconstrained.

ATP and GTP hydrolysis was measured by monitoring the amount of inorganic phosphate released at indicated times (23°C) in reactions (25 ml) using malachite green reagent for phosphate detection. ATP hydrolysis assays were performed in reaction buffer with ATP (1 mM) and FtsA (1 mM). Where indicated, *E. coli* phospholipid vesicles were added (0.5 mg ml^{-1}). *E. coli* total phospholipid extracts (Avanti Polar Lipids) were used to prepare large unilamellar vesicles (LUVs) as previously described (Camberg et al., 2007). LUVs were extruded 15 times through a 100-nm polycarbonate membrane at 65°C to produce SUVs. Small aliquots were frozen at -80°C until use. GTP hydrolysis assays were performed in buffer containing 50 mM MES (pH 6.5), 100 mM KCl and 10 mM $MgCl_2$ with FtsZ (6 mM) and GTP (1 mM). In all ATPase and GTPase assays, unless otherwise stated, total phosphate content was determined at 0, 5 and 10 min using Biomol Green (Enzo Life Sciences) by comparison to a phosphate standard curve. Where indicated, an NADH enzyme-coupled assay was used to measure ATP hydrolysis by FtsA by monitoring absorbance at 340 nm (Graf et al., 2009).

Light scattering assays

Dynamic light scattering (DLS) measurements were made using Zetasizer Nano ZS with a detector angle of 173° and a 4 mW, 633 nm He–Ne laser (Malvern Instruments). To determine size distribution, FtsA (2 μM) alone or with ATP (4 mM), ADP (2 mM), ATPγS (2 mM) or TX-100 (2%), where indicated, were incubated for 30 min, added to a polystyrene cuvette and scanned at 23°C. The intensity-weighted hydrodynamic

diameter profiles are reported as the average of three replicates of 11 scans per replicate.

To monitor nucleotide-dependent phospholipid reorganization by FtsA, His-SUMO-FtsA and FtsA mutant proteins, 90° angle light scattering was performed. Reaction mixtures containing FtsA, His-SUMO-FtsA or FtsA mutant protein (2 μM) with copurified PLs, or detergent-extracted FtsA supplemented with SUVs (100 μg ml^{-1}), where indicated, were monitored for light scatter with time after the addition of 4 mM ATP using an Agilent Eclipse fluorescence spectrophotometer with both excitation and emission wavelengths set to 450 nm with 5 nm slit widths. Baseline readings were collected for at least 3 min, ATP (4 mM) and where indicated EDTA (15 mM), ATPγS (2 mM) or ADP (2 mM) was added and light scattering was measured for up to 120 min.

Assembly and recruitment assays

To measure FtsZ polymer formation by ultracentrifugation, reaction mixtures (25 μl) with FtsZ or FtsZ(R379E) (4 μM), were prepared in buffer containing 50 mM MES (pH 6.5), 100 mM KCl, 10 mM $MgCl_2$, 2 mM GTP and a nucleotide regenerating system containing acetate kinase (25 μg ml^{-1}) and acetyl phosphate (15 mM). Where indicated, FtsA (0–4 μM) and ATP (4 mM) were added. Polymerization reactions were incubated for 5 min at 23°C and then centrifuged at 129,000 x g for 30 min. Pellets were resuspended in equal volume as supernatants and analyzed by SDS-PAGE and coomassie staining.

Phospholipid recruitment assays with FtsA and FtsZ were performed by incubating FtsZ or FtsZ(R379E) (6 μM) with GMPCPP (0.2 mM), GDP (1 mM) or GTP (2 mM), where indicated, in reaction buffer for 3 min and then added to a reaction containing FtsA (2 μM) pre-assembled with SUVs (500 μg ml^{-1}) and ADP (2 mM), ATP (4 mM) or ATPγS (2 mM) and then incubated for an additional 10 min at 30°C. Phospholipid vesicles were collected by low speed centrifugation at 12,000 x g for 12 min. Supernatants and pellets were analyzed by SDS-PAGE and coomassie staining. Percent of protein in the pellet fraction was determined by densitometry using NIH ImageJ.

Trp-DPH FRET assay was performed by incorporation of 1,6-Diphenyl-1,3,5-hexatriene (DPH) (Sigma-Aldrich) into liposomes at 1:500 DPH to lipid (w/w) unless otherwise indicated as described (Masuda et al., 2006). The fluorescence of tryptophan was excited at 285 nm (5 nm slit widths) and emission spectra by FtsA wild type and mutant protein (0–3 μM), after incubation with DPH-liposomes (100 μg ml^{-1}) for 6 min at 30°C and, where indicated, ATP (0.1 mM). DPH emission was scanned from 400 to 500 nm.

Confocal fluorescence microscopy

Cultures of MG1655 containing plasmid pSEB293 (Pichoff and Lutkenhaus, 2005) encoding GFP-FtsA, or mutagenized to contain GFP-FtsA(K86A), were grown overnight on solid LB Lennox media containing ampicillin (100 μg ml^{-1}), and then restreaked onto plates containing arabinose (0.7 nM) and grown for 5 h at 37°C. Cells were applied to a 4% agarose pad containing MOPS [3-(N-morpholino)

propanesulfonic acid] minimal media with 0.5% glycerol and a coverslip was added. Samples were visualized with a Zeiss LSM 700 confocal fluorescence microscope with excitation at 488 nm and 555 nm. Where indicated, a Nomarski prism was used to acquire differential interference contrast (DIC) images. All images were captured on an AxioCam digital camera with ZEN 2012 software. Cell lengths were measured using NIH ImageJ.

To monitor assembly of protein and lipid complexes, FtsZ and FtsZ(R379E) were fluorescently labeled with Alexa Fluor 488 (FL-FtsZ) and cycles of polymerization and depolymerization were performed to collect active, labeled protein as described (Gonzalez et al., 2003; Camberg et al., 2014). FtsA samples containing copurifying phospholipid vesicles were labeled using FM 4–64EX at 250 μg ml^{-1}. Reactions of, where indicated, FtsA-FM4–64EX (1 μM) with FtsA (3 μM) and FL-FtsZ or FL-FtsZ(R379E) (1 μM) with FtsZ or FtsZ(R379E) (3 μM) were mixed in the presence of 4 mM ATP, 2 mM GTP and a regenerating system, applied to a flow chamber. We used a 10 μl flow chamber (thickness 0.08 mm) as described (Bailey et al., 2015) and visualized reactions by confocal fluorescence microscopy. Lipid concentrations of FtsA fractions were determined by incubation of FtsA with FM 4–64 (1.25 μg ml^{-1}). Fluorescence intensity was measured with an Agilent Eclipse fluorescence spectrophotometer using an excitation wavelength of 565 nm and an emission wavelength of 745 nm and 5 nm slit widths and compared to a phospholipid standard curve.

Electron microscopy

Reactions containing assembly buffer mixtures of 4 μM FtsA, 4 mM ATP, 4 μM FtsZ, 0.2 mM GMPCPP and 0.5 mg ml^{-1} SUVs, where indicated, were incubated for 5 min at 23°C, applied to a mesh carbon/formvar coated grid, fixed with glutaraldehyde (1%) and negative stained with uranyl acetate (2%). For whole cell thin sections, bacterial cell pellets were fixed with 2.5% glutaraldehyde in 0.15 M sodium cacodylate buffer (pH 7.4) at 4°C for several days. Samples were rinsed in 0.15 M sodium cacodylate buffer and post-fixed in 1% osmium tetroxide for 1 h at 4°C. Following distilled water rinses, samples were stained en bloc with 2% aqueous uranyl acetate. Pellets were encased in 2% agar, and dehydrated through a graded acetone series and infiltrated and embedded in Spurr's epoxy resin (Ladd Research Industries, Burlington, VT). Semi-thin sections (1 μm) were prepared using a Reichert-Jung Ultracut E ultramicrotome (Leica Biosystems, Buffalo Grove, IL), and stained with methylene blue and azure II. Ultra-thin sections were prepared and retrieved onto 300-mesh thin bar copper grids, and contrasted with uranyl acetate and lead citrate. Sections were examined using a CM-10 electron microscope (FEI, Hillsboro, OR). Images were collected with a model 785 Erlangshen ES1000W CCD camera (Gatan, Pleasanton, CA).

Acknowledgements

We thank Chris LaBreck, Shannon May, Eric DiBiasio and Cathy Trebino for helpful discussions and critical reading of the manuscript, Carol Ayala at the Rhode Island Hospital for expert assistance with EM, Joe Lutkenhaus for pSEB293 and Martin Loose for pML29. We also thank Cal Vary at Maine Medical Center Research Institute

for lipid profiling and identification and Marc Llaguno and Xinran Liu at the Center for Cellular and Molecular Imaging at Yale School of Medicine. Research reported in this publication was supported by the National Institute of General Medical Sciences of the National Institutes of Health under Award Number R01GM118927 to J. Camberg. The content is solely the responsibility of the authors and does not necessarily represent the official views of the National Institutes of Health. This material is based upon work conducted at a Rhode Island NSF EPSCoR research facility, the Genomics and Sequencing Center, supported in part by the National Science Foundation EPSCoR Cooperative Agreement #EPS-1004057.

Conflict of Interest

The authors declare that they have no conflicts of interest with the contents of this article.

References

Aarsman, M.E., Piette, A., Fraipont, C., Vinkenvleugel, T.M., Nguyen-Disteche, M., and den Blaauwen, T. (2005) Maturation of the *Escherichia coli* divisome occurs in two steps. Mol Microbiol 55: 1631–1645.

Alexeeva, S., Gadella, T.W., Jr.,Verheul, J., Verhoeven, G.S., and den Blaauwen, T. (2010) Direct interactions of early and late assembling division proteins in *Escherichia coli* cells resolved by FRET. Mol Microbiol 77: 384–398.

Bailey, M.E., Sackett, D.L., and Ross, J.L. (2015) Katanin severing and binding microtubules are inhibited by tubulin carboxy tails. Biophys J 109: 2546–2561.

Bernard, C.S., Sadasivam, M., Shiomi, D., and Margolin, W. (2007) An altered FtsA can compensate for the loss of essential cell division protein FtsN in *Escherichia coli*. Mol Microbiol 64: 1289–1305.

Bisson-Filho, A.W., Hsu, Y.P., Squyres, G.R., Kuru, E., Wu, F., Jukes, C., et al. (2017) Treadmilling by FtsZ filaments drives peptidoglycan synthesis and bacterial cell division. Science 355: 739–743.

Blattner, F.R., Plunkett, G., 3rd, Bloch, C.A., Perna, N.T., Burland, V., Riley, M., et al. (1997) The complete genome sequence of *Escherichia coli* K-12. Science 277: 1453–1462.

Bork, P., Sander, C., and Valencia, A. (1992) An ATPase domain common to prokaryotic cell cycle proteins, sugar kinases, actin, and hsp70 heat shock proteins. Proc Natl Acad Sci U S A 89: 7290–7294.

Busiek, K.K., Eraso, J.M., Wang, Y., and Margolin, W. (2012) The early divisome protein FtsA interacts directly through its 1c subdomain with the cytoplasmic domain of the late divisome protein FtsN. J Bacteriol 194: 1989– 2000.

Camberg, J.L., Hoskins, J.R., and Wickner, S. (2009) ClpXP protease degrades the cytoskeletal protein, FtsZ, and modulates FtsZ polymer dynamics. Proc Natl Acad Sci U S A 106: 10614–10619.

Camberg, J.L., Johnson, T.L., Patrick, M., Abendroth, J., Hol, W.G., and Sandkvist, M. (2007) Synergistic stimulation of EpsE ATP hydrolysis by EpsL and acidic phospholipids. Embo J 26: 19–27.

Camberg, J.L., Viola, M.G., Rea, L., Hoskins, J.R., Wickner, S., and Scheffers, D.-J. (2014) Location of dual sites in *E. coli* FtsZ important for degradation by ClpXP; one at the C-terminus and one in the disordered linker. PLoS One 9: e94964.

Corbin, B.D., Geissler, B., Sadasivam, M., and Margolin, W. (2004) Z-ring-independent interaction between a subdomain of FtsA and late septation proteins as revealed by a polar recruitment assay. J Bacteriol 186: 7736–7744.

Corbin, B.D., Wang, Y., Beuria, T.K., and Margolin, W. (2007) Interaction between cell division proteins FtsE and FtsZ. J Bacteriol 189: 3026–3035.

Cordell, S.C., Robinson, E.J., and Lowe, J. (2003) Crystal structure of the SOS cell division inhibitor SulA and in complex with FtsZ. Proc Natl Acad Sci U S A 100: 7889–7894.

Dai, K., Xu, Y., and Lutkenhaus, J. (1996) Topological characterization of the essential *Escherichia coli* cell division protein FtsN. J Bacteriol 178: 1328–1334.

Du, S., Pichoff, S., and Lutkenhaus, J. (2016) FtsEX acts on FtsA to regulate divisome assembly and activity. Proc Natl Acad Sci U S A 113: E5052–E5061.

Eriksson, H.M., Wessman, P., Ge, C., Edwards, K., and Wieslander, A. (2009) Massive formation of intracellular membrane vesicles in *Escherichia coli* by a monotopic membrane-bound lipid glycosyltransferase. J Biol Chem 284: 33904–33914.

Errington, J. (2015) Bacterial morphogenesis and the enigmatic MreB helix. Nat Rev Microbiol 13: 241–248.

Feucht, A., Lucet, I., Yudkin, M.D., and Errington, J. (2001) Cytological and biochemical characterization of the FtsA cell division protein of Bacillus subtilis. Mol Microbiol 40: 115–125.

Ford, M.G., Mills, I.G., Peter, B.J., Vallis, Y., Praefcke, G.J., Evans, P.R., and McMahon, H.T. (2002) Curvature of clathrin-coated pits driven by epsin. Nature 419: 361–366.

Fujita, J., Maeda, Y., Nagao, C., Tsuchiya, Y., Miyazaki, Y., Hirose, M., et al. (2014) Crystal structure of FtsA from Staphylococcus aureus. FEBS Lett 588: 1879–1885.

Gayda, R.C., Henk, M.C., and Leong, D. (1992) C-shaped cells caused by expression of an ftsA mutation in *Escherichia coli*. J Bacteriol 174: 5362–5370.

Geissler, B., Elraheb, D., and Margolin, W. (2003) A gainof-function mutation in ftsA bypasses the requirement for the essential cell division gene zipA in *Escherichia coli*. Proc Natl Acad Sci U S A 100: 4197–4202.

Geissler, B., Shiomi, D., and Margolin, W. (2007) The ftsA* gain-of-function allele of *Escherichia coli* and its effects on the stability and dynamics of the Z ring. Microbiology 153: 814–825.

Goehring, N.W., and Beckwith, J. (2005) Diverse paths to midcell: assembly of the bacterial cell division machinery. Curr Biol 15: R514–R526.

Gonzalez, J.M., Jimenez, M., Velez, M., Mingorance, J., Andreu, J.M., Vicente, M., and Rivas, G. (2003) Essential cell division protein FtsZ assembles into one monomerthick ribbons under conditions resembling the crowded intracellular environment. J Biol Chem 278: 37664–37671.

Graf, C., Stankiewicz, M., Kramer, G., and Mayer, M.P. (2009) Spatially and kinetically resolved changes in the conformational dynamics of the Hsp90 chaperone machine. Embo J 28: 602–613.

Haeusser, D.P., and Margolin, W. (2016) Splitsville: structural and functional insights into the dynamic bacterial Z ring. Nat Rev Microbiol 14: 305–319.

Hale, C.A., and de Boer, P.A. (1997) Direct binding of FtsZ to ZipA, an essential component of the septal ring structure that mediates cell division in *E. coli*. Cell 88: 175–185.

Hale, C.A., and de Boer, P.A. (1999) Recruitment of ZipA to the septal ring of *Escherichia coli* is dependent on FtsZ and independent of FtsA. J Bacteriol 181: 167–176.

Herricks, J.R., Nguyen, D., and Margolin, W. (2014) A thermosensitive defect in the ATP binding pocket of FtsA can be suppressed by allosteric changes in the dimer interface. Mol Microbiol 94: 713–727.

Hu, Z., Gogol, E.P., and Lutkenhaus, J. (2002) Dynamic assembly of MinD on phospholipid vesicles regulated by ATP and MinE. Proc Natl Acad Sci 99: 6761–6766.

Krupka, M., Cabre, E.J., Jimenez, M., Rivas, G., Rico, A.I., and Vicente, M. (2014) Role of the FtsA C terminus as a switch for polymerization and membrane association. mBio 5: e02221.

Krupka, M., Rowlett, V.W., Morado, D., Vitrac, H., Schoenemann, K., Liu, J., and Margolin, W. (2017) *Escherichia coli* FtsA forms lipid-bound minirings that antagonize lateral interactions between FtsZ protofilaments. Nat Commun 8: 15957.

Kudryashov, D.S., and Reisler, E. (2013) ATP and ADP actin states. Biopolymers 99: 245–256.

Lara, B., Rico, A.I., Petruzzelli, S., Santona, A., Dumas, J., Biton, J., et al. (2005) Cell division in cocci: localization and properties of the Streptococcus pneumoniae FtsA protein. Mol Microbiol 55: 699–711.

Llinas, P., Isabet, T., Song, L., Ropars, V., Zong, B., Benisty, H., et al. (2015) How actin initiates the motor activity of Myosin. Dev Cell 33: 401–412.

Loose, M., and Mitchison, T.J. (2014) The bacterial cell division proteins FtsA and FtsZ self-organize into dynamic cytoskeletal patterns. Nat Cell Biol 16: 38–46.

Lutkenhaus, J., Pichoff, S., and Du, S. (2012) Bacterial cytokinesis: From Z ring to divisome. Cytoskeleton 69: 778–790.

Martos, A., Monterroso, B., Zorrilla, S., Reija, B., Alfonso, C., Mingorance, J., et al. (2012) Isolation, characterization and lipid-binding properties of the recalcitrant FtsA division protein from *Escherichia coli*. PLoS One 7: e39829.

Masuda, M., Takeda, S., Sone, M., Ohki, T., Mori, H., Kamioka, Y., and Mochizuki, N. (2006) Endophilin BAR domain drives membrane curvature by two newly identified structure-based mechanisms. Embo J 25: 2889–2897.

Metzger, LEt., and Raetz, C.R. (2009) Purification and characterization of the lipid A disaccharide synthase (LpxB) from *Escherichia coli*, a peripheral membrane protein. Biochemistry 48: 11559–11571.

Modi, K., Misra, H.S., and Scheffers, D.-J. (2014) Dr-FtsA, an actin homologue in Deinococcus radiodurans differentially affects Dr-FtsZ and Ec-FtsZ functions in vitro. PLoS One 9: e115918.

Mukherjee, A., Cao, C., and Lutkenhaus, J. (1998) Inhibition of FtsZ polymerization by SulA, an inhibitor of septation in *Escherichia coli*. Proc Natl Acad Sci U S A 95: 2885–2890.

Murakami, K., Yasunaga, T., Noguchi, T.Q., Gomibuchi, Y., Ngo, K.X., Uyeda, T.Q., and Wakabayashi, T. (2010) Structural basis for actin assembly, activation of ATP hydrolysis, and delayed phosphate release. Cell 143: 275–287.

Osawa, M., and Erickson, H.P. (2013) Liposome division by a simple bacterial division machinery. Proc Natl Acad Sci U S A 110: 11000–11004.

Paradis-Bleau, C., Sanschagrin, F., and Levesque, R.C. (2005) Peptide inhibitors of the essential cell division protein FtsA. Prot Engin Des Sel 18: 85–91.

Pelham, R.J., and Chang, F. (2002) Actin dynamics in the contractile ring during cytokinesis in fission yeast. Nature 419: 82–86.

Peter, B.J., Kent, H.M., Mills, I.G., Vallis, Y., Butler, P.J., Evans, P.R., and McMahon, H.T. (2004) BAR domains as sensors of membrane curvature: the amphiphysin BAR structure. Science 303: 495–499.

Pichoff, S., and Lutkenhaus, J. (2002) Unique and overlapping roles for ZipA and FtsA in septal ring assembly in *Escherichia coli*. Embo J 21: 685–693.

Pichoff, S., and Lutkenhaus, J. (2005) Tethering the Z ring to the membrane through a conserved membrane targeting sequence in FtsA. Mol Microbiol 55: 1722–1734.

Pichoff, S., and Lutkenhaus, J. (2007) Identification of a region of FtsA required for interaction with FtsZ. Mol Microbiol 64: 1129–1138.

Pichoff, S., Shen, B., Sullivan, B., and Lutkenhaus, J. (2012) FtsA mutants impaired for self-interaction bypass ZipA suggesting a model in which FtsA's self-interaction competes with its ability to recruit downstream division proteins. Mol Microbiol 83: 151–167.

Pogliano, J., Pogliano, K., Weiss, D.S., Losick, R., and Beckwith, J. (1997) Inactivation of FtsI inhibits constriction of the FtsZ cytokinetic ring and delays the assembly of FtsZ rings at potential division sites. Proc Natl Acad Sci U S A 94: 559–564.

Pollard, T.D., and Wu, J.Q. (2010) Understanding cytokinesis: lessons from fission yeast. Nat Rev Mol Cell Biol 11: 149–155.

Reddy, M. (2007) Role of FtsEX in cell division of *Escherichia coli*: viability of ftsEX mutants is dependent on functional SufI or high osmotic strength. J Bacteriol 189: 98–108.

Rico, A.I., Garcia-Ovalle, M., Palacios, P., Casanova, M., and Vicente, M. (2010) Role of *Escherichia coli* FtsN protein in the assembly and stability of the cell division ring. Mol Microbiol 76: 760–771.

Rould, M.A., Wan, Q., Joel, P.B., Lowey, S., and Trybus, K.M. (2006) Crystal structures of expressed nonpolymerizable monomeric actin in the ADP and ATP states. J Biol Chem 281: 31909–31919.

Shiomi, D., and Margolin, W. (2008) Compensation for the loss of the conserved membrane targeting sequence of FtsA provides new insights into its function. Mol Microbiol 67: 558–569.

Snead, W.T., Hayden, C.C., Gadok, A.K., Zhao, C., Lafer, E.M., Rangamani, P., and Stachowiak, J.C. (2017) Membrane fission by protein crowding. Proc Natl Acad Sci U S A 114: E3258–E3267.

Soderstrom, B., Mirzadeh, K., Toddo, S., von Heijne, G., Skoglund, U., and Daley, D.O. (2016) Coordinated disassembly of the divisome complex in *Escherichia coli*. Mol Microbiol 101: 425–438.

Szwedziak, P., Wang, Q., Bharat, T.A., Tsim, M., and Lowe, J. (2014) Architecture of the ring formed by the tubulin homologue FtsZ in bacterial cell division. eLife 3: e04601. Szwedziak, P., Wang, Q., Freund, S.M., and Lowe, J. (2012) FtsA forms actin-like protofilaments. Embo J 31: 2249–2260. van den Ent, F., Izore, T., Bharat, T.A.,

Johnson, C.M., and Lowe, J. (2014) Bacterial actin MreB forms antiparallel double filaments. eLife 3: e02634.

van den Ent, F., and Lowe, J. (2000) Crystal structure of the cell division protein FtsA from Thermotoga maritima. Embo J 19: 5300–5307.

Viola, M.G., LaBreck, C.J., Conti, J., Camberg, J.L., and Cascales, E. (2017) Proteolysis-dependent remodeling of the tubulin homolog FtsZ at the division septum in *Escherichia coli*. PLoS One 12: e0170505.

Wang, X., Huang,J., Mukherjee, A., Cao, C., and Lutkenhaus, J. (1997) Analysis of the interaction of FtsZ with itself, GTP, and FtsA. J Bacteriol 179: 5551–5559.

Yang, X., Lyu, Z., Miguel, A., McQuillen, R., Huang, K.C., and Xiao, J. (2017) GTPase activity-coupled treadmilling of the bacterial tubulin FtsZ organizes septal cell wall synthesis. Science 355: 744–747.

Yim, L., Vandenbussche, G., Mingorance, J., Rueda, S., Casanova, M., Ruysschaert, J.M., and Vicente, M. (2000) Role of the carboxy terminus of *Escherichia coli* FtsA in self-interaction and cell division. J Bacteriol 182: 6366–6373.

Table 1. Strains and plasmids used in this study.

Strain	**Relevant genotype**	**Source, Reference or Construction**
MG1655	*LAM- rph-1*	(Blattner *et al.*, 1997)
BL21(λde3)	*F- ompT gal dcm lon hsdSB(rB- mB-) λ(de3[lacI lacUV5-T7 gene 1 ind1 sam7 nin5])*	EMD Millipore, USA
JC0390	MG1655 (*ΔaraEp*::*kan*)	(Viola *et al.*, 2017)
Plasmids		
pSEB293	*amp* P_{ara}::*gfp-ftsA*	(Pichoff & Lutkenhaus, 2007)
pBAD-*gfp-ftsA(K86A)*	*amp* P_{ara}::*gfp-ftsA(K86A)*	This study
pET-24b	*kan*, P_{T7} promoter	EMD Millipore, USA
pET-*ftsA*	*kan*	This study
pET-*ftsA(K86A)*	*kan*	This study
pET-*ftsA(R286W)*	*kan*	This study
pET-*ftsA(ΔMTS)*	*kan*	This study
pET-*ftsZ*	*kan*	(Camberg et al., 2009)
pET-*ftsZ(R379E)*	*kan*	(Camberg et al., 2014)
pML29	*amp* P_{T7}::*his-sumo-ftsA*	(Loose & Mitchison, 2014)

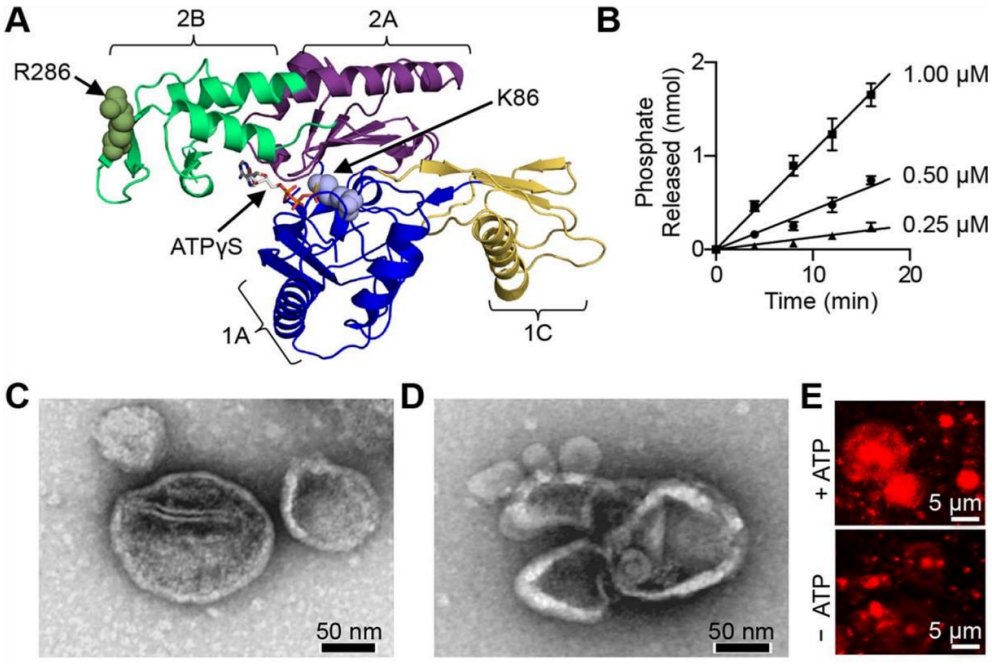
A
2B
2A
R286
K86
ATPγS
1A
1C
B
Phosphate Released (nmol)
2
1
0
0
10
20
Time (min)
1.00 μM
0.50 μM
0.25 μM
C
50 nm
D
50 nm
E
+ ATP
5 μm
– ATP
5 μm

Fig 1. FtsA hydrolyzes ATP rapidly in the presence of liposomes.

A. *E. coli* FtsA (residues 13–381) modeled onto T. maritima FtsA (pdb: 4A2B) (Szwedziak et al., 2012). Subdomains 1A (blue, 13–88, 156– 196, 359–381), 1C (gold, 89–155), 2A (purple, 197–232) and 2B (green, 233–303) are shown, where indicated. Amino acids Arg 286 (green) and Lys 86 (light blue) are shown as Corey-Pauling-Koltun (CPK) models. ATPγS is shown as a stick model. B. Hydrolysis of ATP by FtsA (0.25, 0.50 and 1.00 μM) was monitored with time as described in Experimental Procedures. Data is an average of three replicates represented as mean +/- SEM. C. FtsA (4 μM) was prepared as described in Experimental Procedures and visualized by negative stain TEM. D. FtsA (4 μM) was incubated with ATP (4 mM), prepared and visualized by negative stain TEM. Size bars in C and D are 50 nm. E. FtsA (4 μM) in the absence or presence of ATP (4 mM) was stained with FM 4–64 and then injected into a flow chamber and visualized by confocal FtsZ polymers and soluble fractions containing non-polymerized FtsZ are shown.

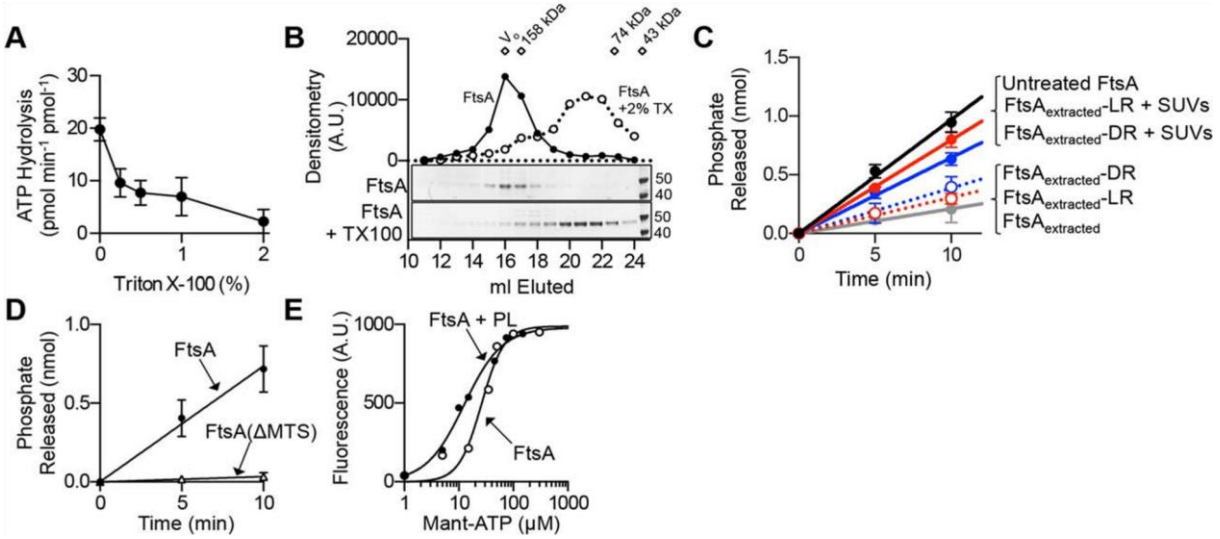
A
ATP Hydrolysis (pmol min-1 pmol-1)
Triton X-100 (%)
B
Densitometry (A.U.)
V0
158 kDa
74 kDa
43 kDa
FtsA
FtsA +2% TX
FtsA + TX100
ml Eluted
C
Phosphate Released (nmol)
Time (min)
Untreated FtsA
FtsAextracted-LR + SUVs
FtsAextracted-DR + SUVs
FtsAextracted-DR
FtsAextracted-LR
FtsAextracted
D
Phosphate Released (nmol)
FtsA
FtsA(ΔMTS)
Time (min)
E
Fluorescence (A.U.)
FtsA + PL
FtsA
Mant-ATP (μM)

Fig 2. Phospholipids are essential for rapid ATP hydrolysis

A. ATP hydrolysis by FtsA was measured over time as described in Experimental Procedures in the presence of increasing concentrations of TX100 detergent (0, 0.25, 0.5, 1, 2%), which was included in the reaction buffer. FtsA used in A contains copurifying PLs and ATP hydrolysis is prevented with increasing TX100. B. Elution profile of FtsA (solid line) and FtsA with 0.5% TX100 (dashed line) by size exclusion chromatography. Fractions were analyzed by SDS-PAGE and densitometry. V_O denotes the void volume. FtsA used in B contains copurifying PLs and the elution profile shifts in the presence of TX100, which solubilizes lipid vesicles. C. Detection of phosphate released in reactions of untreated FtsA containing copurifying PLs (1 μM), or FtsA (1 μM) extracted with 2% TX100 (FtsA-extracted) and then treated with a detergent removal spin column (FtsA-extracted-DR), or with lipid removal agent (250 μg ml^{-1}) (FtsA-extracted-LR) and reconstituted with SUVs (500 μg ml^{-1}), where indicated. Phosphate was detected at 0, 5 and 10 minutes by malachite green reagent. D. ATP hydrolysis of FtsA (1 μM) or FtsA(ΔMTS) (1 μM), where indicated, was monitored over time. FtsA used in D contains copurifying PLs. E. FtsA (2 μM) was extracted from copurifying PLs and then exchanged into buffer without detergent and incubated with mant-ATP (1 to 250 mM) in the presence (open circles) and absence (closed circles) of SUVs (500 μg ml^{-1}). Mant-ATP fluorescence was monitored as described in Experimental Procedures. Data from A, C and D are an average of three replicates represented as mean +/- SEM.

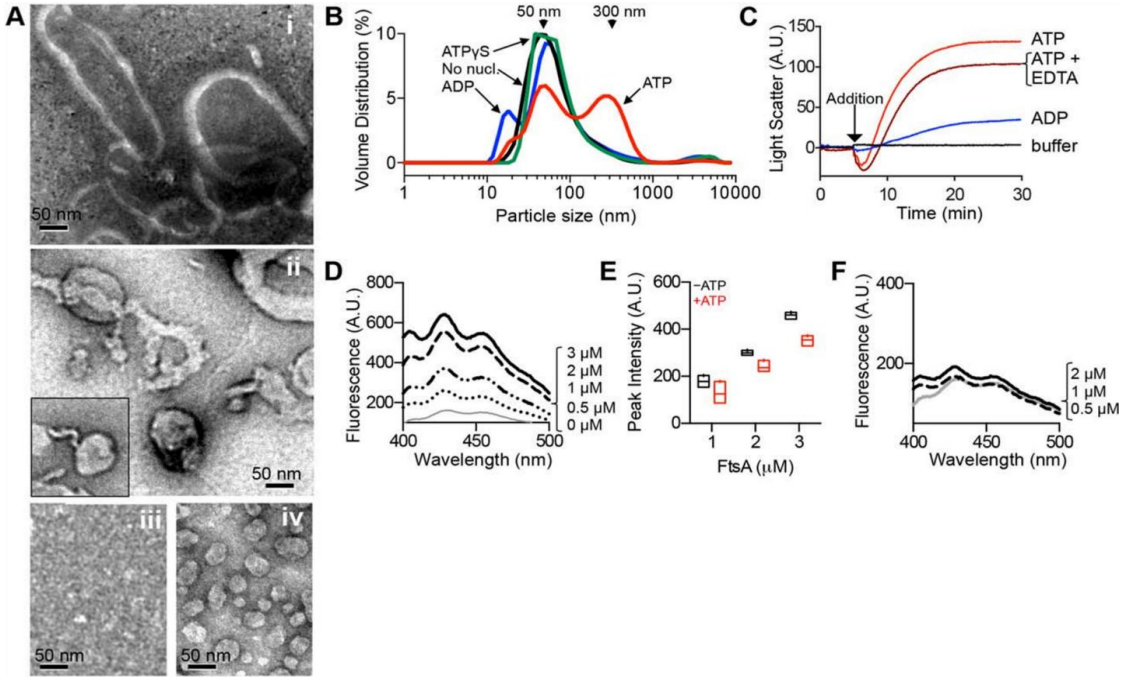
A
i
50 nm
ii
50 nm
iii
50 nm
iv
50 nm
B
50 nm
300 nm
ATPγS
No nucl.
ADP
ATP
Volume Distribution (%)
Particle size (nm)
C
Addition
ATP
ATP + EDTA
ADP
buffer
Light Scatter (A.U.)
Time (min)
D
3 μM
2 μM
1 μM
0.5 μM
0 μM
Fluorescence (A.U.)
Wavelength (nm)
E
-ATP
+ATP
Peak Intensity (A.U.)
FtsA (μM)
F
2 μM
1 μM
0.5 μM
Fluorescence (A.U.)
Wavelength (nm)

Fig. 3. The C-terminal MTS of FtsA inserts into SUVs and is modified by ATP.

A. TEM of FtsA (3 μM) extracted from copurifying PLs and supplemented with SUVs (500 μg ml^{-1}) and ATP (4 mM) (i and ii). Prior to the addition of SUVs and ATP, FtsA was extracted from copurifying PLs with 2% TX100, then exchanged into buffer without detergent (i) and also treated with a detergent removal spin column ($FtsA_{extracted}$-DR) (ii and inset). In control reactions, extracted FtsA ($FtsA_{extracted}$-DR) shows no apparent structures (iii) and exogenous SUVs (500 μg ml^{-1}) alone (iv) are uniform and approximately 50 nm. Size bars are 50 nm. B. Dynamic light scatter of FtsA (2 μM), as described in Experimental Procedures, alone or incubated with ATP (4 mM), ADP (2 mM) or ATPγS (2 mM) for 30 min at 23°C and scanned 11 times. Plots shown are an average of three independent experiments, each with 11 scans. FtsA used in B contains copurifying PLs. C. Reaction mixtures containing FtsA (2 μM) were monitored by 90° light scatter as described in Experimental Procedures. A baseline was collected for 5 min, then ATP (4 mM) with and without EDTA (15 mM), ADP (2 mM) or buffer was added, and signal monitored for an additional 25 min. FtsA used in C contains copurifying PLs. D. Dose-dependent FRET efficiency from the FtsA W408 and W415 tryptophan donors, both in the MTS, to DPH incorporated into liposomes(100 μg ml^{-1}) (1:500 w/w) was examined by emission of DPH fluorescence as described in Experimental Procedures. Traces show increasing FtsA concentrations (0, 0.5, 1.0, 2.0 and 3.0 mM). FtsA used in D contains copurifying PLs and DPH-treated SUVs were added. E. Box and whiskers plot of FRET efficiency of several FtsA concentrations (0.5, 1.0 and 2.0 mM) in the presence (red) or absence (black) of

ATP (4 mM). The box encompasses the maximum and minimum values. The line within each box represents the median (n 5 3). F. FRET efficiency of increasing concentrations of FtsA(ΔMTS) (0.5, 1.0 and 2.0 mM) to DPH incorporated in liposomes (100 μg ml^{-1}). Data in B-D and F are representative of three trials.

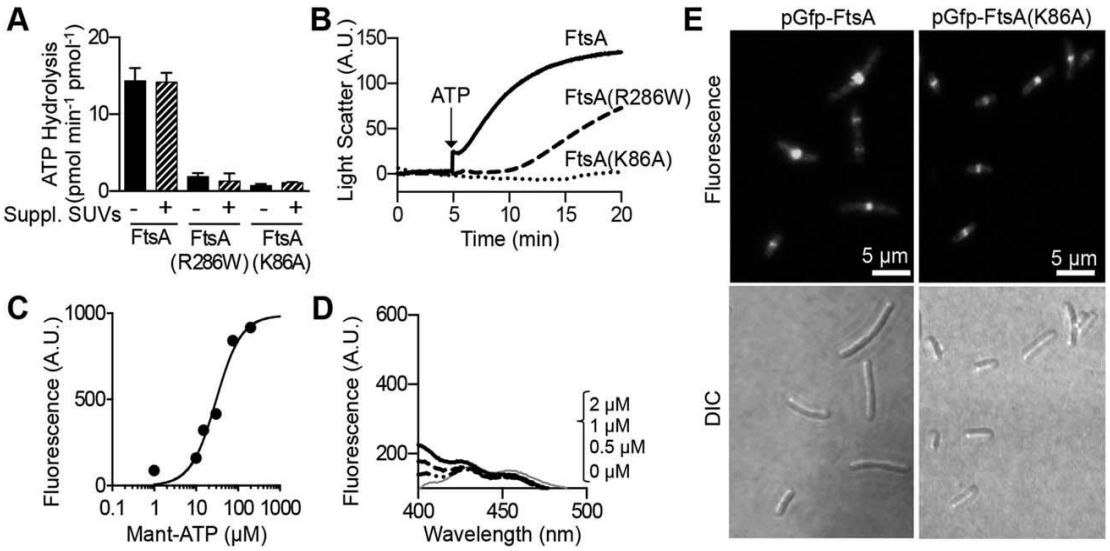
A
ATP Hydrolysis (pmol min-1 pmol-1)
20
10
0
Suppl. SUVs - + - + - +
FtsA
FtsA (R286W)
FtsA (K86A)
B
Light Scatter (A.U.)
150
100
50
0
ATP
FtsA
FtsA(R286W)
FtsA(K86A)
0 5 10 15 20
Time (min)
C
Fluorescence (A.U.)
1000
500
0
0.1 1 10 100 1000
Mant-ATP (μM)
D
Fluorescence (A.U.)
600
400
200
2 μM
1 μM
0.5 μM
0 μM
400 450 500
Wavelength (nm)
E
pGfp-FtsA
pGfp-FtsA(K86A)
Fluorescence
DIC
5 μm
5 μm

Fig. 4. FtsA(K86A), which contains a mutation in a loop near the active site, is defective for function.

A. ATP hydrolysis by FtsA (1 μM), FtsA(K86A) (1 μM) or FtsA(R286W) (1 μM), with and without supplemental SUVs (500 μg ml^{-1}), where indicated. Data is an average of three replicates represented as mean +/- SEM. FtsA wild type and mutant protein used in A contain copurifying PLs. B. Phospholipid reorganization by FtsA (2 μM), FtsA(K86A) (2 μM) or FtsA(R286W) (2 μM) were monitored by 90° angle light scatter. A baseline signal was measured for 5 min then ATP was added and monitored for 60 min. Data is representative of three replicates. FtsA wild type and mutant protein used in B contain copurifying PLs. C. Binding of FtsA(K86A) to mant-ATP monitored by measuring fluorescence emission at increasing mant-ATP concentrations as described in Experimental procedures. D. FRET efficiency of increasing concentrations of the FtsA(K86A) MTS to DPH incorporated in liposomes as described in Experimental procedures. E. Confocal fluorescence and differential interference contrast (DIC) microscopy of wild type cells (MG1655) expressing GFP-FtsA or GFP-FtsA(K86A) induced under growth conditions described in Experimental procedures. Size bars are 5 μm.

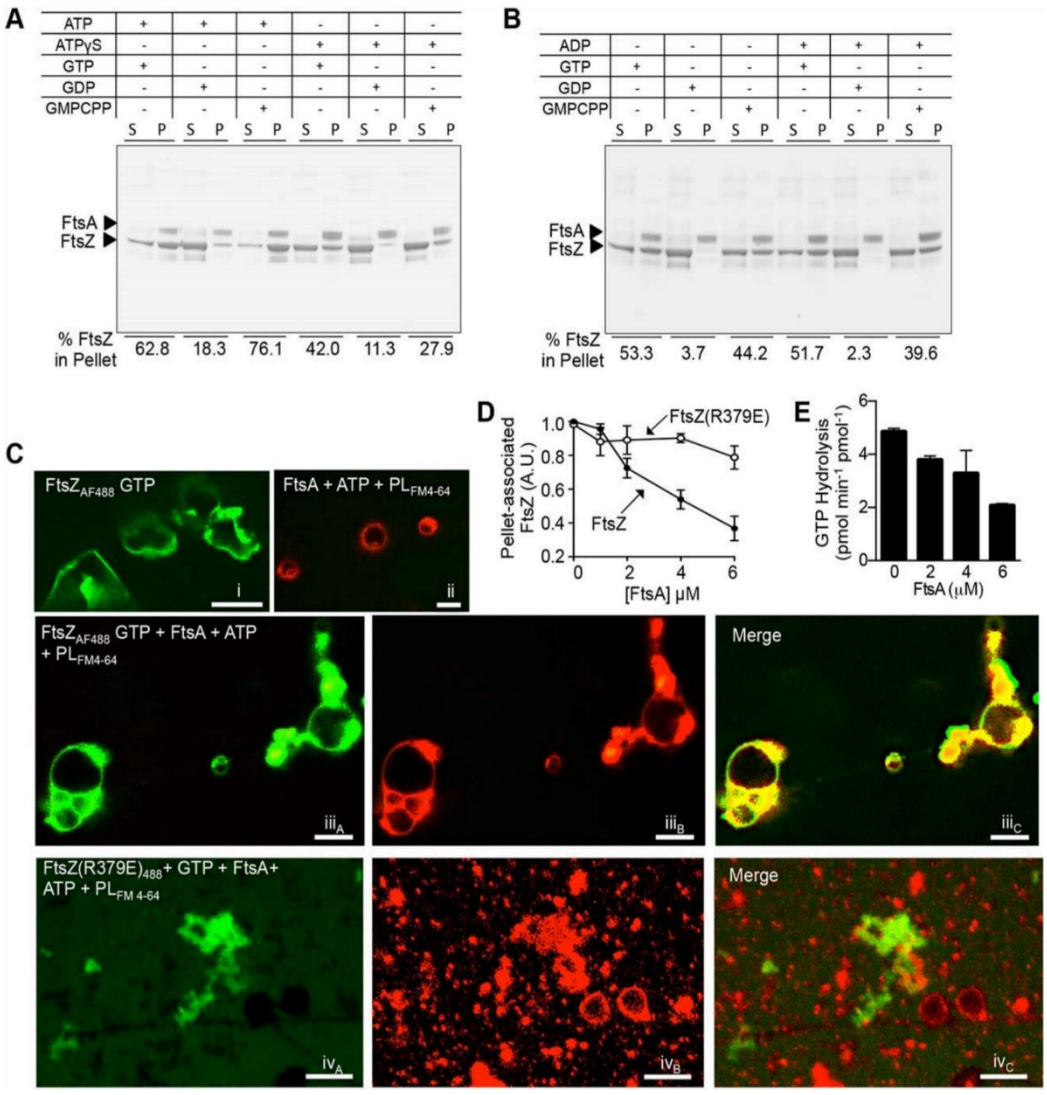
A
ATP
ATPγS
GTP
GDP
GMPCPP
S P
FtsA
FtsZ
% FtsZ in Pellet
62.8 18.3 76.1 42.0 11.3 27.9
B
ADP
GTP
GDP
GMPCPP
S P
FtsA
FtsZ
% FtsZ in Pellet
53.3 3.7 44.2 51.7 2.3 39.6
C
FtsZAF488 GTP
i
FtsA + ATP + PLFM4-64
ii
FtsZAF488 GTP + FtsA + ATP + PLFM4-64
iiiA
iiiB
Merge
iiiC
FtsZ(R379E)488+ GTP + FtsA+ ATP + PLFM 4-64
ivA
ivB
Merge
ivC
D
Pellet-associated FtsZ (A.U.)
FtsZ(R379E)
FtsZ
[FtsA] μM
E
GTP Hydrolysis (pmol min-1 pmol-1)
FtsA (μM)

Fig. 5. FtsA recruits FtsZ to phospholipids and destabilizes steady state FtsZ polymers.

A. Phospholipid recruitment assays with reaction mixtures of FtsZ (6 mM) with GTP, GDP or GMPCPP, as indicated, were pre-assembled and added to pre-incubated mixtures of FtsA (2 mM) and SUVs (500 μg ml^{-1}) with ATP or ATPγS then fractionated as described in Experimental Procedures. Supernatants and resuspended pellets were visualized by SDS-PAGE and quantified by densitometry. The ratio of copurifying to exogenous lipids was 1:2. B. Phospholipid recruitment assay, as in A, but reaction mixtures of FtsZ (6 mM) with GTP, GDP or GMPCPP, as indicated, were preassembled and added to pre-incubated mixtures of FtsA (2 mM) and SUVs with or without ADP then fractionated as previously. C. Confocal fluorescence microscopy was performed in a chamber slide containing FL-FtsZ polymerized with GTP (green) (i) or FtsA, with copurifying PLs stained with FM 4–64 (red) and ATP (ii). Reactions containing FtsA, with copurifying FM 4–64 stained vesicles, ATP, GTP and FL-FtsZ (iii) or FL-FtsZ(R379E) (iv) were assembled and visualized as described in Experimental Procedures. Size bars indicate 5 mm. D. Reactions of FtsA (0 to 6 mM) and, where indicated, FtsZ or FtsZ(R379E) (4 mM), with GTP (2 mM) and ATP (4 mM) were incubated for 5 min, then fractionated by ultracentrifugation. Pellets were visualized by SDS-PAGE and quantified by densitometry. FtsA used in D contains copurifying PLs. E. GTP hydrolysis assays of FtsZ (6 mM) incubated with GTP (1 mM) and increasing concentrations of FtsA (0 to 6 mM) were monitored over time and assayed for free phosphate as described in Experimental Procedures. Data from D and E are an average of three replicates represented as mean +/- SEM.

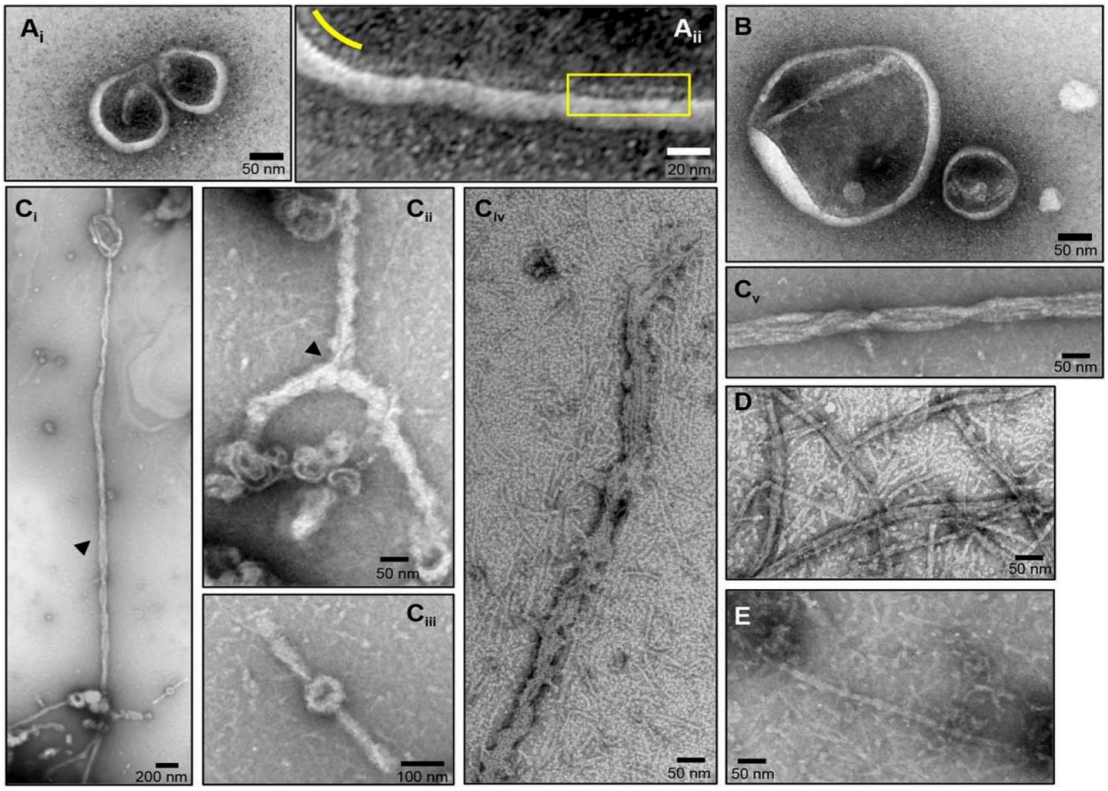
A$_i$
50 nm
A$_{ii}$
20 nm
B
50 nm
C$_i$
200 nm
C$_{ii}$
50 nm
C$_{iii}$
100 nm
C$_{iv}$
50 nm
C$_v$
50 nm
D
50 nm
E
50 nm

Fig. 6. Reconstruction of synthetic proto-ring complexes.

A. FtsA (4 mM) visualized by negative stain TEM with SUVs (500 μg ml^{-1}) and ATP (4 mM). Size bars are 50 nm in Ai and 20 nm in Aii. Yellow line denotes region of negative membrane curvature with FtsA aligned on the surface; yellow box encompasses FtsA aligned on the membrane surface in a region of neutral curvature. The ratio of copurifying to exogenous lipids is 1:1. B. FtsA (2 μM) was visualized by TEM, as in A, in the presence of FtsZ (4 mM). The ratio of copurifying to exogenous lipids is 1:2. C. Synthetic proto-ring complexes were assembled by incubation of FtsA (2 mM), FtsZ (4 mM), ATP (4 mM), GMPCPP (0.2 mM) and SUVs (500 μg ml^{-1}), then visualized by TEM (i-v). Arrows indicate regions of helical twists and/or branches. The ratio of copurifying to exogenous lipids in is 1:2. D. FtsZ (4 mM) with GMPCPP was visualized by TEM. E. TEM, as in D, but FtsZ was incubated with GMPCPP and SUVs (500 μg ml^{-1}). TEM in A-E was performed as described in Experimental procedures.

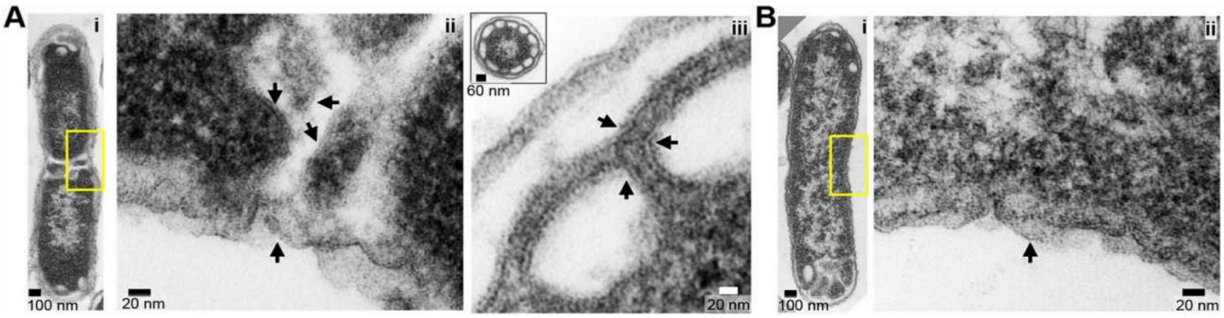
A
i
100 nm
ii
20 nm
60 nm
iii
20 nm
B
i
100 nm
ii
20 nm

Fig. 7. Membrane distortion and intracellular vesicle formation in cells overexpressing FtsA.

A, B. In A, *E. coli* BL21(de3) cells overexpressing FtsA from pET-ftsA (A) or empty vector (B) were grown, fixed, prepared as thin sections and visualized by negative stain TEM as described in Experimental Procedures. Yellow box highlights a region of the septum viewed at higher magnification (Aii, Bii); arrows indicated discernible membranes. In Aiii, clusters of membrane-lined regions accumulated at the cell poles (inset, polar cross-section) of cells overexpressing FtsA, but were rarely observed in cells containing the control vector (Bi).

Supporting Information
Fig. S1

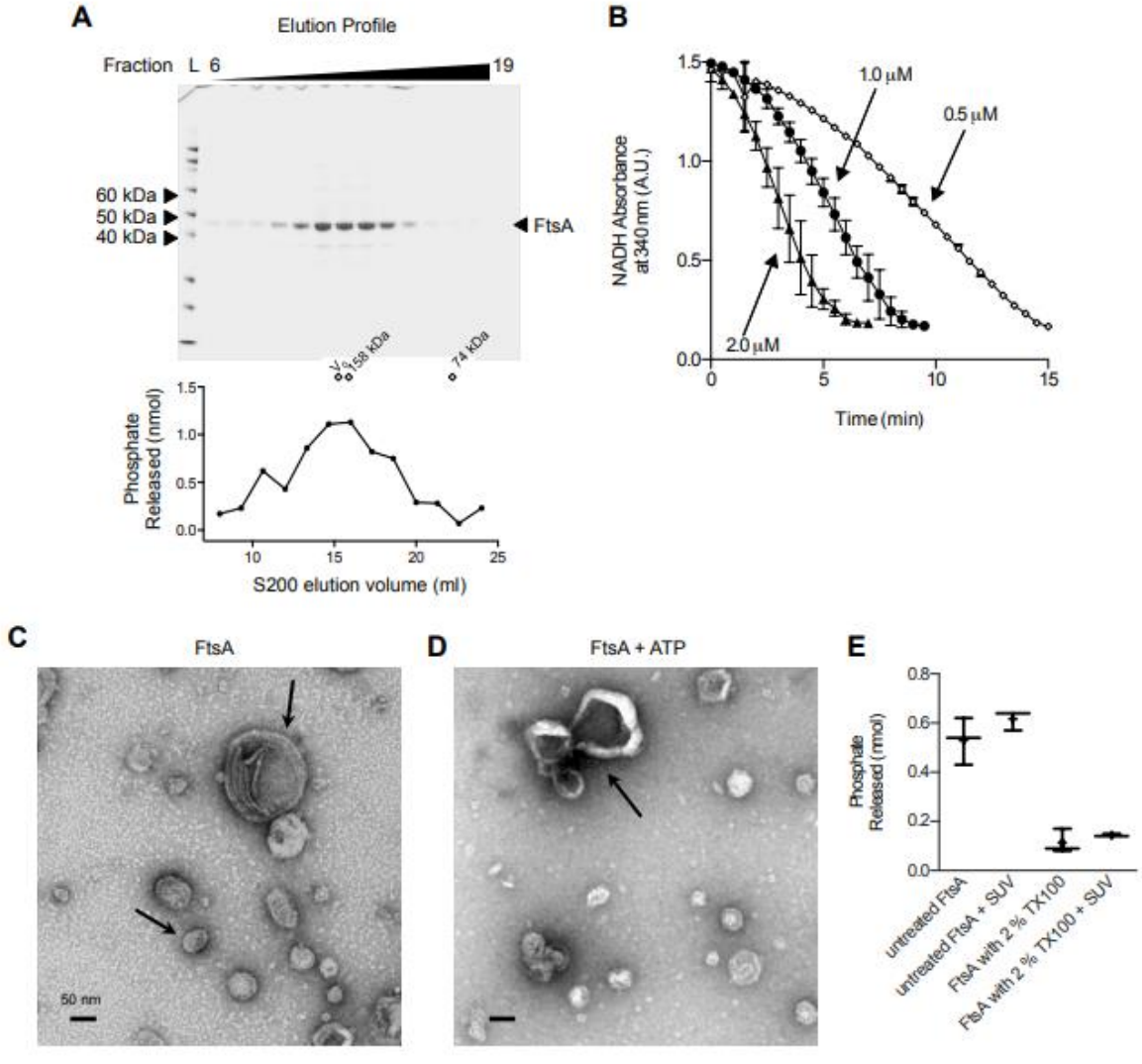

Fig S1. ATP hydrolysis activity trace of purified FtsA and survey of copurified PLs.

A. Elution profile of FtsA by size exclusion chromatography (upper) fractions were analyzed by SDS-PAGE. Equal volume samples from each elution fraction were tested for ATP hydrolysis (lower) by malachite green phosphate detection assay, as described in Experimental Procedures. B. Steady-state ATP hydrolysis by FtsA was monitored by an NADH coupled reaction, as described in Experimental Procedures. FtsA (0.5, 1.0 and 2.0 μM) was incubated with ATP (5 mM), NADH (0.25 mM), phosphoenolpyruvate (1 mM), and 0.2 mg of pyruvate kinase, 0.05 mg of lactic dehydrogenase (all components from Sigma-Aldrich). Reactions were monitored by NADH-associated absorbance at 340 nm for 20 minutes and quantified by comparison to a NADH standard curve. Data are an average of three replicates represented as mean ± SEM. C-D. FtsA (4 μM) and copurified PL vesicles were incubated alone (C) or with ATP (D) and visualized by negative stain TEM, as described in Experimental Procedures. E. Hydrolysis of ATP by FtsA (1 μM) with 2 % TX100 and SUVs, where indicated, was measured after 5 min as described in Experimental Procedures. All measurements were background corrected using no protein controls. Data from three replicates are represented as a box and whiskers plot.

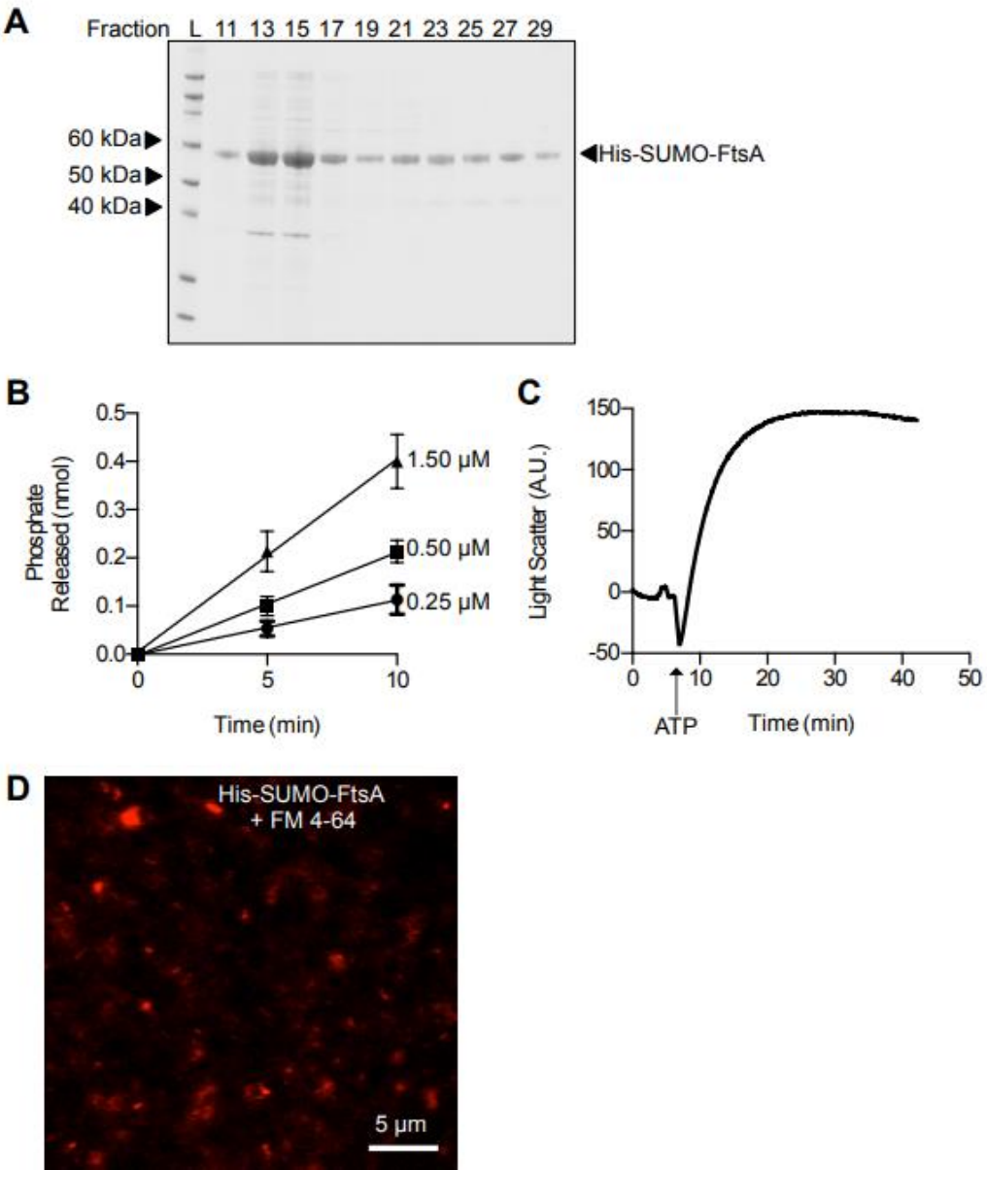
A
Fraction L 11 13 15 17 19 21 23 25 27 29
60 kDa
50 kDa
40 kDa
His-SUMO-FtsA
B
Phosphate Released (nmol)
0.5
0.4
0.3
0.2
0.1
0.0
0
5
10
Time (min)
1.50 μM
0.50 μM
0.25 μM
C
Light Scatter (A.U.)
150
100
50
0
-50
0
10
20
30
40
50
ATP
Time (min)
D
His-SUMO-FtsA
+ FM 4-64
5 μm

Fig. S2. **His-SUMO-FtsA hydrolyzes ATP and reorganizes phospholipid vesicles.**

A. Elution profile of His-SUMO-FtsA by size exclusion chromatography. Fractions were analyzed by SDS-PAGE and densitometry. B. Hydrolysis of ATP by His-SUMO-FtsA (0.25, 0.50 and 1.50 μM) was monitored with time as described in Experimental Procedures; phosphate was detected by malachite green. Data is an average of three replicates represented as mean ± SEM. C. Reaction mixtures containing His-SUMO-FtsA (2 μM) were monitored by 90^{o} light scatter as described in Experimental Procedures. A baseline was collected for 5 min, then ATP was added and the signal was monitored for an additional 40 min. Data is representative of three trials. D. His-SUMO-FtsA was stained with FM4-64 and injected into a flow chamber and visualized by confocal fluorescence microscopy.

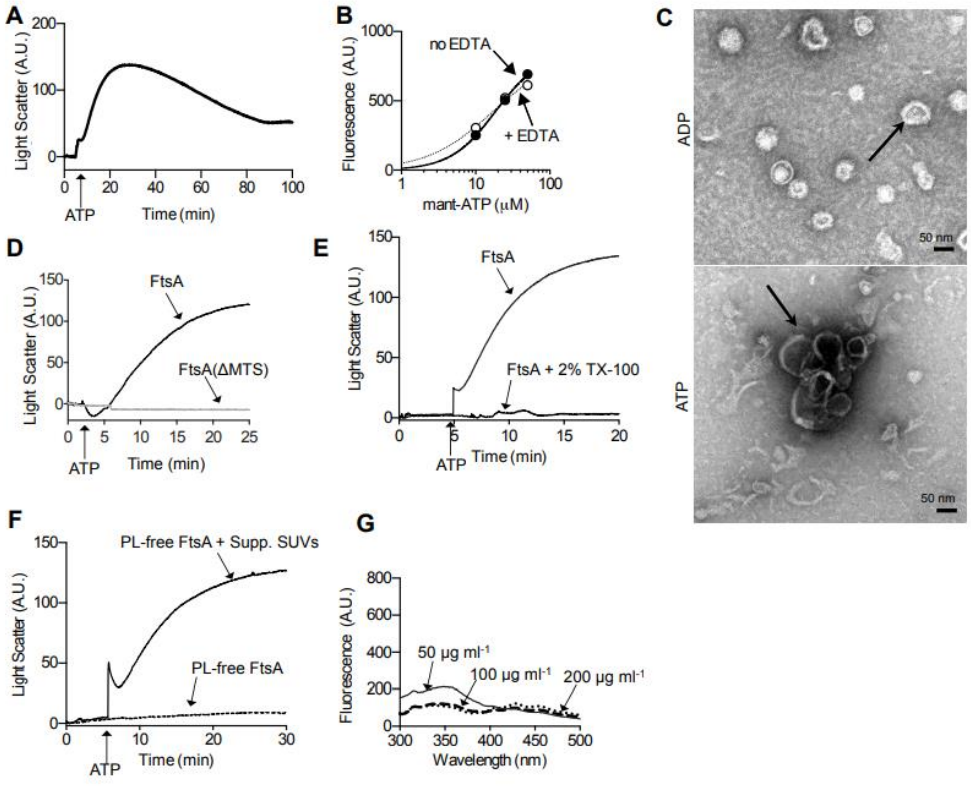
A
Light Scatter (A.U.)
200
100
0
0 20 40 60 80 100
ATP
Time (min)
B
Fluorescence (A.U.)
1000
500
0
no EDTA
+ EDTA
1 10 100
mant-ATP (μM)
C
ADP
50 nm
ATP
50 nm
D
Light Scatter (A.U.)
150
100
50
0
FtsA
FtsA(ΔMTS)
0 5 10 15 20 25
ATP
Time (min)
E
Light Scatter (A.U.)
150
100
50
0
FtsA
FtsA + 2% TX-100
0 5 10 15 20
ATP
Time (min)
F
Light Scatter (A.U.)
150
100
50
0
PL-free FtsA + Supp. SUVs
PL-free FtsA
0 10 20 30
ATP
Time (min)
G
Fluorescence (A.U.)
800
600
400
200
0
50 μg ml-1
100 μg ml-1
200 μg ml-1
300 350 400 450 500
Wavelength (nm)

Fig. S3

Nucleotide-induced changes in light scatter by FtsA require an intact MTS and PLs. A. 90° angle light scatter, as in Experimental Procedures, of FtsA (2 μM), was performed with ATP added after 5 min and reactions were monitored for 100 min. Data are representative of three trials. B. Binding of FtsA (2 μM) to mant-ATP in the presence or absence of EDTA (15 mM) was monitored by measuring fluorescence emission at increasing mant-ATP concentrations (10, 25, 50 μM) as described in Experimental Procedures. C. FtsA (4 μM) and SUVs were incubated with ADP (upper) or with ATP (lower) and visualized by negative stain TEM, as described in Experimental Procedures. At 4 μM FtsA, the ratio of copurifying to exogenous lipids was 1:1. D. 90° angle light scatter of FtsA and FtsA(ΔMTS) (2 μM) was performed. A baseline signal was measured for 5 min then ATP was added and reactions were monitored for 25 min. Data are representative of three trials. E. 90° Light scatter of FtsA (2 μM) and ATP in the presence and absence of 2% TX100 and monitored for 20 min. Data are representative of three trials. F. 90° Light scatter of FtsA (2 μM), that was extracted with detergent and then exchanged into assembly buffer without detergent, and ATP was added with or without exogenous PLs (SUV 500 μg ml-1) and monitored for 25 min. Data are representative of three trials. G. FRET efficiency with increasing concentrations of PL vesicles (50, 100, 200 μg ml-1) by DPH (100 μg ml-1) incorporated in liposomes, performed as described in Experimental Procedures. Data are representative of three trials.

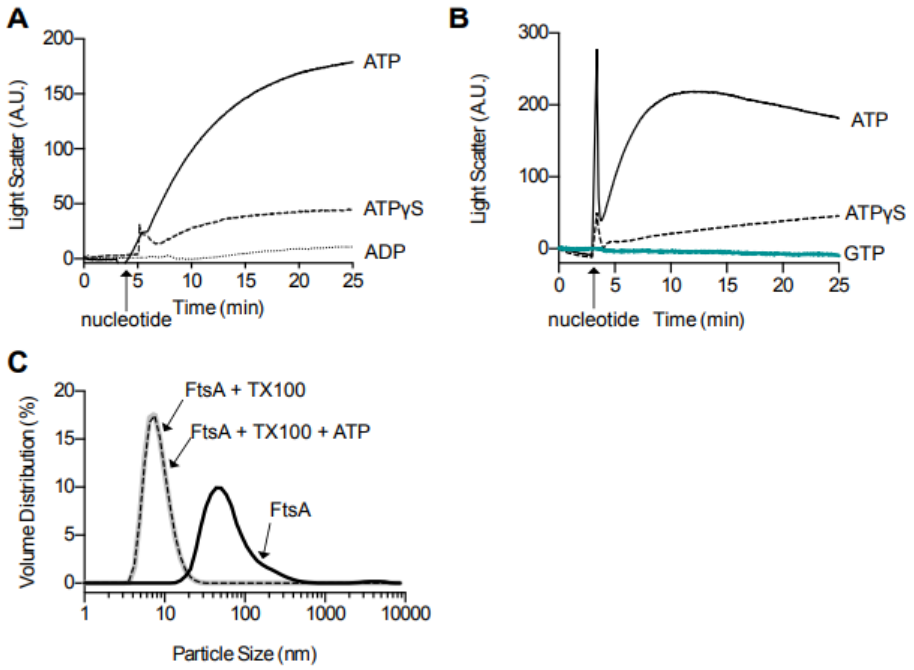
A
Light Scatter (A.U.)
200
150
100
50
0
ATP
ATPγS
ADP
0
5
10
15
20
25
nucleotide
Time (min)
B
Light Scatter (A.U.)
300
200
100
0
ATP
ATPγS
GTP
0
5
10
15
20
25
nucleotide
Time (min)
C
Volume Distribution (%)
20
15
10
5
0
FtsA + TX100
FtsA + TX100 + ATP
FtsA
1
10
100
1000
10000
Particle Size (nm)

Fig. S4

FtsA PL reorganization and particle size distribution under varying nucleotide conditions. A. 90° angle light scatter was monitored, as described in Experimental Procedures, of FtsA (2 μM), with ATP (4 mM), ADP (2 mM) or ATPγS (2 mM) added after 5 min. Reactions were monitored for 25 min. Data is representative of three trials. B. 90° angle light scatter was monitored as in 'A' of FtsA (2 μM), with ATP (4 mM), ATPγS (4 mM) or GTP (4 mM) added after 5 min. Reactions were monitored for 25 min. Data is representative of three trials. C. Dynamic light scatter of FtsA (2 μM), as in Experimental Procedures, incubated with and without ATP in the presence or absence of TX100 (2 %) for 30 min at 23 °C and scanned 11 times. Plots shown are an average of 3 independent experiments, each with 11 scans.

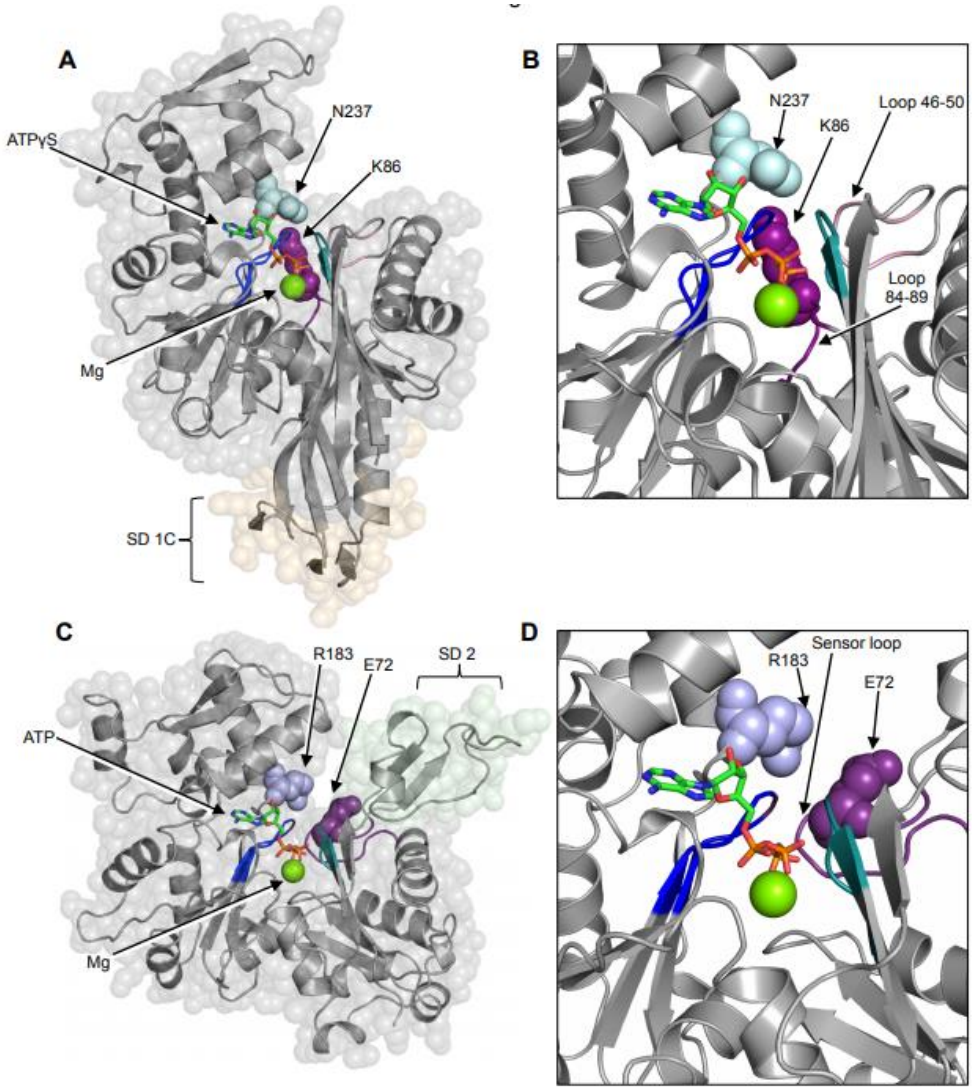
A
ATPγS
N237
K86
Mg
SD 1C
B
N237
K86
Loop 46-50
Loop
84-89
C
ATP
R183
E72
SD 2
Mg
D
R183
Sensor loop
E72

Fig. S5

Comparison of FtsA and actin active sites. A. *E. coli* FtsA (residues 13-381) modeled onto *T. maritima* FtsA (pdb: 4A2B) (Szwedziak et al., 2012). Subdomain '1C' (gold, 89-155) is shown. Amino acids Lys 86 (purple) and Asn 237 (light blue) are shown as CPK models. ATPγS is shown as a stick model and magnesium is shown as a green sphere. B. *E. coli* FtsA active site, as in A, highlighting positions bearing similarity to phosphate binding loops P1 (teal, 16-20) and P2 (blue, 210-217), putative sensor loop (purple, 84-89) and an additional candidate sensor loop (pink, 46-50). C. S. cerevisiae actin (residues 4-375) (pdb: 1YAG) (Vorobiev et al., 2003). Subdomain 2 (green, 89-155) is shown. Amino acids Glu 72 (purple) and Arg 183 (light blue), which forms a salt bridge at the rear of the active site (Murakami et al., 2010), are shown as CPK models. ATP is shown as a stick model and magnesium is shown as a green sphere. D. S. cerevisiae actin active site, as C, highlighting positions of phosphate binding loops P1 (teal, 11-16) and P2 (blue, 154-161) and sensor loop (purple, 70-78) (Kudryashov & Reisler, 2013, Vorobiev et al., 2003).

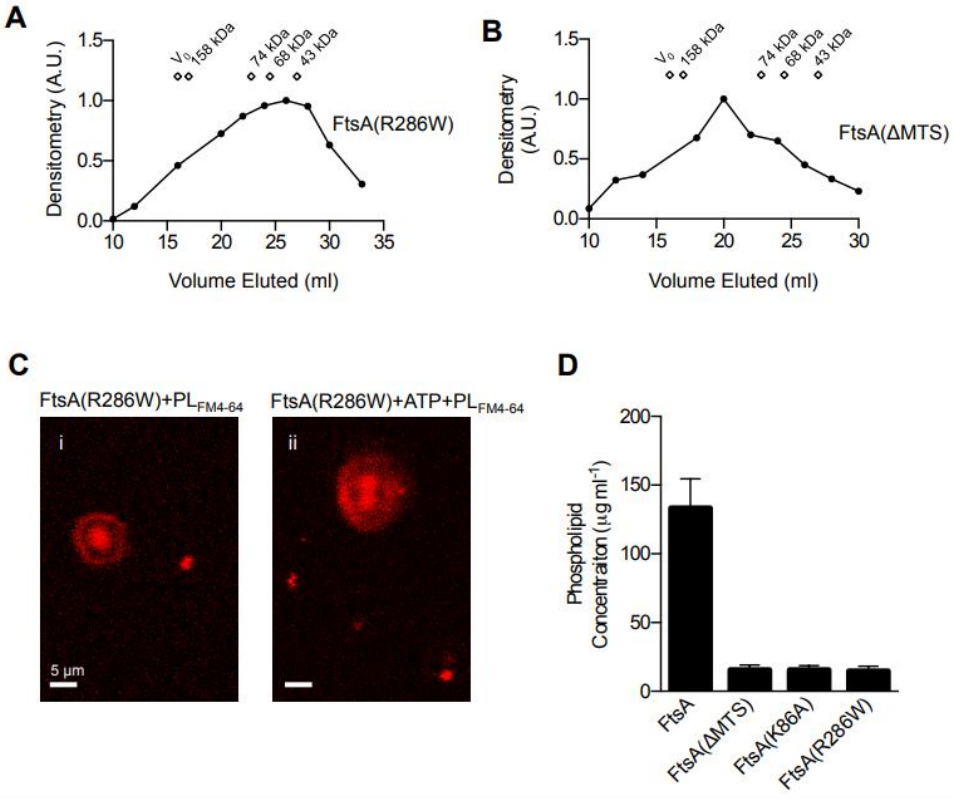
A
Densitometry (A.U.)
1.5
1.0
0.5
0.0
10
15
20
25
30
35
Volume Eluted (ml)
V_0
158 kDa
74 kDa
68 kDa
43 kDa
FtsA(R286W)
B
Densitometry (A.U.)
1.5
1.0
0.5
0.0
10
15
20
25
30
Volume Eluted (ml)
V_0
158 kDa
74 kDa
68 kDa
43 kDa
FtsA(ΔMTS)
C
FtsA(R286W)+PL_{FM4-64}
FtsA(R286W)+ATP+PL_{FM4-64}
i
ii
5 µm
D
Phospholipid Concentration (µg ml^{-1})
200
150
100
50
0
FtsA
FtsA(ΔMTS)
FtsA(K86A)
FtsA(R286W)

Fig. S6

Characterization of FtsA(R286W) and lipid content of FtsA mutant proteins. A. Elution profile of FtsA(R286W) by size exclusion chromatography. Elution profile was plotted by densitometry of band intensities after SDS-PAGE of eluting fractions and coomassie staining and compared to known protein standards. Vo indicates the position of the void volume. B. Elution profile of FtsA(ΔMTS) by size exclusion chromatography. Elution profile was plotted by densitometry of band intensities after SDS-PAGE of eluting fractions and coomassie staining and compared to known protein standards. Vo indicates the position of the void volume. C. Purified FtsA(R286W) was stained with FM4-64 and injected into a flow chamber and visualized by confocal fluorescence microscopy in the presence (i) or absence (ii) of ATP. Size bar indicates 5μm. D. Purified samples of FtsA or FtsA mutant proteins (1 μM) were stained with FM 4-64 (1.25 μg ml-1). Fluorescence was measured and compared to a standard curve of known PL concentration as described in Experimental Procedures.

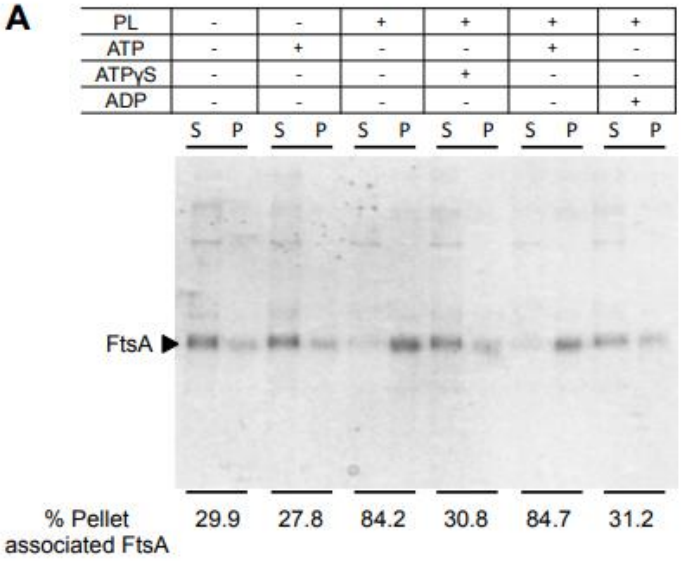
A
PL - - + + + +
ATP - + - - + -
ATPγS - - - + - -
ADP - - - - - +
S P S P S P S P S P S P
FtsA
% Pellet associated FtsA
29.9 27.8 84.2 30.8 84.7 31.2
B
PL - + + +
FtsA - - + +
ATP - - - +
GTP + + + +
P S P S P S P S
FtsA
FtsZ
C
FtsA + + + + + -
ATP - + + + + -
GTP + + - - + +
GMPCPP - - + - - -
GDP - - - + - -
PL + + + + + +
P S P S P S P S P S P S
FtsA
FtsZ(R379E)
% FtsZ(R379E) in Pellet
6.4 35.6 14.8 35.5 3.7 1.9

Fig. S7. FtsA-dependent recruitment of FtsZ to PLs. A. Phospholipid recruitment assay, as described in Experimental Procedures, with reaction mixtures of FtsA (2 μM) incubated in the presence or absence of PL vesicles and indicated nucleotide conditions. Supernatants and resuspended pellets were visualized by SDS-PAGE. B. Phospholipid recruitment assays with reaction mixtures of FtsZ (6 μM) and guanine nucleotide as indicated, were added to FtsA (2 μM), SUVs and adenine nucleotide, then fractionated as described in Experimental Procedures. Supernatants and resuspended pellets were visualized by SDS-PAGE. C. Phospholipid recruitment assay, as B, but with FtsZ(R379E), FtsA and nucleotide conditions as indicated.

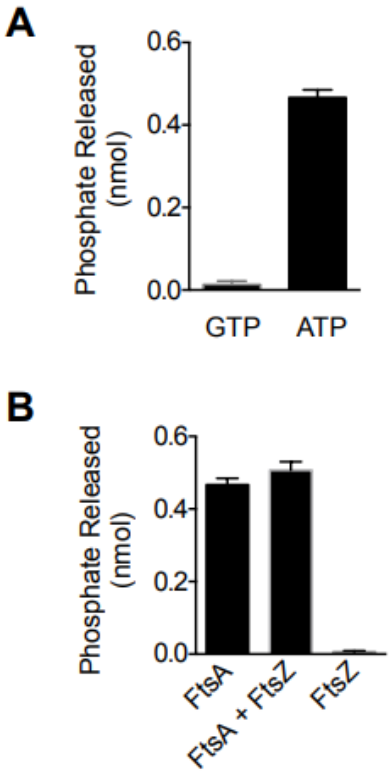
A
Phosphate Released (nmol)
0.6
0.4
0.2
0.0
GTP
ATP
B
Phosphate Released (nmol)
0.6
0.4
0.2
0.0
FtsA
FtsA + FtsZ
FtsZ

Fig. S8. Nucleotide Hydrolysis by FtsA and FtsZ. A. Hydrolysis of GTP or ATP by FtsA (1 μM) was monitored with time as described in Experimental Procedures, and phosphate was detected by malachite green reagent. B. Hydrolysis of ATP by FtsA (2 μM) and/or FtsZ (6 μM) was monitored with time as described in Experimental Procedures, and phosphate was detected by malachite green reagent. Data in A and B are an average of three replicates represented as mean ± SEM.

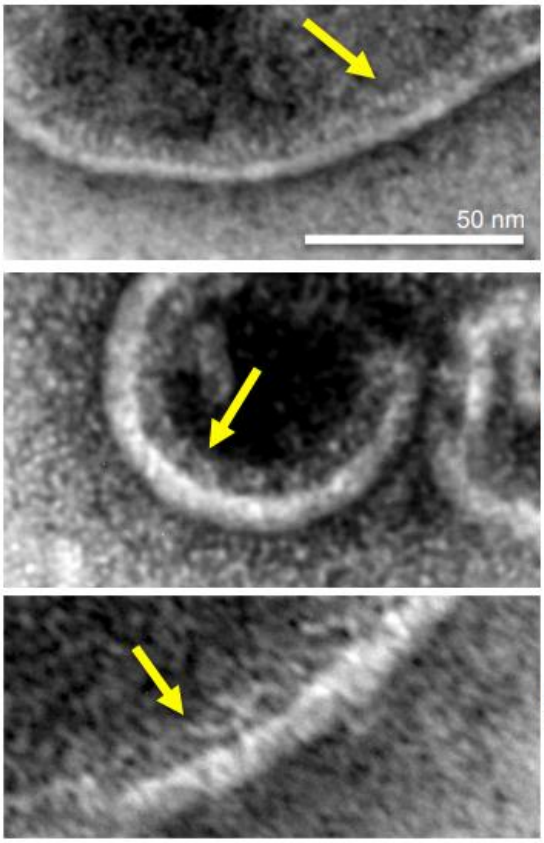

Detergent-solubilized FtsA
Resupplemented with SUVs
and ATP

FtsA with copurifying vesicles
Resupplemented with SUVs
and ATP

FtsA with copurifying vesicles
and ATP

Fig. S9. TEM of putative FtsA protomers, consistent in size with FtsA cytoplasmic domains, aligned on a phospholipid surface. Shown are images of detergent-extracted FtsA supplemented with SUVs (upper), FtsA with copurified vesicles and supplemented with exogenous PLs (middle), or FtsA with copurified vesicles (lower); all were incubated with ATP and visualized by TEM. High resolution images show nodules aligning on PL surface indicated by arrowheads. Size bars indicate 50 nm.

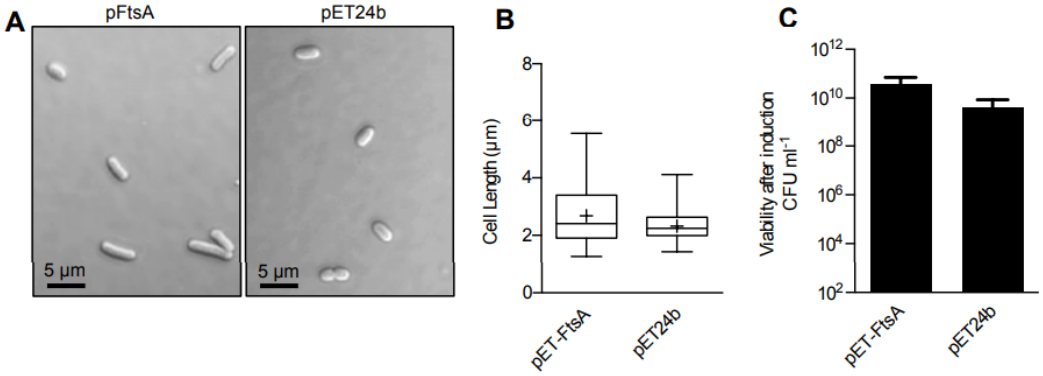
A
pFtsA
pET24b
5 µm
5 µm
B
Cell Length (µm)
0
2
4
6
8
pET-FtsA
pET24b
C
Viability after induction
CFU ml-1
10^2
10^4
10^6
10^8
10^10
10^12
pET-FtsA
pET24b

Fig. S10. BL21 cells overexpressing FtsA are similar in length and viability to cells with empty vector A. Confocal differential interference contrast (DIC) microscopy of BL21 expressing FtsA or empty vector induced with 0.5 mM IPTG for 20 hours at 16 °C. Size bars are 5 μm. Individual cells were chosen as representative of the population. B. Cells expressing FtsA (n=174) or empty vector (n=117), from (A), were measured for length using NIH ImageJ. Cells lengths are shown as a box-and-whisker plot. The extent of the box encompasses the interquartile range of the cell length, and whiskers extend to the maximum and minimum values. The line within each box represents the median and the cross within each box represents the mean. C. Cell viability after 20 h of induction 16 °C was determined by measuring colony forming units (CFU ml−1) of cultures expressing FtsA or containing empty vector.

Row	Index	Peak Name[2]	Group[2]	FtsA(ΔMTS) Mean 1	FtsA Mean 2	Difference[3]	p-value
183	52	PE 34:1 (FA 18:1)	PE	315.81	9117.05	-8801.24	0.0489
200	38	PE 33:1 (FA 16:0)	PE	153.42	3100.77	-2947.35	0.0499
195	49	PE 34:1 (FA 16:0)	PE	123.76	3019.57	-2895.82	0.0495
155	26	PE 32:1 (FA 16:1)	PE	98.04	2799.56	-2701.52	0.0465
179	47	PE 34:2 (FA 18:1)	PE	35.96	1278.76	-1242.79	0.0484
176	27	PE 32:1 (FA 16:0)	PE	39.23	992.38	-953.15	0.0483
139	20	PE 30:0 (FA 14:0)	PE	19.47	960.28	-940.81	0.0454
181	117	CL 78:7 (FA 19:1)	CL	16.41	663.44	-647.03	0.0488
194	61	PE 35:1 (FA 16:0)	PE	28.70	495.76	-467.06	0.0494
143	64	PE 35:1 (FA 18:1)	PE	19.85	482.07	-462.21	0.0457
199	106	PE 37:2 (FA 19:1)	PE	16.96	453.87	-436.91	0.0499
132	193	CL 68:1 (FA 18:1)	CL	12.63	407.24	-394.61	0.0449
16	1765	TAG 50:6+NH4 (-FA 20:5 (NH4))	TAG	0.00	387.12	-387.12	0.0363
198	113	CL 78:7 (FA 17:1)	CL	15.66	372.92	-357.26	0.0498
40	1756	TAG 46:5+NH4 (-FA 20:5 (NH4))	TAG	0.00	313.98	-313.98	0.0384
95	1388	MADAG 46:2+NH4 (-FA 16:1 (NH4))	MADAG	4.98	282.16	-277.19	0.0419
72	152	PS 37:2 (FA 18:1)	PS	2.60	278.92	-276.32	0.0406
153	35	PE 33:2 (FA 17:1)	PE	11.24	241.47	-230.23	0.0464
133	29	PE 32:1 (FA 18:1)	PE	5.43	235.05	-229.62	0.0450
48	191	PE 33:2 (FA 16:1)	PE	3.66	214.99	-211.33	0.0394
184	102	PG 34:1 (PA,PG,PI,CL,PIP,PIP3)	PG	11.29	215.95	-204.66	0.0489
94	307	CL 82:5 (FA 17:1)	CL	0.00	202.82	-202.82	0.0419
202	157	CL 84:5 (FA 18:1)	CL	8.48	203.70	-195.23	0.0500
129	501	CL 70:4 (FA 18:1)	CL	0.00	194.10	-194.10	0.0443
83	363	CL 74:7 (FA 18:1)	CL	0.00	152.79	-152.79	0.0412
20	422	PE 31:1 (FA 17:1)	PE	0.00	150.47	-150.47	0.0366
130	645	CL 78:4 (FA 17:1)	CL	0.00	139.98	-139.98	0.0444
113	194	PE 32:2;1 (LPE e)	PE	3.63	142.53	-138.90	0.0430
188	37	PE 33:1 (FA 16:1)	PE	5.55	141.99	-136.44	0.0491

[1] MS/MS was performed to determine identity and comparative distribution of lipids as described in Liaw, L., I. Prudovsky, R.A. Koza, R.V. Anunciado-Koza, M.E. Siviski, V. Lindner, R.E. Friesel, C.J. Rosen, P.R. Baker, B. Simons & C.P. Vary, (2016) Lipid Profiling of In Vitro Cell Models of Adipogenic Differentiation: Relationships With Mouse Adipose Tissues. *J Cell Biochem* **117**: 2182-2193.

[2] Lipid groups are defined as PE, phosphatidylethanolamine; CL, cardiolipin; TAG, tracylglycerol; MADAG, monoalkyl diacylglycerol; and PS, phosphatidylserine.

[3] Difference is defined by the relative signal intensity from FtsA(ΔMTS) Mean 1 minus the relative signal intensity from FtsA Mean 2 for controlled compare samples.

Table S1: MS/MS identification of major lipid species present in FtsA and FtsA(ΔMTS)

1. MS/MS was performed to determine identity and comparative distribution of lipids as described in Liaw, L., I. Prudovsky, R.A. Koza, R.V. Anunciado-Koza, M.E. Siviski, V. Lindner, R.E. Friesel, C.J. Rosen, P.R. Baker, B. Simons & C.P. Vary, (2016) Lipid Profiling of In Vitro Cell Models of Adipogenic Differentiation: Relationships With Mouse Adipose Tissues. J Cell Biochem 117: 2182-2193. 2. Lipid groups are defined as PE, phosphatidylethanolamine; CL, cardiolipin; TAG, tracylglycerol; MADAG, monoalkyl diacylglycerol; and PS, phosphatidylserine. 3. Difference is defined by the relative signal intensity from FtsA(ΔMTS) Mean 1 minus the relative signal intensity from FtsA Mean 2 for controlled compare samples.

Manuscript IV

Publication status: Formatted for *Journal of Molecular Biology*

Title: Nucleotide-dependent polymerization and lateral membrane-association by the cell division protein FtsA

Authors: Joseph Conti1[1], Evelyn M. Siler[1], Jodi L. Camberg[1,2]*

Author Affiliations:

[1]Department of Cell and Molecular Biology,

College of Environment and Life Sciences,

University of Rhode Island, Kingston, RI, USA

[2]Department of Nutrition and Food Sciences

The University of Rhode Island

Kingston, RI 02881

***Corresponding author**: Jodi L. Camberg,

120 Flagg Road, Kingston, RI, 02881;

Tel: (401)874-4961;

Email: cambergj@uri.edu

Keywords: cell division; FtsA; divisome; polymerization; actin-like

Abbreviations: MTS, membrane targeting sequence; PL, phospholipid; SUV, small unilamellar vesicle; TEM, transmission electron microscopy; ADP, Adenosine diphosphate; ATP- γ-S, adenosine 5′-[γ-thio]triphosphate; ATP, Adenosine triphosphate; *E. coli*, *Escherichia coli*; EDTA, ethylenediaminetetraacetic acid; FtsA, filamentous temperature sensitive mutant A; GTP, Guanosine-5'-triphosphate; GDP-AlF3, Guanosine-5'-diphosphate-aluminum fluoride; TIRF, total internal reflection fluorescence; PG, peptidoglycan; PLs, phospholipids

Abstract

The prokaryotic cell division protein FtsA is an actin-like ATPase that is highly conserved among prokaryotes and is essential in *Escherichia coli*. FtsA directly recruits polymers of FtsZ to the cytoplasmic face of the inner membrane mediated by a C-terminal membrane targeting sequence (MTS) which intercalates into the lipid bilayer. In vitro, FtsA purified from *E. coli* directly reorganizes phospholipid (PL) architecture and remodels dynamic FtsZ polymers. Truncated FtsA mutant proteins from *Streptococcus pneumoniae* and *Thermotoga maritima* missing the C-terminal MTS (FtsAΔMTS) have been reported to polymerize in the presence of ATP. To determine if *E. coli* FtsAΔMTS undergoes a large conformational change in the presence of nucleotide we performed biophysical assays and transmission electron microscopy (TEM) using purified *E. coli* FtsAΔMTS in the presence of ATP. We observed that FtsAΔMTS incubated with ATP forms high molecular weight complexes, which assemble in a concentration-dependent manner and are polymers by TEM. To determine if nucleotide affects PL engagement by FtsA, we performed sedimentation assays in the presence and absence of nucleotide. We observed that FtsA binds PLs with and without ATP and that FtsAΔMTS is unable to bind PLs when ATP is omitted. However, FtsAΔMTS is recruited to PLs in the presence of ATP suggesting that FtsAΔMTS associates with PLs by an ATP-dependent interaction. Together, these results suggest that FtsA forms ATP-dependent polymers and that FtsA contains a surface-exposed residues which mediate a secondary site of membrane association that is ATP-dependent. These studies provide insight into a highly conserved interaction during early prokaryotic cell division.

Introduction

The hallmark of bacterial cell division is the formation of protein structure called the Z-ring which assembles at the septum. The Z-ring consists of two highly conserved proteins, FtsZ and FtsA (Haeusser & Margolin 2016). FtsZ is a homolog of the eukaryotic cytoskeletal protein tubulin and, in vitro, polymerizes in the presence of GTP (Mukherjee & Lutkenhaus 1998). In vivo, the regulated assembly of staggered bundles of FtsZ polymers forms the Z-ring (Lutkenhaus et al. 2012). FtsA, which shares structural homology with the actin family of proteins, contains a highly conserved 15 residue C-terminal MTS (Pichoff & Lutkenhaus 2005). FtsA binds to the C-terminal region of FtsZ and tethers the Z-ring to the inner face of the cytoplasmic membrane (van den Ent & Löwe 2000; Szwedziak et al. 2012). In *E. coli*, FtsA and FtsZ arrive first and simultaneously at the site of cell division and assemble into a nascent Z-ring which acts as a scaffold to sequentially recruit at least 10 additional essential cell division proteins (Söderström et al. 2016). FtsN, a bitopic membrane protein that activates peptidoglycan synthesis, is directly recruited to the Z-ring by FtsA (Shiomi & Margolin 2008; Busiek et al. 2012; Du et al. 2016). Recruitment of FtsN marks the formation of a mature Z-ring and acts as a landmark to recruit late septal proteins that insert additional peptidoglycan at the division site (Rico et al. 2010).

There are several potential mechanisms by which the Z-ring and its downstream components may generate the constrictive force to overcome the turgor pressure of the cell and achieve septation(Osawa & Erickson 2018). During cell

division, constrictive force may be generated by the activity and assembly or disassembly of cytoskeletal structures. In addition, generation of new cell membrane at the site of cell division may also contribute to the overall force applied during division as older membrane becomes displaced. Constrictive force generated on the cytoplasmic face of the division septum may be generated by the Z-ring. X-ray crystallography and negative stain TEM show two distinct conformations of FtsZ polymers, a straight polymer or a bent polymer, FtsZ binding non-hydrolyzable GTP promotes straight polymers and polymers containing GTP adapt various degrees of curvature(Lu et al. 2000) and therefore it was suggested that bending force may be coupled to constriction (Li et al. 2007). Constrictive force generated on the cytoplasmic face of the septum may also be generated by FtsZ polymers treadmilling whereby a polymer grows at one end and disassembles at the opposite end, and the directional motion may provide directional force. Evidence for FtsZ filaments undergoing treadmilling comes from in vivo and in vitro observations by TIRF-microscopy which both support that FtsZ undergoes treadmilling and that movement of FtsZ polymers depends on the rate of GTP-hydrolysis and occurs coordinately with FtsA (Loose & Mitchison 2013; Bission-Filho et al. 2017).

Constrictive force generated on the periplasmic face of the division septum is generated by periplasmic proteins that synthesize peptidoglycan at the nascent division site (Gray et al. 2015). FtsN, which has been localized to the Z-ring by FtsA, interacts with additional downstream division proteins to engage peptidoglycan synthesis and remodeling, including murein transpeptidases and glycosyltransferases. Specifically,

this model suggests septal wall synthesis inserts PG at site of cell division to generate force for constriction.

Polymerization of FtsA has been reported by multiple groups (Krupka et al. 2014; Szwedziak et al. 2012; Szwedziak et al. 2014). FtsA is classified as a bacterial actin-like protein due to sequence homology in the enzymatic pocket and structural homology in the FtsA domain architecture (Bork et al. 1992). A more prototypical bacterial actin-like protein, MreB, has four domains (1A, 1B, 2A, 2B) which are spatially organized homologously to the four domains of actin (1-2, 3-4), however, the 1B subdomain of MreB is absent from FtsA and a large sequence insertion is present below subdomain 1A and so this region is referred to as the FtsA 1C switch domain (van den Ent et al. 2014). MreB and actin both form ATP-dependent paired-helical filaments which each exhibit directionality (van den Ent et al. 2014). Observations by electron microscopy suggest FtsA, in the presence of ATP, forms straight single-stranded polymers (Szwedziak et al. 2014). In addition, FtsA has been reported to form a 12-subunit ring-shaped polymer with an inner diameter of 20 nm (Schoenemann et al. 2018). It is unclear how an FtsA polymer functions in cell division, one hypothesis is an FtsA mini-ring opposes FtsZ bundling which promotes stabilization of long-range FtsZ protofilaments (Schoenemann et al. 2018). An alternative hypothesis is that FtsA polymers which form on the membrane may directly reorganize the phospholipid (PL) bilayer (Conti et al. 2017). FtsA hydrolyzes ATP rapidly and performs ATP-dependent lipid reorganization and both functions required an intact MTS (Conti et al. 2017). Polymerization of FtsA is regulated by ATP-binding (Szwedziak et al. 2012), but proteins that bind FtsA, which include FtsN (Geissler et al. 2003) or FtsEX (Du et al.

2016), are thought to inhibit FtsA polymerization. This finding agreed with earlier reports that FtsA can disrupt PL vesicles in the presence of ATP (Krupka et al. 2014) and a separate group which found FtsZ bound to PL vesicles by a mutant FtsA protein could occasionally generate complete scission of the PL vesicles (Osawa & Erickson 2013).

Here, we investigate the role of the FtsA-MTS in FtsA-mediated membrane reorganization. A mutant FtsA protein lacking the C-terminal 15 amino acid MTS (FtsAΔMTS) forms large molecular weight complexes by sedimentation assay and light scatter and appear as polymers by TEM. These polymers are concentration-dependent and fail to assemble when ATP is omitted from the reaction. FtsA binds PLs in the presence or absence of nucleotide (Conti et al. 2017). Interestingly, we report FtsAΔMTS associates to PLs in the presence of ATP and fails to sediment with PLs when nucleotide is omitted. We propose a model of FtsA-mediated lipid remodeling activity: FtsA is anchored to the membrane by the endogenous MTS independent of the nucleotide state. Upon binding ATP, FtsA polymerizes and a surface-exposed site on FtsA associates with the membrane. Upon hydrolysis of ATP by FtsA the filament depolymerizes and the surface exposed region of FtsA dissociates from the membrane yet remains associated to the membrane through the MTS. Rapid ATP hydrolysis may then promote cycles of FtsA membrane association and dissociation.

Results

FtsAΔMTS assembles into polymers in a concentration-dependent manner in presence of ATP

There are several bacterial actin-like proteins that assemble into polymers including MreB, ParM (Bharat et al. 2015; Petek & Mullins 2014; van den Ent et al. 2014) and a C-terminally truncated mutant FtsA purified from *Streptococcus penumoniae* (Krupka et al. 2014). Therefore, we tested if FtsA from *E. coli*, truncated to remove the C-terminal membrane targeting sequence (FtsAΔMTS), could form stable polymers in the presence of nucleotide. To investigate if FtsAΔMTS can form a high molecular weight complexes, we purified FtsAΔMTS and performed sedimentation assays of FtsAΔMTS in the presence and absence of ATP. Increasing concentrations of FtsAΔMTS (4-24 μM) were incubated in the presence and absence of ATP, and then reactions were fractionated by ultracentrifugation. Supernatant and pellet fractions were visualized by SDS-PAGE and coomassie staining. We observed that in the absence of ATP, FtsAΔMTS was soluble and remained predominantly localized to the supernatant (Fig. 1a). However, when FtsAΔMTS was incubated in the presence of ATP, we observed a concentration-dependent shift in the distribution of FtsAΔMTS to the ultracentrifugation pellet (Fig. 1a). Notably, in reactions containing 24 μM FtsAΔMTS and ATP, 60% of FtsAΔMTS fractionated with the pellet, compared to 14% when ATP was omitted. In reactions containing 16 μM FtsAΔMTS with ATP, 26% of the protein was detected in the pellet compared to 12% when ATP was omitted (Fig. 1b) suggesting that oligomers assemble cooperatively above a critical concentration. These results indicate that ATP promotes a large molecular weight complex capable of sedimentation at 129,000 *x g*.

To confirm these results, we used 90°-angle light scattering to detect the assembly of large FtsAΔMTS complexes. Reactions containing FtsAΔMTS were incubated and measured to determine a baseline light scatter signal, then, upon addition of ATP, we continue to monitor the light scattering signal for at least 15 min (Fig. 1c). We observed that in reactions containing FtsAΔMTS the addition of ATP promotes a large increase in light scatter which reaches a plateau after approximately 10 minutes (Fig. 1c). To further characterize the concentration-dependency of FtsAΔMTS assembly we incubated reactions containing increasing concentrations of FtsAΔMTS, monitored each for a baseline light scatter signal, then upon addition of ATP continued to monitor light scatter. We observed that reactions containing ATP and increasing concentrations of FtsAΔMTS promotes increasing magnitude of light scatter (Fig. 1c). These results suggest that FtsAΔMTS, in the presence of ATP, promotes an increase in light scatter consistent with the formation of high molecular weight complexes.

To further investigate the requirement for ATP in the assembly of FtsAΔMTS complexes and determine if nucleotide hydrolysis is important for assembly, we compared several ATP analogs for the ability to support complex formation. We observed that addition of ATP promotes light scatter whereas reactions of FtsAΔMTS containing ADP or FtsAΔMTS with ATP and excess EDTA to chelate Mg^{2+} failed to induce light scatter (Fig. 1d). This result indicates that FtsAΔMTS assembles into large molecular weight complexes which are concentration-dependent and that magnesium-dependent ATP hydrolysis may be important for assembly.

To test if the FtsAΔMTS complexes detected by light scatter and sedimentation assays are polymers, we performed negative staining and TEM on mixtures of FtsA,

ATP and PLs. In reactions containing FtsAΔMTS, ATP and SUVs we observed single-stranded polymers ranging up to 800 nm in length (Fig. 2a, upper). The polymers were approximately 6 nm in width (Fig. 2a, lower). Under identical reaction conditions but omitting SUVs observed polymers suggesting SUVs are not essential for polymer formation (Fig. 2b). Importantly, in reaction mixtures of FtsAΔMTS omitting nucleotide we observed only background staining with no large identifiable structures by TEM (Fig. 2c,d). These results demonstrate that incubation of FtsAΔMTS with ATP promotes polymer formation. The observed polymers were approximately 10 nm in width which is consistent with FtsAΔMTS forming a single-stranded protofilament (Fig. 2b).

ATP induces membrane association of FtsAΔMTS to phospholipid vesicles

FtsA has been reported to copurify with PLs and bind small unilamellar vesicles (SUVs) independent of the nucleotide state (Conti et al. 2017). To determine if FtsAΔMTS can interact with SUVs we performed PL recruitment assays of FtsAΔMTS (4μM) in the presence of SUVs (250 μg ml^{-1}) with or without nucleotide. In the absence of nucleotide approximately 4% of FtsAΔMTS fractionates to the SUV-associated pellet, surprisingly, this amount increases to 41% when the reaction is supplemented with ATP (Fig. 3a). Importantly, ATP-dependent interaction between FtsAΔMTS and SUVs is disrupted by increasing concentrations of KCl (Fig. 3b) suggesting FtsAΔMTS binds to SUVs by an electrostatic interaction.

To determine the nucleotide dependency of FtsAΔMTS association to SUVs we performed additional low-speed sedimentation assays. We incubated reactions

containing FtsAΔMTS and SUVs with varying nucleotides (Fig. 3c). We incubated FtsAΔMTS with SUVs and ATP at a physiological concentration of salt (300mM KCl) and then determined if FtsAΔMTS fractionates with the SUV-associated pellet or remaines in the soluble supernatant. In the presence of ATP, 22% of FtsAΔMTS is pellet-associated; however, with reactions containing FtsAΔMTS, SUVs and ADP, only approximately 2% of FtsAΔMTS is detected in the pellet (Fig 3c). Additionally, in reactions containing FtsAΔMTS and SUVs in the presence of ATPγS, ATP with excess EDTA or omitting nucleotide, less FtsAΔMTS was detected in the SUV-associated pellet, suggesting that ATP hydrolysis promotes the interaction between FtsAΔMTS and the membrane (Fig. 3d).

Additionally, we tested if FtsAΔMTS can hydrolyze ATP under reaction conditions that promote membrane assocation. We observed rapid ATP hydrolysis by FtsA and slow ATP hydrolysis by FtsAΔMTS in the presence PLs (Fig. S1) which is consistent with previous reports (Conti et al. 2018). Taken together, these results suggest that FtsA contains a secondary-site of membrane association which associates with the membrane in an ATP-dependent manner.

Surface-exposed residues of FtsA may be important for a secondary membrane interaction.

FtsA engages the membrane directly through a C-terminal MTS, which is critical for FtsA function in vivo (Pichoff & Lutkenhaus 2005). To probe FtsAΔMTS membrane-association we performed site-directed mutagenesis on a helix of FtsA which contains several surface-exposed residues with positively charged side-groups

(Fig. 4a). We identified three residues in this helix, Lys325 His326 His327, as a putative site that may interact with a negatively charged PL surface. To determine if the FtsA 325-327 region is important for ATP-dependent membrane association we constructed and purified the substitution mutant proteins FtsA325AAA and FtsA325AAAΔMTS, which contain a substitution of residues 325-327 for triple alanine, then performed PL association assays in the presence and absence of ATP. FtsA and FtsA325AAA each contain an intact MTS and fractionate with the PL-associated pellet (Fig. 4b). FtsAΔMTS exhibited ATP-dependent PL-association; however, the double-mutant protein FtsA325AAAΔMTS showed significantly reduced membrane association in the presence and absence of ATP (Fig. 4b). To determine if this deficit is due to an inability to self-associate caused by the substitution we measured ATP hydrolysis, if the rate of ATP hydrolysis is intact this suggests amino acid residues 325-327 do not affect FtsA self-association. FtsA and FtsA325AAA hydrolyze ATP rapidly (Fig. 4c) whereas FtsAΔMTS and FtsA325AAAΔMTS are defective for ATP hydrolysis (Fig. 4c). These results suggest the 325 region does not affect ATP hydrolysis consistent with a model whereby FtsA325AAAΔMTS maintains wildtype subunit-subunit interaction. Additionally, FtsA325AAAΔMTS did not promote ATP-dependent light scatter (Fig. S2a). Taken together, this suggests the 325 region of FtsA is important for ATP-dependent membrane association via a second region outside of the MTS.

Discussion

FtsA is a bacterial actin-like ATPase that directly binds to the membrane via its C-terminal MTS, and the interaction is independent of the nucleotide occupancy

(Conti et al. 2017). Here, we report FtsA truncated to remove the MTS, producing FtsAΔMTS, binds to the membrane in an ATP-dependent manner (Fig. 3), likely mediated by surface-exposed residues on FtsA (Fig. 4b). FtsAΔMTS association to SUVs can be disrupted by increasing ionic strength indicating the secondary site of membrane association likely associates with PLs through an electrostatic interaction (Fig. 3a,b). Additionally, in sedimentation assays we show FtsAΔMTS forms polymers in the presence of ATP in a concentration-dependent manner, which we observed by TEM, and upon omission of ATP we were unable to observe polymers (Fig. 1a,b; Fig. 2). To chelate magnesium from the enzymatic pocket of FtsAΔMTS we incubated the protein with EDTA, in a reaction a reaction containing FtsAΔMTS, EDTA and ATP we failed to observe ATP-dependent light scatter (Fig. 1c) suggesting nucleotide hydrolysis may be important for assembly of FtsAΔMTS into polymers. Considering the rate of ATP hydrolysis of FtsAΔMTS is 95% slower than native FtsA (Fig. 4c), it seems plausible that the slow rate of ATP hydrolysis by FtsAΔMTS may stabilize a conformation of FtsA which promotes assembly of long polymers whereby upon rapid hydrolysis the FtsA polymer disassembles.

What then is the function of an FtsA polymer during cell division? Previously, we have shown ATP-binding by FtsA promotes reorganization of PL membranes and recruitment of FtsZ polymers to the membrane (Conti et al. 2017). Additionally, we showed that without PLs FtsA hydrolyzes ATP slowly and FtsA bound to PLs hydrolyzes ATP rapidly (Conti et al. 2017). Our model of FtsA polymerization proposes that FtsA is anchored to the membrane through its endogenous MTS and ATP promotes formation of a short polymer of FtsA. The FtsA polymer may have two

functions, the first is dynamic recruitment of FtsZ polymers. A single subunit of FtsA could tether several subunits of an FtsZ polymer to the membrane, as FtsA polymerizes the molar ratio between the FtsA polymer to the FtsZ polymer reaches an equimolar concentration, at this stoichiometry the FtsA polymer may destabilize the FtsZ filament causing localized disassembly. The second function of an FtsA polymer may be to mediate membrane reorganization: FtsA anchors to the membrane through intercalation of the MTS into the lipid bilayer independent of nucleotide. As FtsA binds ATP the secondary site of lipid-association interacts with the membrane and upon ATP hydrolysis FtsA remains tethered to the membrane through the MTS but the secondary site of membrane association dissociates. This produces an attractive model whereby ATP-binding promotes both polymerization and an additional contact with the membrane, following ATP-hydrolysis, dissociation of one point of contact of FtsA from the membrane and depolymerization; as long as FtsA remains tethered to the membrane through the MTS then rapid cycles of ATP-dependent membrane-binding and polymerization could exert mechanical force on the membrane to promote lipid reorganization.

The ability of another bacterial actin-like protein, MreB, to distort a PL bilayer has been well-characterized. Whereas cell length is primarily regulated by the Z-ring and downstream components, collectively referred to as the divisome, longitudinal growth is regulated by a protein complex referred to as the elongasome. The core of this complex is MreB which binds the membrane on the cytoplasmic face of the bilayer and localizes cell-wall synthesis enzymes (Shi et al. 2018). Species-specific mutations in MreB affect aspects of MreB polymers including the degree of bending or extent of

branching or variable thickness of MreB polymers and across a variety of species accumulation of MreB correlates with regions of cell curvature (Shi et al. 2018). In rod shaped bacteria, the small molecule A22 induces depolymerization and mislocalization of MreB leading to diffuse, rather than specifically localized, cell wall assembly, which leads to a loss of rod shape over several generations (Ursell et al. 2014; Gitai et al. 2005). These findings suggest changes at the molecular level of MreB can fine-tune the cell shape over a large range. Similarly, we propose polymers of FtsA can also fine-tune the shape of the septum by forming polymers which distort the membrane and remodel the long-range FtsZ protofilaments.

Regardless of the specific function of the FtsA polymer, several reports obtained from in vivo genetic studies have suggested that interactions between FtsA and other division proteins, including ZipA, FtsN and FtsEX, may prevent FtsA self-association, promoting monomerization(Pichoff et al. 2012; Du et al. 2016; Pichoff et al. 2015). Therefore, FtsA-interacting proteins may function to inhibit polymerization, thereby regulating cycles of ATP binding and release and cycles of membrane reorganization. Further study will be required to determine the precise roles of FtsA-interacting proteins with respect to polymerization or membrane remodeling by FtsA and to determine if there is equilibrium between FtsA monomers and polymers associated with the membrane.

Materials and Methods

Plasmids, protein expression and purification

E. coli MG1655 expressing pET-24b *ftsA* and site-specific mutants in *ftsA* were constructed by site-directed mutagenesis of *ftsA* expression plasmids using the QuikChange mutagenesis system (Agilent) and confirmed by sequencing. FtsA and FtsA mutant proteins were expressed in BL21 carrying pET vectors encoding wild type or mutant FtsA and purified as previously published (Conti et al. 2017). Eluting fractions were analyzed for purity of FtsA content by SDS-PAGE and coomassie staining: all protein samples used were judged >95% pure. Protein concentrations were determined by bradford assay with comparison to a bovine serum albumin standard curve using Bio-Rad Protein Determination Reagent and concentrations are reported as FtsA monomers.

Nucleotide hydrolysis assay

ATP hydrolysis was measured by monitoring the amount of inorganic phosphate released at indicated times using malachite green reagent for phosphate detection. ATP hydrolysis assays were performed in Reaction Buffer (200 mM KCl, 10 mM $MgCl_2$, 50 mM Tris pH 7.5) with ATP (1 mM) and FtsA (1 µM) and, where indicated, *E. coli* PL vesicles were added (0.5 mg ml^{-1}). *E. coli* total PL extracts (Avanti Polar Lipids) were used to prepare small unilamellar vesicles as previously described (Conti et al. 2017). In all ATPase assays total phosphate content was determined at 5 min using Biomol Green (Enzo Life Sciences) by comparison to a phosphate standard curve.

Light scattering assays

To monitor nucleotide-dependent PL reorganization by FtsA and FtsA mutant proteins, 90°-angle light scattering was performed. Reaction mixtures containing Reaction Buffer and either FtsA, or FtsA mutant protein, where indicated, were monitored for

light scatter with time before and after the addition of 4 mM ATP using an Agilent Eclipse fluorescence spectrophotometer with both excitation and emission wavelengths set to 450 nm with 5 nm slit widths. Baseline readings were collected for at least 3 min, ATP (4 mM) and where indicated EDTA (15 mM), ATPγS (2 mM) or ADP (2 mM) was added and light scattering was measured for up to 30 min.

Assembly and recruitment assays

FtsAΔMTS polymer formation was determined by a sedimentation assay. Reaction mixtures (25 µl) with FtsA or FtsA mutant proteins, at indicated concentrations, were prepared in Reaction Buffer with 4 mM ATP. Polymerization reactions were incubated for 5 min at 23°C and then centrifuged at 129,000 x g for 30 min. Pellets were resuspended in equal volume as supernatants and analyzed by SDS-PAGE and coomassie staining.

PL recruitment assays with FtsAΔMTS were performed by incubating 4 µM protein with ATP (4 mM), ADP (2 mM) or ATPγS (2 mM) and SUVs (500 µg ml^{-1}) then incubated for 5 min at 30°C. SUVs were collected by low speed centrifugation at 12,000 x g for 12 min. Supernatants and pellets were analyzed by SDS-PAGE and coomassie staining. Percent of protein in the pellet fraction was determined by densitometry using NIH ImageJ.

Electron microscopy

Reactions containing assembly buffer mixtures of 20 µM FtsAΔMTS, 4 mM ATP and, where indicated, 0.5 mg ml^{-1} SUVs, were incubated for 5 min at 23°C, applied to a mesh carbon/formvar coated grid, fixed with glutaraldehyde (1%) and negative stained

with uranyl acetate (2%) and were examined using a JEOL JEM-2100F Transmission Electron Microscope (Peabody, MA).

Acknowledgements

We thank Christopher J. LaBreck, Eric DiBiasio and Cathy Trebino. We would also like to thank Janet Atoyan for sequencing assistance performed at the Rhode Island Genomics and Sequencing Center, which is supported in part by the National Science Foundation under EPSCoR Grants Nos. 0554548 & EPS-1004057. Research reported in this publication was supported by the National Institute of General Medical Sciences of the National Institutes of Health under Award Number R01GM118927 to J. Camberg. The content is solely the responsibility of the authors and does not necessarily represent the official views of the National Institutes of Health.

References

Bharat, T.A.M., Murshudov G.N., Sachse, C., & Lowe J., 2015. Structures of actin-like ParM filaments show architecture of plasmid-segregating spindles. *Nature*. 523, 106-110 2015(07)

Bisson-Filho, A.W., Hsu, Y.P., Squyres, G.R., Kuru, K., Wu, F., VanNieuwenhze, M.S., Brun, Y.V., & Garner, E.C., et al., 2017. Treadmilling by FtsZ filaments drives peptidoglycan synthesis and bacterial cell division. *Science*, 17(2)355;6326 pp.1–6.

Bork, P., Sander, C. & Valencia, A, 1992. An ATPase domain common to prokaryotic cell cycle proteins, sugar kinases, actin, and hsp70 heat shock proteins. *Proc Natl Acad of Sci*, 89(16), pp.7290–4.

Busiek, K.K., Eraso, J.M., Wang, Y., & Margolin W. 2012. The Early Divisome Protein FtsA Interacts Directly through Its 1c Subdomain with the Cytoplasmic Domain of the Late Divisome Protein FtsN. *J Bacteriol*, Apr; 194(8) pp.1989–2000.

Conti, J., Viola, M.G. & Camberg, J.L., 2017. FtsA reshapes membrane architecture and remodels the Z-ring in Escherichia coli. *Mol Microbiol*, Feb;107(4):558-576.

Du, S., Pichoff, S. & Lutkenhaus, J., 2016. FtsEX acts on FtsA to regulate divisome assembly and activity. *Proc Natl Acad of Sci*, Aug 23;113(34):E5052-61

Van den Ent, F., Izore, T., Bharat, T.A.M., Johnson, C.M., & Lowe, J. 2014.

Bacterial actin MreB forms antiparallel double filaments. *eLife*, 2014(3):e02634, pp.1–22.

Van den Ent, F. & Löwe, J., 2000. Crystal structure of the cell division protein FtsA from Thermotoga maritima. *The EMBO journal*, 19(20), pp.5300–5307.

Geissler, B., Elraheb, D. & Margolin, W., 2003. A gain-of-function mutation in ftsA bypasses the requirement for the essential cell division gene zipA in Escherichia c m oli. *Proc Natl Acad of Sci*, 100(7), pp.4197–202.

Gray, A.N., Egan, A.J.F., Veer, I.L., Verheul J., den Blaauwen T., Typas, A., Cross, C.A., Vollmer, W., et al., 2015. Coordination of peptidoglycan synthesis and outer membrane constriction during Escherichia coli cell division. *eLife*, 4(MAY):e07118, pp.1–29.

Haeusser, D.P. & Margolin, W., 2016. Splitsville: structural and functional insights into the dynamic bacterial Z ring. *Nature reviews. Microbiology*, 14(5), pp.305–319.

Krupka, M., Cabre, E.J., Jimenez, M., Rivas, G., Rico, A.I. & Vicente, M. 2014. Role of the FtsA C terminus as a switch for polymerization and membrane association. *mBio*, 5(6):e022221-14, pp.1–9.

Li, Z., Trimble, M.J., Brun, Y.V., Jensen, G.J. 2007. The structure of FtsZ filaments in vivo suggests a force-generating role in cell division. *EMBO J.*, 26(22), pp.4694–4708.

Loose, M. & Mitchison, T.J., 2013. The bacterial cell division proteins FtsA and

FtsZ self-organize into dynamic cytoskeletal patterns. *Nature Cell Biology*, 16(1), pp.38–46.

Lu, C., Reedy, M. & Erickson, H.P., 2000. Straight and Curved Conformations of FtsZ Are Regulated by GTP Hydrolysis. *J. Bacteriol*., 182(1), pp.164–170.

Lutkenhaus, J., Pichoff, S. & Du, S., 2012. Bacterial cytokinesis: From Z ring to divisome. *Cytoskeleton*, 69(10), pp.778–790.

Mukherjee, A. & Lutkenhaus, J., 1998. Dynamic assembly of FtsZ regulated by GTP hydrolysis. *EMBO J.*, 17(2), pp.462–469.

Osawa, M. & Erickson, H.P., 2013. Liposome division by a simple bacterial division machinery. *Proc Natl Acad of Sci*, 110(27), pp.11000–4.

Osawa, M. & Erickson, H.P., 2018. Turgor Pressure and Possible Constriction Mechanisms in Bacterial Division. *Front Microbiol.*, 9(January), pp.1–7.

Petek, N.A. & Mullins, R.D., 2014. Bacterial actin-like proteins: Purification and characterization of self-assembly properties. *Methods in Enzymology*, 540, pp.19–34.

Pichoff, S., Shen, B., Sullivan, B., & Lutkenhaus, J. 2012. FtsA mutants impaired for self-interaction bypass ZipA suggesting a model in which FtsA's self-interaction competes with its ability to recruit downstream division proteins. *Molecular Microbiology*, 83(1), pp.151–167.

Pichoff, S., Du, S. & Lutkenhaus, J., 2015. The bypass of ZipA by overexpression of FtsN requires a previously unknown conserved FtsN motif essential for FtsA – FtsN interaction supporting a model in which FtsA monomers recruit

late cell division proteins to the Z ring. *Mol Microbiol.*, 95(February), pp.971–987.

Pichoff, S. & Lutkenhaus, J., 2005. Tethering the Z ring to the membrane through a conserved membrane targeting sequence in FtsA. *Molecular Microbiology*, 55(6), pp.1722–1734.

Rico, A.I., Garcia-Ovalle, M., Palacio, P., Casanova, M., & Vicente M. 2010. Role of Escherichia coli FtsN protein in the assembly and stability of the cell division ring. *Molecular Microbiology*, 76(3), pp.760–771.

Shi, H., Bratton, B.P., Gitai, Z., & Huang, K.C. 2018. How to Build a Bacterial Cell: MreB as the Foreman of E. coli Construction. *Cell*, 172(6), pp.1294–1305.

Shiomi, D. & Margolin, W., 2008. Compensation for the loss of the conserved membrane targeting sequence of FtsA provides new insights into its function. *Mol Microbiol.* 67(January), pp.558–569.

Söderström, B., Mirzadeh, K., Toddo, S., von Heijne, G., Skoglund, U. & Daley, D.O. 2016. Coordinated disassembly of the divisome complex in Escherichia coli. *Molecular Microbiology*, 101(3), pp.425–438.

Szwedziak, P., Wang, Q., Freund, S.M., Lowe, J., 2012. FtsA forms actin-like protofilaments. *EMBO J.*, 16;31(10), pp.2249–2260.

Szwedziak, P., Wang, Q., Tsim, M., & Lowe, J. 2014. Architecture of the ring formed by the tubulin homologue FtsZ in bacteria. *eLife*, 3:e04601.

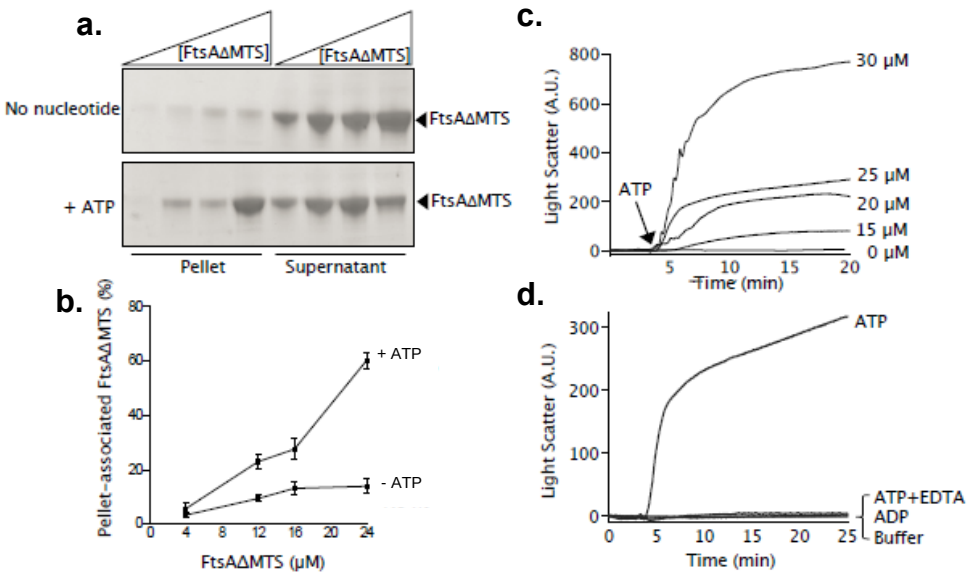
a.
[FtsAΔMTS]
[FtsAΔMTS]
No nucleotide
+ ATP
FtsAΔMTS
FtsAΔMTS
Pellet
Supernatant
b.
Pellet-associated FtsAΔMTS (%)
+ ATP
- ATP
FtsAΔMTS (μM)
c.
Light Scatter (A.U.)
ATP
30 μM
25 μM
20 μM
15 μM
0 μM
Time (min)
d.
Light Scatter (A.U.)
ATP
ATP+EDTA
ADP
Buffer
Time (min)

Figure 1. FtsAΔMTS in the presence of ATP induces large protein complexes

(a) Reactions containing FtsAΔMTS (4-24 μM) and ATP (4 mM), where indicated, were incubated at room temperature for 5 minutes and then fractionated by ultracentrifugation. Supernatants and pellets were analyzed by SDS-PAGE and coomassie staining. (b) Quantitation of FtsA by densitometry comparing relative abundance of FtsA associated with the pellet in the presence or absence of ATP. (c) Reactions with increasing concentration of FtsAΔMTS were monitored by 90° light scatter as described in Materials and Methods. A baseline was collected for 4 min, then ATP (4 mM) was added, and signal monitored for an additional 20 min. (d) Reaction mixtures containing FtsAΔMTS (25 μM) were monitored by 90° light scatter as described in Materials and Methods. A baseline was collected for 5 min, then ATP (4 mM) with and without EDTA (15 mM), ADP (2 mM) was added, and signal monitored for an additional 20 min.

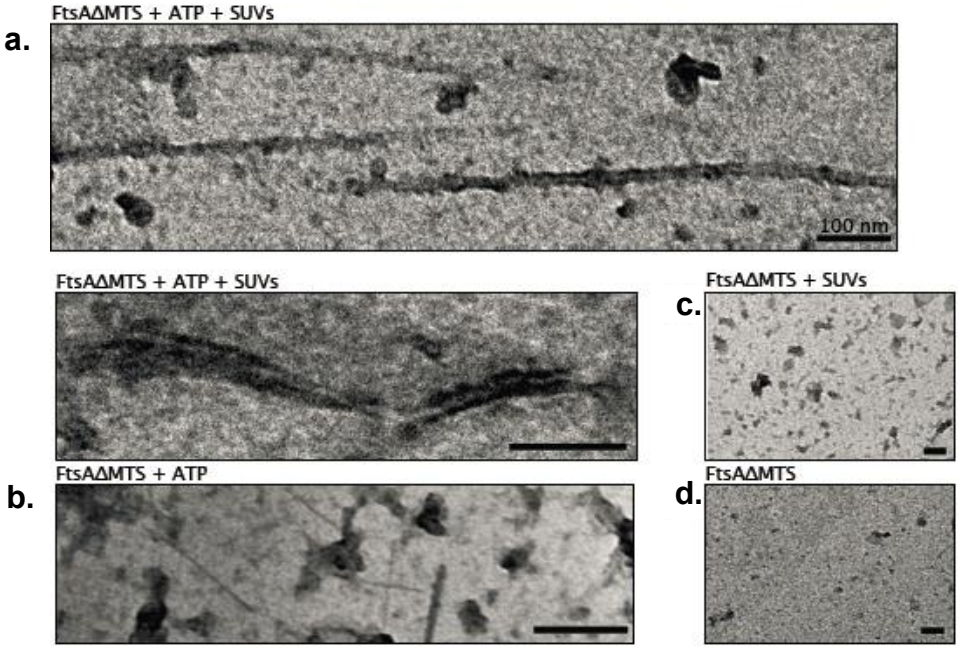
a.
FtsAΔMTS + ATP + SUVs
100 nm
FtsAΔMTS + ATP + SUVs
b.
FtsAΔMTS + ATP
c.
FtsAΔMTS + SUVs
d.
FtsAΔMTS

Figure 2. FtsAΔMTS forms ATP-dependent filaments

(a) Upper and lower, FtsA (20 µM) was incubated with ATP (4 mM), prepared and visualized by negative stain TEM. Size bar is 100 nm. (b) FtsA (20 µM) in the presence of ATP (4 mM) and PL vesicles were prepared and visualized by negative stain TEM. (c) FtsA (20 µM) incubated with SUVs in the absence of nucleotides were prepared and visualized by negative stain TEM. (d) Reaction containing FtsA, as in c, but omitting SUVs was prepared and visualized by negative stain TEM.

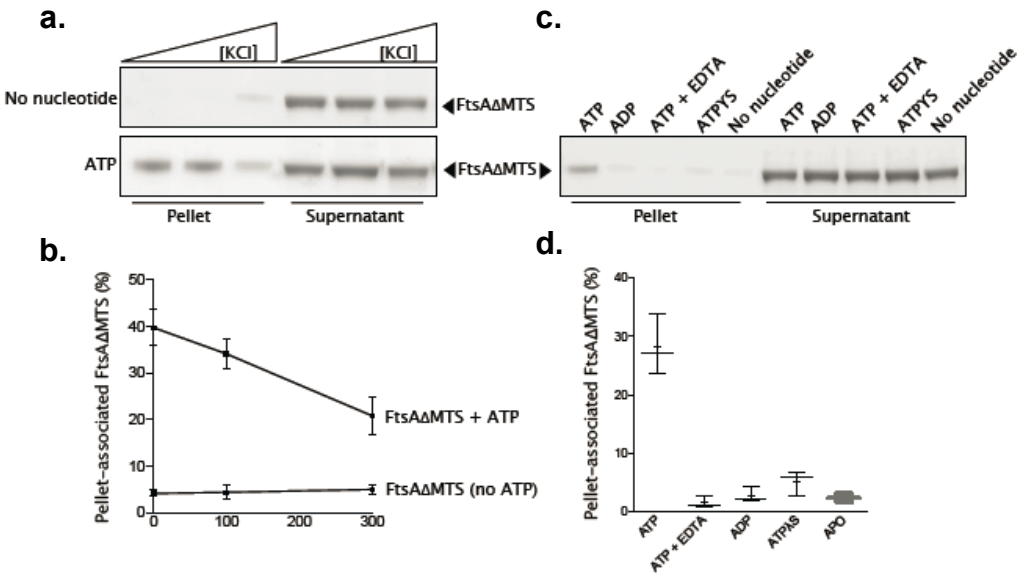
a.
[KCl]
[KCl]
No nucleotide
ATP
FtsAΔMTS
FtsAΔMTS
Pellet
Supernatant
c.
ATP
ADP
ATP + EDTA
ATPγS
No nucleotide
ATP
ADP
ATP + EDTA
ATPγS
No nucleotide
Pellet
Supernatant
b.
Pellet-associated FtsAΔMTS (%)
50
40
30
20
10
0
0
100
200
300
FtsAΔMTS + ATP
FtsAΔMTS (no ATP)
d.
Pellet-associated FtsAΔMTS (%)
40
30
20
10
0
ATP
ATP + EDTA
ADP
ATPγS
APO

Figure 3. ATP induces membrane association of FtsAΔMTS to phospholipid vesicles

(a) Sedimentation assay to determine membrane association, as described in Materials and Methods, with reaction mixtures of FtsAΔMTS (4 μM) and SUVs (0.5 mg ml-1), incubated in the presence or absence ATP (4mM) and increasing concentrations of KCl (0, 100, 300 mM KCl). Supernatants and resuspended pellets were visualized by SDS-PAGE. (b) Densitometry of the band corresponding to FtsA to compare relative abundance of FtsA associated with the pellet-associated SUVs. (c) PL binding assay, as in a., of FtsAΔMTS (4 μM) and 300 mM KCl incubated with ADP (2 mM), ATPγS (2 mM) or ATP (4 mM) with or without EDTA (15 mM). (d) Densitometry of the band corresponding to FtsA to compare relative abundance of FtsA associated with the pellet-associated PL vesicles.

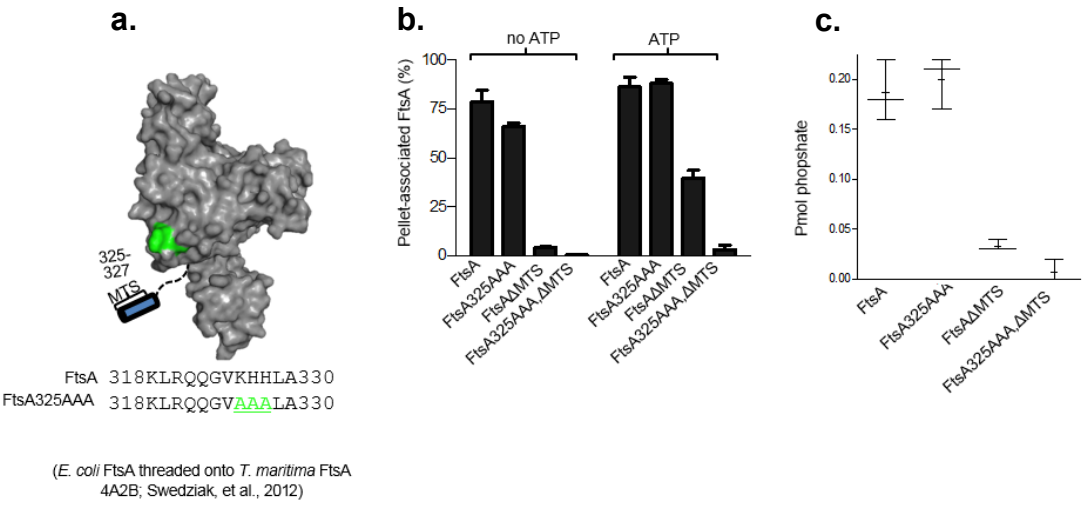
a.
325-
327
MTS
FtsA 318KLRQQGVKHHLA330
FtsA325AAA 318KLRQQGVAAALA330
(E. coli FtsA threaded onto T. maritima FtsA
4A2B; Swedziak, et al., 2012)
b.
no ATP
ATP
Pellet-associated FtsA (%)
100
75
50
25
0
FtsA
FtsA325AAA
FtsAΔMTS
FtsA325AAA,ΔMTS
c.
Pmol phopshate
0.20
0.15
0.10
0.05
0.00
FtsA
FtsA325AAA
FtsAΔMTS
FtsA325AAA,ΔMTS

Figure 4. Surface-exposed residues of FtsA may be important for a secondary membrane interaction

(a) *E. coli* FtsA (residues 13–381) modeled onto *T. maritima* FtsA (pdb: 4A2B) (Szwedziak et al., 2012). Surface exposed residues are shown highlighting amino acids at position 325, KHH (green). (b) PL binding sedimentation assay, as described in Materials and Methods, with reaction mixtures of FtsA or FtsA mutant proteins (4 μM) and PL vesicles, incubated in the presence or absence ATP (4mM) and 300 mM KCl. Supernatants and resuspended pellets were visualized by SDS-PAGE. (c) Hydrolysis of ATP by FtsA or FtsA mutant proteins (1 μM) were monitored with time as described in Materials and Methods, and phosphate was detected by malachite green reagent. Data is an average of three replicates represented as mean +/- SEM.

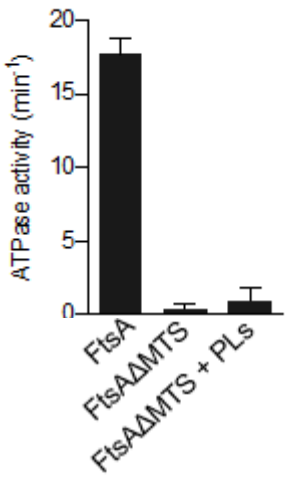
20
15
10
5
0
ATPase activity (min-1)
FtsA
FtsAΔMTS
FtsAΔMTS + PLs

Fig. S1. Nucleotide Hydrolysis by FtsA and FtsAΔMTS in the presence and absence of SUVs.

(a) Hydrolysis of ATP by FtsA or FtsAΔMTS (1 μM), with or without phospholipids, were monitored with time as described in Materials and Methods, and phosphate was detected by malachite green reagent. Data is an average of three replicates represented as mean +/- SEM.

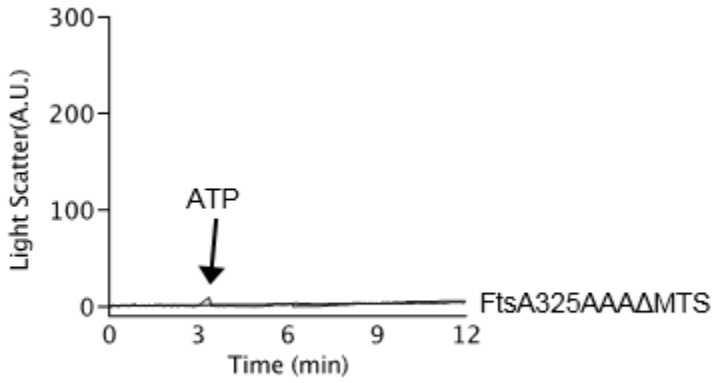
300
200
100
0
Light Scatter(A.U.)
ATP
FtsA325AAAΔMTS
0
3
6
9
12
Time (min)

Fig. S2. FtsA325AAAΔMTS in the presence of ATP fails to promote increase in light scatter.

(a) FtsA325AAAΔMTS (10 μM) was monitored by 90° light scatter as described in Materials and Methods. A baseline was collected for 3 min, then ATP (4 mM) with was added, and signal monitored for an additional 8 min.